Experimental study of methane decarbonization to produce hydrogen using a laminar premixed flame

by

Farjad Falahati

A thesis submitted in partial fulfillment of the requirements for the degree of

Master of Science

Department of Mechanical Engineering
University of Alberta

Abstract

Hydrogen is a promising source of energy with various applications. The most common method of producing hydrogen is steam reforming of methane; however, thermal cracking of methane can be used alternatively for hydrogen production with less CO_2 emissions. In this study, thermal cracking of methane in the products of premixed air-fuel flames was studied. A quartz cylinder filled with insulation blocks was used as the reaction chamber with the placed flame placed at the inlet to create the reaction zone and methane was injected into the flame. The exhaust products were then sampled and passed through a gas chromatography analyzer to determine the methane conversion efficiency into hydrogen as the main goal of this study. Two types of premixed flames (*i.e.*, methane and propane-based fuels) that were slightly fuel rich to minimize free-oxygen were used to study methane cracking.

The temperature distribution along the center-line inside the reaction chamber was measured for both flames. The highest temperature recorded in the reaction chamber was 1170 °C and 1135 °C for propane and methane flame, respectively, and it dropped dramatically further from the flame in the reaction chamber for both flames. Methane conversion into hydrogen with the premixed air-propane flame was measured for various flow rates of pyrolysis methane from 0 to 5 l_n/min for a fixed flow rate flame. The highest measured conversion efficiency for this flame was 69% when the pyrolysis methane flow rate of 0.5 l_n/min. The same sets of experiments were done with a premixed air-methane flame, and the highest measured methane conversion to hydrogen of 78% was obtained with the pyrolysis methane flow rate of 0.5 l_n/min. The gas chromatography

analysis showed the efficiency of methane conversion into solid carbon was very low as the carbon atoms mainly preferred to form CO when in contact with the hot products of combustion.

Preface

This thesis is original work by Farjad Falahati. Part of Chapters 2 and 3 of this thesis have been published as Farjad Falahati, Mohammad Javad Afroughi, Jason S. Olfert, and Larry W. Kostiuk. “Preliminary experimental study of methane decarbonization using a laminar premixed flame”. In *Proceedings of Combustion Institute - Canadian Section, Spring Technical Meeting*, Montreal, Canada, May 15 - 18, 2017.

Acknowledgements

I would like to express my sincere gratitude to my supervisors Professors Larry W. Kostiuk and Jason S. Olfert for their continuous support during the whole of my study. I greatly appreciate their patience in motivating me and sharing their knowledge for all challenges I had. Conversations with them always kept me at higher level of thinking and were true inspirations.

I am also grateful for my friends and lab mates for their support, friendship and help.

Special thanks go to my parents and my brother for providing me support during my whole life and believing me all along. I owe it to you all!

Farjad Falahati

January, 2018

Table of Contents

List of Tables

List of figures

CHAPTER 1. INTRODUCTION

1.1 Background

Human activities affect the environment on a global scale, causing a dramatic increase in greenhouse gas emissions, decreasing the pH of oceans, and increasing atmospheric temperature [1]. Greenhouse gases, in particular, CO_2, are the main cause of climate change. Greenhouse gas emissions have increased significantly since industrialization. The concentration of carbon dioxide in the atmosphere has risen about 35% from the beginning of the industrialization [2]. Combustion of natural gas, coal, and oil are the main sources of greenhouse gas emissions. Where oil's share of these emissions is 39%, natural gas stands for 20% of greenhouse gas emissions and the balance comes from coal [1]. Natural gas is seen as a cleaner fuel compared to other fossil fuels when used in power plants, industries, and transportation [2] because a greater proportion of its chemical enthalpy is associated with hydrogen instead of carbon. The main source of energy will continue to be the combustion of fossil fuels at least for next 50 years [3]. If the current CO_2 emissions rate continues, then in a half a century the atmospheric concentration of CO_2 will be twice, and will profoundly affect climate [3].

There are different parameters that affect CO_2 concentration in the atmosphere from combustion of fossil fuels. For controlling and decreasing CO_2 emissions various actions can be taken, such as controlling population growth, and reducing the per capita emission rate by increasing energy efficiency, as well as improving and implementing renewable energies technologies. Alternate strategies consider carbon capture and storage/usage, which can either be done after the combustion as CO_2 or the removal of the carbon from the fossil fuels as elemental carbon before combustion [4].

Reducing CO_2 emissions from the direct burning of natural gas is one the main concerns of current studies. The motivation of this research was to find an alternative

way of natural gas usage. Natural gas primarily consists of methane, which can be decomposed into black carbon and a carbon-free fuel in the form of hydrogen [1].

$$CH_4\ (g)\ \rightarrow C\ (s) + 2H_2\ (g) \qquad \Delta H^0 = 74.49\ \text{kJ/mole} \tag{1-1}$$

This reaction does not occur spontaneously at normal temperatures and pressures, but does occur at elevated temperatures (>1100 K) in the absence of oxygen, and is known as thermal decomposition or pyrolysis [5]. Hydrogen produced from this reaction can be used as the heat source in many industries and carbon black is a valuable raw material. The energy needed to raise the temperature of the methane can be provided with various sources. Once this reaction is established, the hydrogen produced in the pyrolysis of methane can be used as the feedstock for the process of thermal decomposition of methane, ideally burning only 15% of the produced hydrogen would be enough to run the process [6]. Furthermore, the produced black carbon can be collected and could potentially be used in various industries such as rubber goods, plastics, inks, paints, etc. Nowadays, carbon is used in structural materials, technological equipment and chemical industries [7].

1.2 Motivation

The specific motivation for this work is to convert natural gas into hydrogen. Hydrogen produced from this process is a clean fuel that can be used in industrial facilities with no carbon emissions. In the proposed process, natural gas will be decomposed into hydrogen and carbon; carbon would be separated from natural gas in the form of black carbon. Figure 1-1 shows the proposed overall process of natural gas decomposition. Thermal cracking of natural gas should occur at a high temperature and oxygen-free environment. The proposed process explored in this thesis; the products of a slightly fuel-rich premixed flame would create the high-temperature environment for pyrolysis of natural gas, having a premixed flame to provide the energy needed for decomposition the cost of the process is less than electrical power.

A confined premixed burner is considered, air and fuel are mixed prior to combustion and flow rates should be adjusted so there will be no oxygen in the products. The adiabatic flame temperature of premixed air and methane is approximately 1950 ^{0}C and then natural gas will be injected into this high-temperature region. As result, the injected natural gas will start to form carbon black and hydrogen, the produced carbon black can be separated by a cyclone, and the stream of hydrogen-rich gases will leave the cyclone ready for afterburning. The emissions of CO_2 can be eliminated completely if some of the produced hydrogen were combusted to sustain the pyrolysis process but would require using of twice as much natural gas to meet the same heating load.

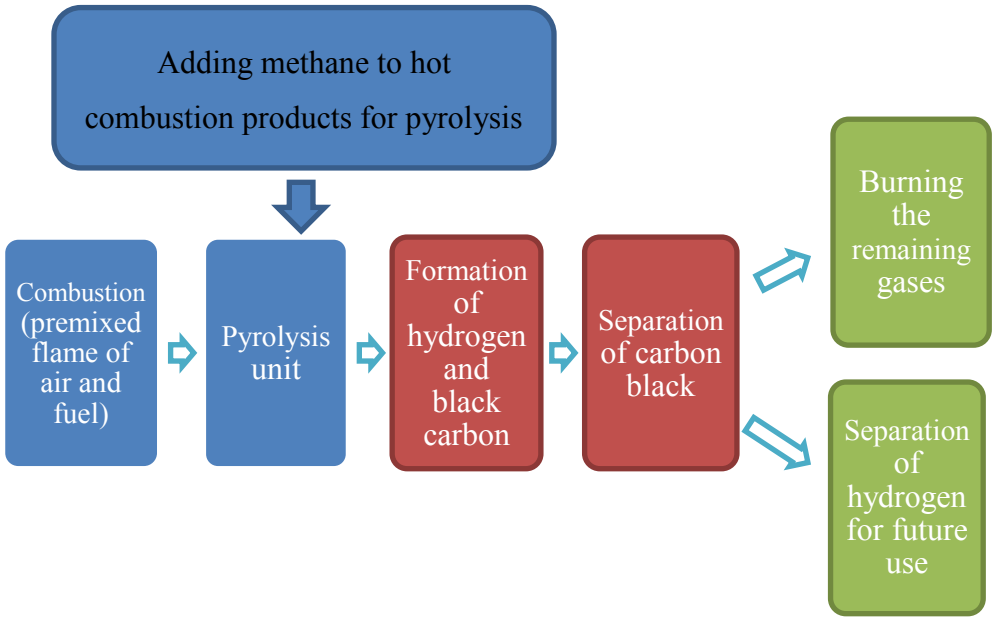

Figure 1-1 -Natural gas pyrolysis scheme

1.3 Hydrogen as Fuel

Hydrogen is a promising replacement for fossil fuel as it has higher energy production when considered its oxidation on a mass basis. The lower heating value of

hydrogen is 2.4 higher than methane. Currently, 0.1 Gt of hydrogen is produced in Canada each year which is mostly (about 98%) from fossil fuel reforming [1]. Hydrogen's applications are in oil refineries, as well as ammonia and methanol production [8]. Hydrogen fuel cells are a rapid growing technology and potential clean power source as it is quiet and free of any hazardous material [9]. Hydrogen production development is needed to make fuel cells an economically favorable power source in automobiles. Hydrogen production is expected to increase to 104-309 Mt by 2050 [10]. Different methods are used to produce hydrogen among which are: steam methane reforming (SMR), coal gasification, biomass gasification, thermal decomposition of methane [1], electrochemical processes and water-splitting cycle [11], Water splitting cycle is more environment friendly than common methods such as SMR, partial oxidation of heavy oils and coal gasification as the hydrogen production process doesn't produce any CO_2 [12]. Hydrogen can be produced by decomposition of water as follow [13]:

$$H_2O \rightarrow H_2 + \frac{1}{2}O_2 \qquad \Delta H^0 = 241.93 \text{ kJ/mole} \qquad (1\text{-}2)$$

If hydrogen is to be produced by renewable energies, the cost of renewable sources must decrease dramatically so the produced hydrogen can be economically possible [14]. Water is the largest source of hydrogen, but water splitting needs much energy (241.93 kJ/mole compared to 74.49 kJ/mole) to produce hydrogen than natural gas decomposition. The amount of available natural gas sources makes it an ideal choice for hydrogen production with less input energy comparing to water [15]. In the following section, steam reforming and thermal cracking of methane will be explained as two common methods of hydrogen production, a comparison between these two methods would be presented and advantages of thermal cracking will be shown.

1.4 Methods for Hydrogen production

1.4.1 Steam methane reforming (SMR)

Producing hydrogen using steam methane reforming releases about 13.7 kg CO_2 per kg of hydrogen produced [16]. The steam reforming process can be defined by the following reactions [4]:

$$\text{Steam reforming } CH_4 + H_2O \rightarrow CO + 3H_2 \quad (1\text{-}3)$$

$$\text{Water Shift } CO + H_2O \rightarrow CO_2 + H_2 \quad (1\text{-}4)$$

$$\text{Overall reactions } CH_4 + 2H_2O \rightarrow CO_2 + 4H_2 \quad (1\text{-}5)$$

Natural gas reacts with steam to produce hydrogen and CO; since CO is a toxic gas it will be reacted with steam again to produce extra hydrogen and CO_2 in water shift reaction. This process happens in a metal alloy tube over a nickel catalyst, at pressure range of 30-60 atm and temperature range of 800-1000 °C. Produced CO_2 is needed to be removed from hydrogen either by solvent absorption and stripping or by adsorption and stripping, then this CO_2 can be sequestered [4]. There are three methods for carbon dioxide storage which are: geological, ocean and mineral. Geological can be done in oil and gas reservoirs, coal seams or saline aquifer. There are many drawbacks associated with geological storage such as leakage to atmosphere, CO_2 is dangerous for human for concentration greater than 1.5% (atmospheric concentration is 0.038%), death of small animals who live in low-level enclosed areas and change water pH and impacts on marine life [17].

1.4.2 Thermal decomposition of methane (TDM)

Thermal decomposition of methane, equation (1-1), is a cleaner way to produce hydrogen with no CO_2 emissions. Lane and Spath [18] estimated the selling price of hydrogen by thermal decomposition of natural gas is about 7-21 $/GJ, which is dependent on the selling price of produced carbon. Carbon black produced from methane cracking sells for approximately $300 to $4000 per tonne depending on its quality [19]. Carbon black is a valuable material with various applications in industry. About 70% of carbon

black is used in tire industry, 20% for rubber products and rest in non-rubber products [20]. Annual world carbon black production is roughly 9 Mt [21]. According to American Society for Testing and Materials (ASTM) designation used for medium thermal black made from thermal cracking of natural gas is N990 with average primary particle diameter of 320 nm [20]. Thermal carbon has high loading capacity and low tensile strength and reinforcement and can be used in wire insulation, hose, O-rings and tire inner liners [20]. The possibility of making thermal cracking a commercial process depends on characteristic of produced carbon, mainly the size of produced particles [22].

In the methane cracking reaction, equation (1-1), the Arrhenius equation defines the reaction kinetics as follow [23]:

$$k = k_0 e^{\frac{-E_a}{RT}} \tag{1-6}$$

k_0 = Pre-exponential factor, 1/s

E_a = Activation energy, kJ/mole

R = Universal gas constant of 8.314 J/mole·K

T = Reaction temperature, K

The rate of reaction (mole/$m^3 \cdot s$) can be defined as:

$$r_{CH_4} = -kC_{CH_4} \tag{1-7}$$

$C_{\mathrm{CH_4}}$ = methane concentration mole/m^3

The activation energy of methane cracking is dependent on residence time, temperature, reactor type and presence of catalyst [24]. A summary of different values of pre-exponential factor and activation energy found in studies is presented in Table 1-1. Figure 1-2 shows the rate constant (1/s) as the function of T (K) for given numbers in table 1-1.

Table 1-1-Different values of activation energy kJ/mole from different studies [23]

Name	Pre-exponential factor 1/s	Activation energy kJ/mole
Steinberg [25]	$5.4*10^{13}$	135
Kevorkian [26]	$1.3*10^{14}$	389.112
Patrianakos [27]	$1.0*10^{14}$	400
Paxman [23]	$5.43*10^{15}$	420.7

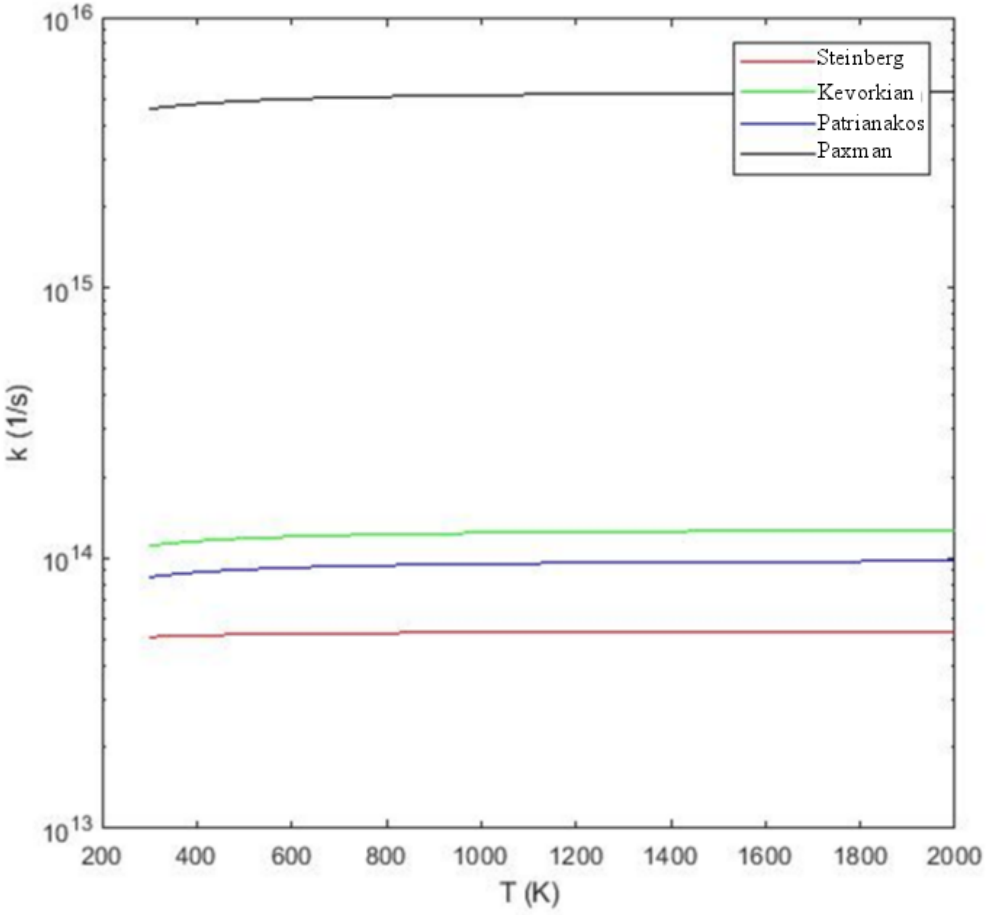

Figure 1-2 - Rate constant (1/s) as function of T (K) for four different studies.

There are different studies which have tried to define methane cracking mechanism at high temperatures. Skinner [28] defined the pyrolysis of methane in a stepwise reaction as follow:

$$CH_4 \rightarrow C_2H_6 \rightarrow C_2H_4 \rightarrow C_2H_2 \rightarrow C \qquad (1\text{-}8)$$

Kevorkian *et al* [26] suggested another mechanism for methane pyrolysis, they used a shock-tube in temperature range of 1383 ^{0}C to 1692 ^{0}C,

$$\begin{gathered} CH_4 <=> CH_2 + H_2 \\ CH_2 + CH_4 <=> CH_3 + CH_3 \\ CH_3 + CH_3 <=> C_2H_6 => \text{Products} \\ CH_2 + H_2 <=> CH_3 + H \\ CH_4 + H <=> CH_3 + H_2 \\ CH_2 + H_2 <=> CH_4 \end{gathered} \tag{1-9}$$

The reaction mechanism of methane cracking is not well defined. Production of some by-products like C_2H_2, C_2H_4 and polyaromatic hydrocarbons (PAHs) need a more complex reaction scheme to be defined [12]. Billaud [29] described the reaction mechanics using 119 reactions. In methane cracking reaction higher pressures are better for higher rates of reactions [25]. Methane pyrolysis needs relatively high temperatures, using a catalyst can reduce the temperature. Most common catalysts that are used in this process are carbon and metal-based catalysts [1].

Different heating sources can be applied to methane cracking among which are solar energy, plasma, molten metal bath and flame [30]. Assuming the efficiency of methane cracking is 80%, the energy needed to produce one mole of hydrogen considering the enthalpy of reaction would be 47.28 kJ per mole of H_2 [15]. Part of the produced hydrogen in thermal cracking can be used as the fuel for the process. Considering higher heating value of hydrogen combustion which is 284.51 kJ per mole of H_2 the moles of hydrogen needed to provide 46.55 kJ/mole for thermal cracking would be 0.33 mole of hydrogen per mole of CH_4 [15]. In fact, by burning about 15% of produced hydrogen the heat for the process can be provided. In this case, there will be no CO_2 emission, but the thermal efficiency of this process is about 53.3% which is relatively low. Burning

methane as the fuel increases the efficiency to 58.1% but will release about 0.05 mole of CO_2 per mole of CH_4 [15].

1.4.3 Thermal decomposition of methane vs steam methane reforming

The cost of hydrogen produced by thermal cracking of methane is \$58/1000 m^3 H_2 which is lower than that for SMR \$67/1000 m^3 H_2 [31]. Another advantage of methane cracking over SMR is that separation and storage of carbon produced in it is much easier than CO_2 produce in SMR [1]. In SMR process for capturing and sequestering the produced CO_2 will lead to 40% of energy lost in the whole process [4], cause is needed to be liquefied and pumped in certain areas for storage [15], which has its own disadvantages as discussed in section 1.4.1; on the other hand in thermal cracking sequestering of carbon black takes less energy as it is a stable solid material comparing to CO_2 which is a reactive gas or low-temperature liquid [4]. An approximate cost estimate shows that producing hydrogen by SMR and thermal cracking costs the same before separation of CO_2 or C, since capturing C is easier than CO_2 then thermal cracking would be a less expensive process [15]. Energy input per mole of hydrogen is lower than SMR [1]. In SMR method by producing one mole of hydrogen there will be 0.3 moles of CO_2 [3] or 11.9 kg of CO_2 per kg of H_2 [32]. Hydrogen produced by thermal cracking of methane which is a CO_2 free process and carbon black is valuable industry material. Produced hydrogen can also be used as the feedstock for the process, burning 15% of the produced hydrogen can keep the process going [3]. The energy needed for thermal cracking can come from solar energy, nuclear energy or combustion. For providing temperature over 1227 ^{0}C a concentration factor of 3000 is needed if using solar energy [33][34]. But more improvement is needed to have solar furnaces that can provide that temperature. Using nuclear power to provide energy for methane cracking is controversial due to the nuclear waste concerns [15].CO_2 emissions would be zero in thermal cracking if the heat needed for the process were provided by solar or nuclear energy; if CO_2 were taxed that would help thermal cracking to be economically feasible. Energy efficiency in thermal cracking is 84.5 % which is higher than SMR which is 83% [3]. If the heat needed for thermal cracking is provided by natural gas combustion, the produced CO_2 and hydrogen can react to produce methanol [4].

1.5 Methane conversion in TDM

1.5.1 Experimental studies

In this section, a summary of couple experimental studies in methane cracking is discussed. Temperature and residence time are the main parameters that were studied in methane conversion into hydrogen by thermal decomposition. Abánades *et al* [3] studied thermal cracking in a heated furnace and tried to investigate the effect of temperature, residence time and tube material. At 1000 °C they reached hydrogen yield of 10% for residence time of 16 s and about 40% for 96 s. Paxman *et al* [23] studied molten media methane cracking, they used a perfectly mixed reactor; in the reactor, at 1100 °C their experiment shows 60% of methane conversion. Rodat *et al* [24] investigated methane decomposition in graphite tubular reactors. The heat for the reaction was provided by a medium-scale solar reactor (10 kW). They investigate the effect of residence time, temperature and methane mole fraction on methane conversion to hydrogen and carbon. The maximum methane conversion rate was 98% at 1497^0C. Operating temperature has a huge impact on thermal cracking [23]. For temperatures over 1350 ^{0}C, the residence time effect becomes negligible [3]. For this temperature range, full conversion of methane would occur with H_2 as the main product [3]. Using different tube materials such as quartz, graphite and silicon carbide had similar results in hydrogen conversion rate [3]. Increasing pressure leads to less methane conversion as a result higher temperatures are needed to have complete decomposition [25]. Adding a catalyst, like carbon, would increase the reaction rate [35].

1.5.2 Numerical studies

Different equations should be considered to model methane cracking, such as, heat transfer by conduction and convection, particle and gas radiation, nucleation and growth of carbon black and reactions of methane dissociation. Methane pyrolysis can be modeled by Gibbs minimization method to determine the equilibrium concentration. For doing so, first all the product species would be determined, then by considering the conservation of mass the concentration of each species that minimize the Gibbs energy will be specified [36]. Gautier *et al* [22] investigated the effects of various operating temperatures and

pressures on methane conversion rate. For atmospheric pressure at 1326 °C, the conversion rate with their model is 44.1% and it increases to 100% at 1726 °C. Steinberg's model [15] used a first-order mass and energy balance for methane cracking reaction. At temperatures over 800^0C at atmospheric pressure the methane conversion is almost complete, *i.e.*, over 95% of gas phase hydrogen. Younesi *et al* [36] used the combustion reactions to define methane pyrolysis. Their model was a modified mechanism from Appel *et al* [37] in which they used data from GRI-Mech 1.2 and defined pyrolysis of methane. Thermodynamic data were taken from NASA-Lewis thermodynamic database [38]. Their model shows at 1000 °C for atmospheric pressure and long residence time methane conversion rate is about 80%. Rodat *et al* [12] did a simulation using Dsmoke code that can model details of PAHs and soot formation; it uses 240 species and 14,000 reactions. It is valid for different chemical reaction such as combustion, steam cracking of alkane and oxidative pyrolysis. Increasing temperatures over a specific amount does not convert methane into hydrogen, as other species like acetylene will be formed, which decrease the hydrogen yield [36]. The peak value of the hydrogen production decreases as the pressure increases for temperatures less than 1200 °C [36].

1.6 Contribution

There is no complete study about methane pyrolysis using a premixed laminar flame as the source of thermal energy for the reaction. Most of the experimental researches in this area, *e.g.*, [3], were done using a shock tube as the reaction tube where temperature and residence time can be controlled and methane conversion into hydrogen and carbon was measured for various temperatures and residence times. Many researches, *e.g.*, [23], tried to investigate methane cracking in presence of a catalyst or in a molten metal bath. There are some numerical projects, *e.g.*, [12], that modeled the kinetic associated with methane pyrolysis. Trying to investigate methane pyrolysis using the high-temperature products of a premixed flame in a set-up was done for the first time in this project. This set-up is not capable of setting the temperature to a certain value like shock tubes, but it is more likely to be a commercial idea, as it does not use any advance reacting tube and it uses natural gas instead of electricity or solar energy as the energy source. Natural gas is

readily available and it would be less expensive than electricity. Having a relatively large reacting tube in this project makes it easy to separate and collect black carbon produced during the pyrolysis and paves the way to develop an industrial scale set-up.

1.7 Objectives

The goal of this study was to establish an experimental setup to investigate methane pyrolysis using an inverted premixed flame for the first time. The set-up was designed to provide a flow of methane through an inverted laminar premixed flame inside an enclosed, oxygen-free environment and observe and measure the conversion of methane into hydrogen. Concentrations of the products were measured at the exhaust using gas chromatography in order to determine the methane conversion into hydrogen. The temperature distribution inside the chamber was measured in order to find the relation between temperature and the conversion rate of methane.

1.8 Thesis outline

In this first chapter a basic literature review was done for studies in methane cracking, chapter 2 contains the details of the experimental set-up. In chapter 3 the results of methane conversion from the experiment by running methane flow through the products, either a propane or methane premixed flame are shown and discussed. Chapter 4 contains conclusion and recommendations for future work.

CHAPTER 2. EXPERIMENTAL SET-UP

2.1 Introduction

The goal of the study is to investigate pyrolysis of natural gas using a premixed laminar flame as the high-temperature source in a lab scale set-up. The main structure of the experimental setup consists of a quartz cylinder as the reactor, a burner that stabilizes the premixed laminar flame, a frame that supports the reacting cylinder and its end plates, and exhaust tube that goes into a fume hood. Sampling the products of the reaction was done by extracting gases from the exhaust tube and sending the sample into a heat exchanger to remove water and then to a gas chromatography analyzer. Temperature measurement was done using a K-type thermocouple inside the reacting cylinder. In this chapter, the set-up used for this study is discussed in detail. The full setup is shown in Figure 2-1, and the next ten sections describe the individual components in detail.

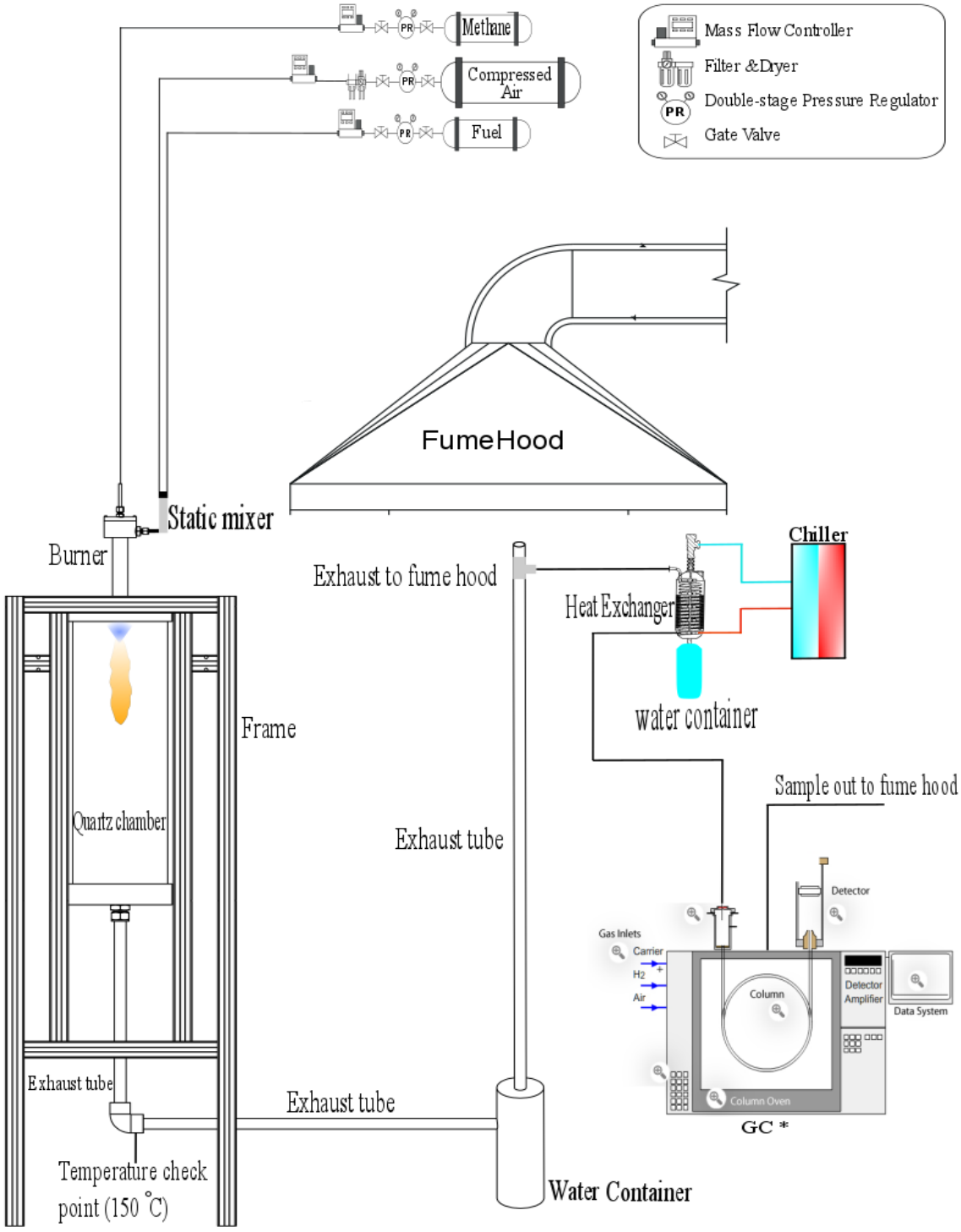

Figure 2-1- Schematic of the experiment and sampling setup – pyrolysis with the propane flame

*The GC schematic is taken from [39]

2.2 Burner

Hatchard *et al*. [40] developed a burner based on a premixed flame for use in an ultra-low emissions furnace that could be either laminar or turbulent flow, and this burner was modified for the current application. The burner tube, shown in Figure 2-2, has an outside diameter (OD) of 3.33 cm and an inside diameter (ID) of 2.69 cm, it is 21.19 cm long and made of 316 stainless steel. Two-millimeter solid-glass beads fill a 5.08 cm section of the burner tube and are used to stop the flame from flashing back passed the burner.

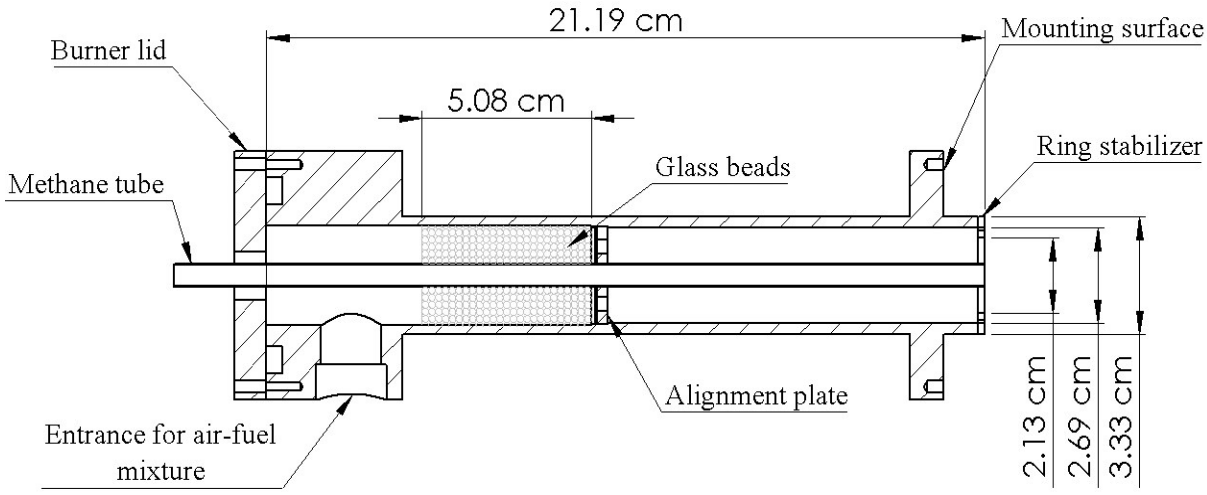

Figure 2-2 – Burner drawing - All dimensions in mm

A ring is used to stabilize the flame, the recirculation of the flow behind the ring helps the flame to be stable by providing a fixed ignition site [41]. This ring has a clearance between itself and the burner's inner diameter. This clearance affects the emission levels, as this clearance increases there will be more unburned hydrocarbon and CO [42]. This ring has an outside diameter of 2.7 cm and located at the center of the burner, which will provide a 0.16 cm clearance. The alignment plate keeps the methane tube centrally aligned, and a 15 x 15 mesh screen was placed on top of the alignment plate to prevent 2 mm glass beads from falling out.

Figure 2-3 is the 3D model of the burner with its mounting face, the inlet port for the premixed fuel and air, and the lid. Figure 2-4 shows end views of the ring stabilizer and mounting planes to show how the ring is mounted to the burner with the three screws. Figure 2-5 shows an actual image of the burner with the flame.

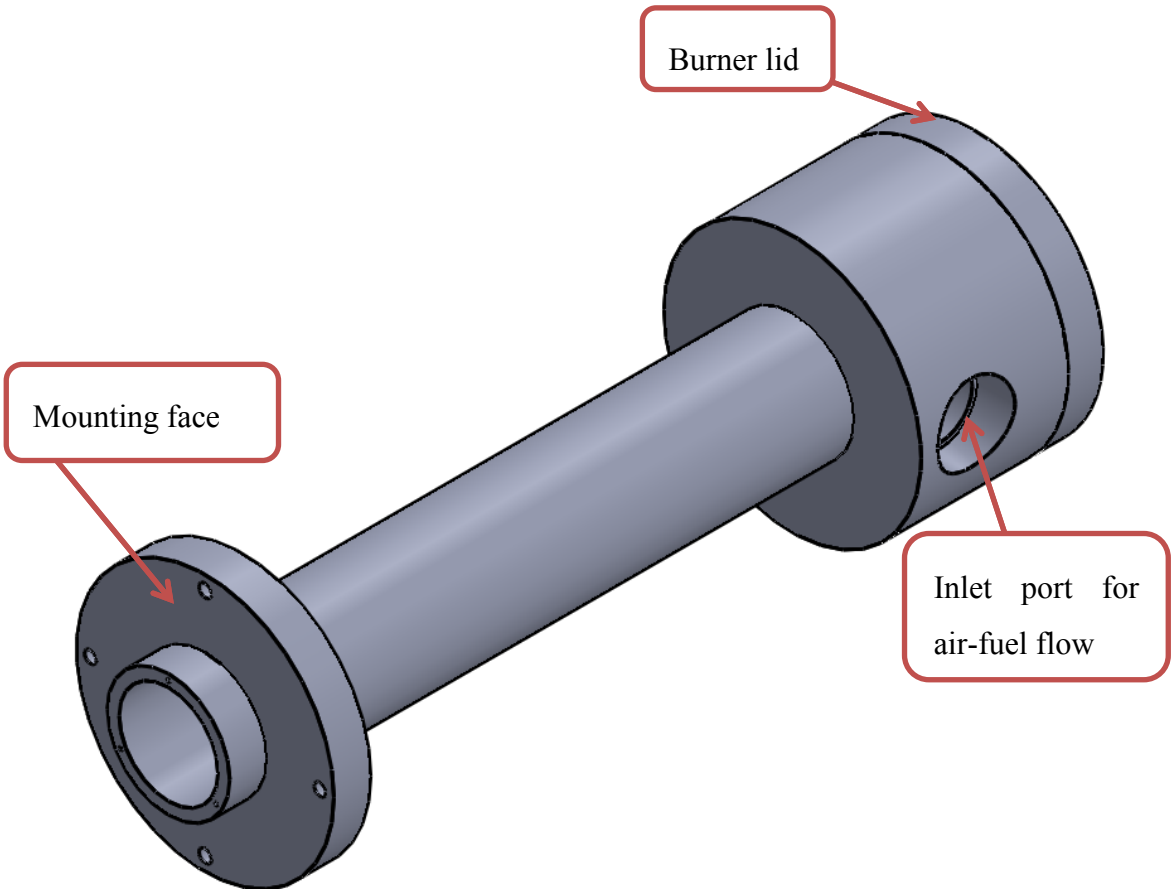

Figure 2-3 – Burner 3D model

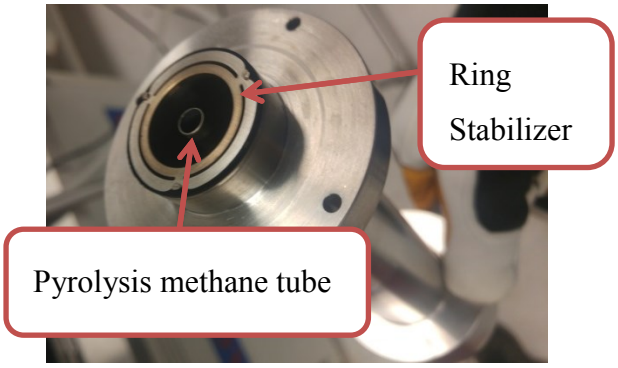

Figure 2-4 – Actual image of the ring stabilizer, also shows the tube in the center of burner that will supply the methane for pyrolysis

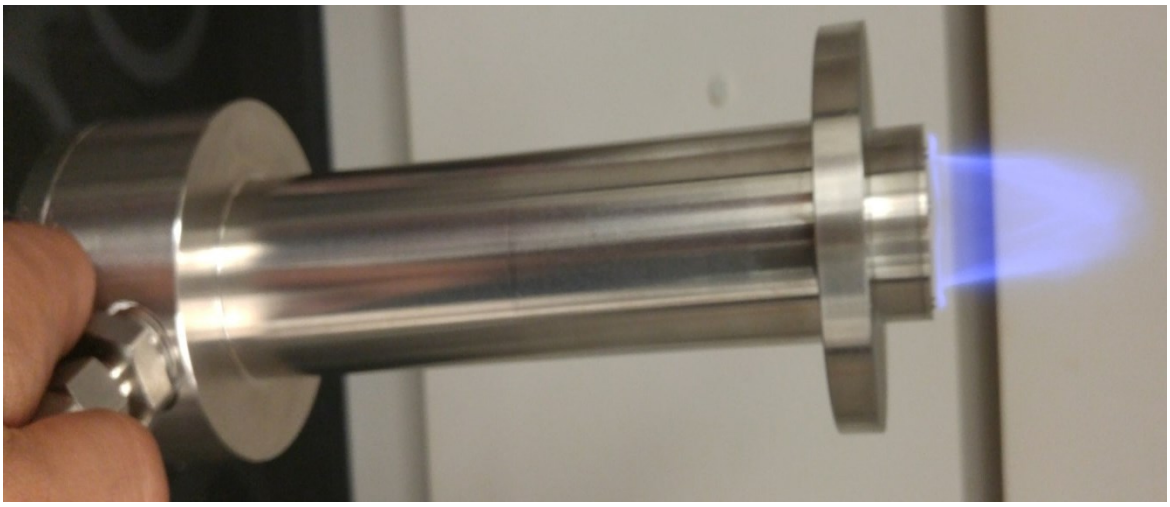

Figure 2-5 - Actual burner with the flame

Air and fuel for the premixed flame, are metered separately and mixed in a static mixer, and then enter the side of the burner through a 1.27 cm NPT fitting. According to the flow rates for this set-up, a 6 blades static mixer was used. Figure 2-6 shows a small screen mesh was added to the Swagelok fitting attached to the burner to stop glass beads from going into the static mixer when held in the upright orientation.

Figure 2-6 - Mesh screen on the Swagelok

Methane for pyrolysis is introduced through a tube that is located in the middle of the burner, which is aligned at the center of the burner using an alignment plate in the middle of the burner. The methane tube ends at the same plane as the burner surface but is adjustable. Different materials and diameters were examined for the methane tube during the experiment. Having the methane tube in direct contact with the flame causes the flame to flashback. When the methane tube is sticking outside of the burner as shown in Figure 2-7 (b) and Figure 2-8 (b) the temperature on the tube will increase and depending on the tube material after a certain time the heat will be conducted along the tube and eventually will cause the flame to move upward inside the burner. Tubes with 0.635 cm diameter and different materials were examined to investigate the stability of the flame. Copper, stainless steel, and ceramic tubes were tested for the methane flow. The critical parameter in this experiment was the thermal conductivity coefficient. The results showed that flashback of the flame happens after a longer time when using a copper tube. For copper tubing 3 different diameters were tested, 0.3175, 0.635 and 1.27 cm; increasing the diameter would lead to a longer time before flashback but since the tube was placed inside the burner it would take a bigger area inside the burner and cause the air-fuel flow to become non-laminar. Having the methane tube sticking out of the burner would cause flashback with any material or diameter.

As shown in Figure 2-7 (a) and Figure 2-8 (a) when the methane tube is placed at the same plane at the burner surface the flame is stable. A 0.635 cm diameter copper tube was used for the pyrolysis methane flow.

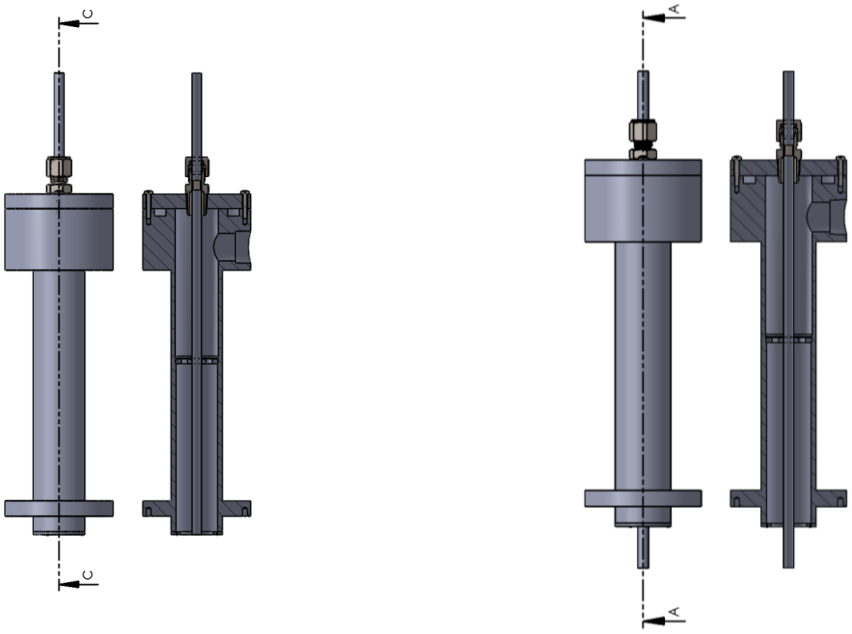

(a) (b)

Figure 2-7 - Methane tube position - drawings

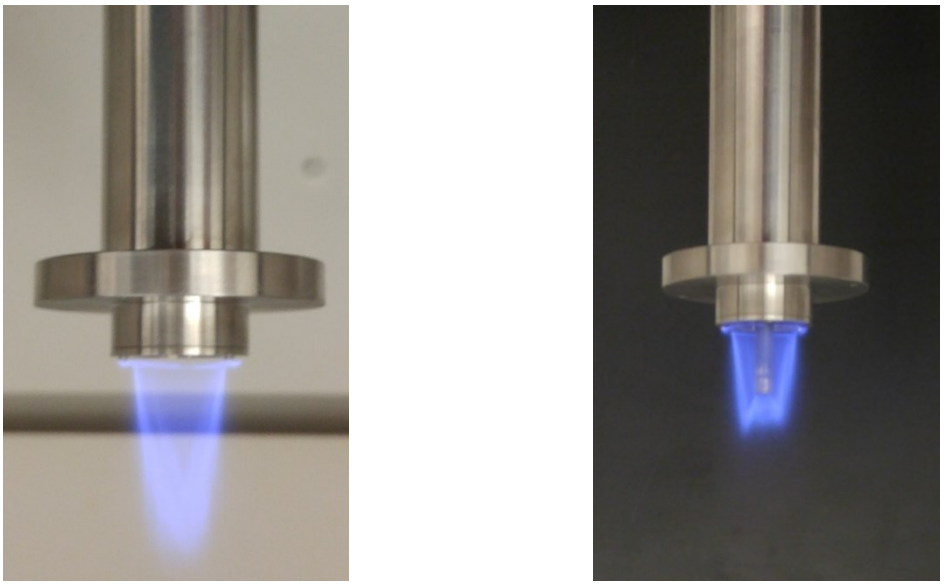

(a) (b)

Figure 2-8 - Methane tube position - experiment

(a) The flame is stable when pyrolysis tube sits at burner outlet surface. (b) When pyrolysis tube sticks outside flashback happens.

2.3 Reactor Chamber and End Fittings

A quartz reactor chamber was chosen so that the flame can be seen at all time, and to help visualize some of the reactions. It also turned out to be important in observing flashback events so that the fuel and methane flow could be turned off immediately. Figure 2-8 shows the quartz which is 68 cm long with OD of 20.6 cm and ID of 20 cm. As it is shown in Figure 2-9 the quartz tube was then closed at both ends with two stainless steel endplates. These stainless steel fittings were designed to close the quartz cylinder and seal it by means of high-temperature silicone O-rings. The materials used for the O-rings was not handle the high temperatures and needed to be replaced occasionally. The top cap drawing can be seen in Appendix A. The burner sits on the top stainless steel fitting and is sealed by a silicon O-ring. Two pins were used to adjust the burner onto the top fitting and then two 3 mm screws, sitting 90 degrees apart from the pins are used to tighten the burner into the steel fitting and seal it.

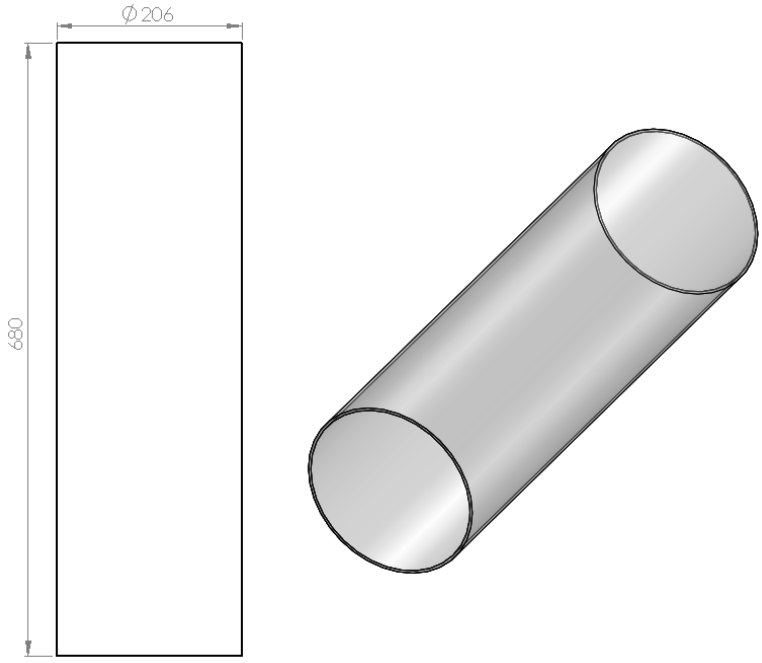

Figure 2-8 - Glass quartz drawing - all dimensions in mm

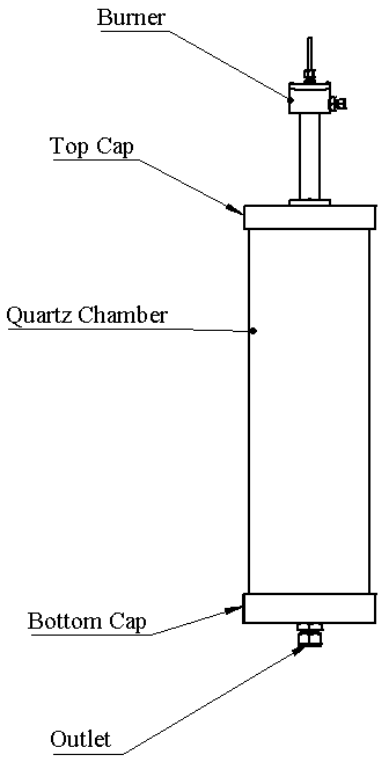

Figure 2-9 – Assembly of burner, quartz chamber, and end caps

The bottom steel fitting can be seen in Appendix A, has a 2.5 cm hole in the middle, which sends the exhaust from the quartz chamber to the fume hood through a 2.5 cm tube. As shown in Figure 2-10 (b) the 2.5 cm exhaust tube goes to a T-port 3-way ball valve. The valve outlet is attached to a filter holder from one side to collect carbon particles and it is attached to a 2.5 cm stainless steel tube from the other side that goes into the fume hood. This tube goes through a container before going to the fume hood. The container is for collecting the condensing water in the products. The container has a 2.5 cm cap at the bottom that can be used to empty it out after it fills with water. A tube from other side of the container goes into the fume hood and sends exhaust into the fume hood.

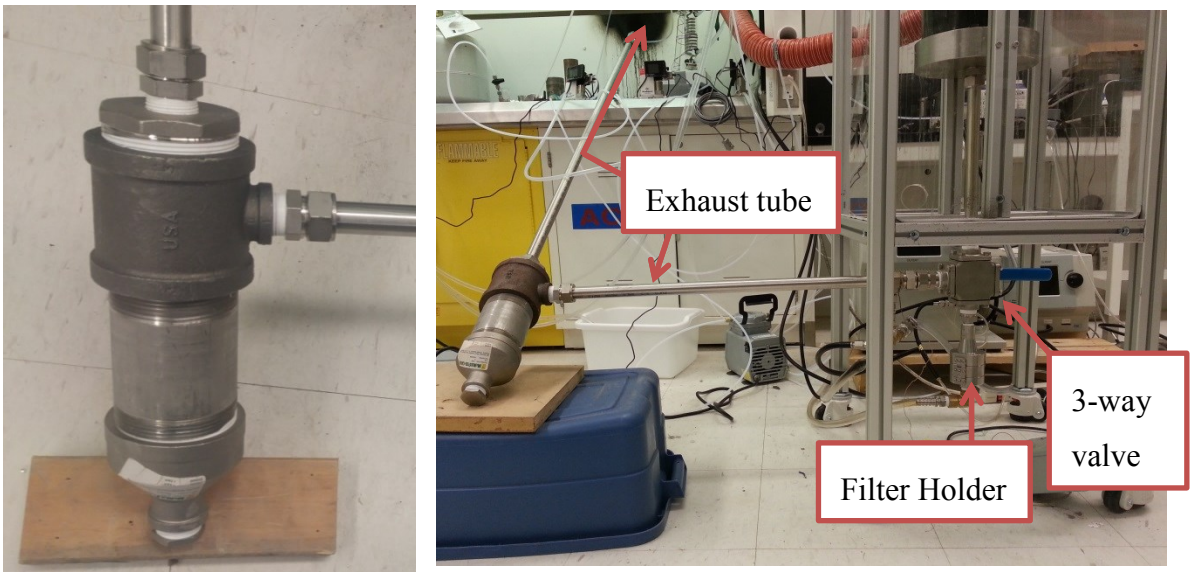

(a) (b)

Figure 2-10 - (a) water container (b) exhaust tube

2.4 Insulation blocks

The quartz chamber could be filled with cylindrical insulation blocks in order to provide a smaller volume (shorter residence time) of high temperature inside the chamber. These blocks were made of alumina silicate ceramic. The maximum working temperature of these blocks is 1098°C, with low linear thermal expansion and thermal conductivity of less than 1 $\frac{W}{m \cdot K}$ [43]. Thirteen blocks with the thickness of 5.08 cm and one block with the thickness of 1.905 cm filled the 68 cm quartz chamber. The outside diameter of blocks is 19.3 cm that gives 0.7 cm clearance between each block and the quartz chamber. There is a 4 cm hole in the middle of all blocks made by a waterjet cutter that provides a small reaction volume with a higher temperature.

Figure 2-11 shows some modifications were made to a few blocks. The top 4 blocks, the thin one, and three thick ones had a 0.5 cm slit cut, so when running the experiment

the flame can be seen through these slits and if any flashbacks happens the flows could be shut off immediately. A pick-up tool was designed to load the insulation blocks into the reaction chamber, details of this tool can be found in Appendix C. Due the high uncertainties of the effects on the temperature after adding insulation blocks a model was simulated using COMSOL to study the effects of insulation blocks on temperature distribution. Details of this simulation are shown in Appendix D. The models proved that insulation blocks are needed to reach the needed temperature for pyrolysis reaction.

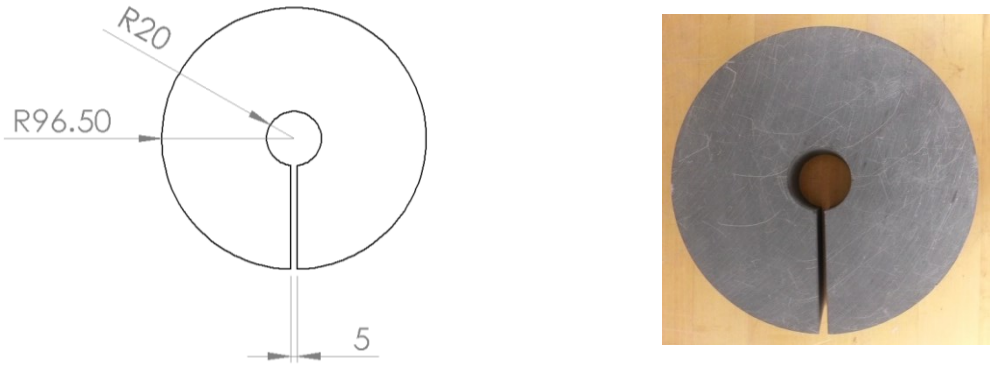

Figure 2-11 - Insulation block with a slit - all dimension in mm

2.5 Sampling line

The reactor products were extracted by a sample line from the 2.5 cm exhaust tube inside the fume hood. Figure 2-12 shows a 0.3175 cm tube goes into a heat exchanger. This heat exchanger consists of a glass coil that the sample goes through and a container at the bottom of the coil to collect the condensed water. The heat exchanger is cooled by a recirculating chiller with Cooling Capacity of 500 watts (Cole Parmer model # RK-13042-21). This chiller has force/suction pump that circulates cool water at 5 °C around the coil and condenses the water in the sample so the mole fraction of water would be 0.9%. This relative dry sample goes into a 0.3175 cm tube and through an inline filter. This line goes into a diaphragm pump, which sends the sample to a gas chromatography (GC) analyzer. At the outlet of the gas analyzer the flow can be controlled by a needle

valve, the needle valve helps to adjust the approximate flow rate needed for sampling; The outlet line which is a 0.625 cm tube goes back into the fume hood.

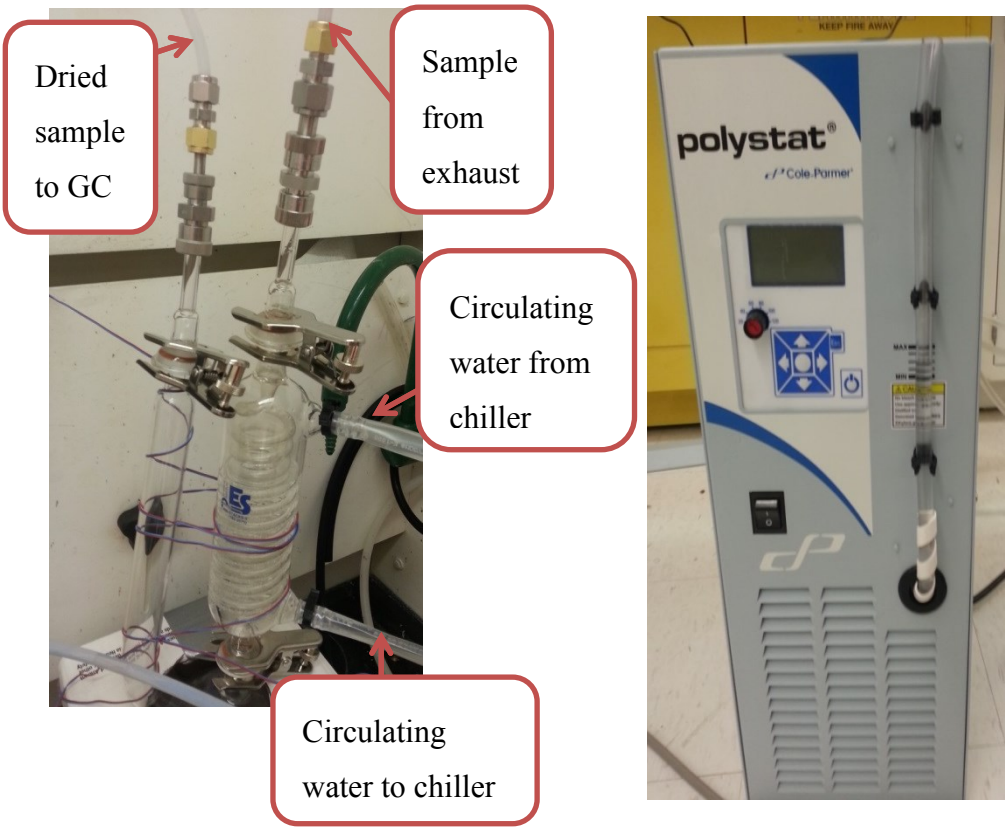

(a) (b)

Figure 2-12 - (a) heat exchanger (b) Chiller

2.6 Frame for Support and Confinement

The quartz chamber and the burner were held inside a metal frame with polycarbonate faces. This frame keeps the quartz chamber in position, additionally; any leakage from the reactor will be confined inside the frame and sucked out by a vacuum pump. This pump with an airflow capacity of 3000 slpm is connected to a duct hose with OD of 7.62 cm and goes to the fume hood. As shown in Figure 2-13 there is a 7.50 cm hole on the side of the frame with a steel flange that holds one side of the duct hose inside the frame and the other side is attached to the inlet of the pump. The frame components are 40x40 mm aluminum rails. Four-millimeter thick polycarbonate plates are installed on the sides of the frame with a rubber seal. As shown in Figure 2-14 the quartz chamber

hangs in the middle of the frame and is supported by two columns. These two columns are attached to two other columns at the bottom of the frame in order to carry the weight of reactor and insulation blocks. The frame sits on 4 castors that make it easy to move the whole set-up and they can be locked to keep the frame in the place.

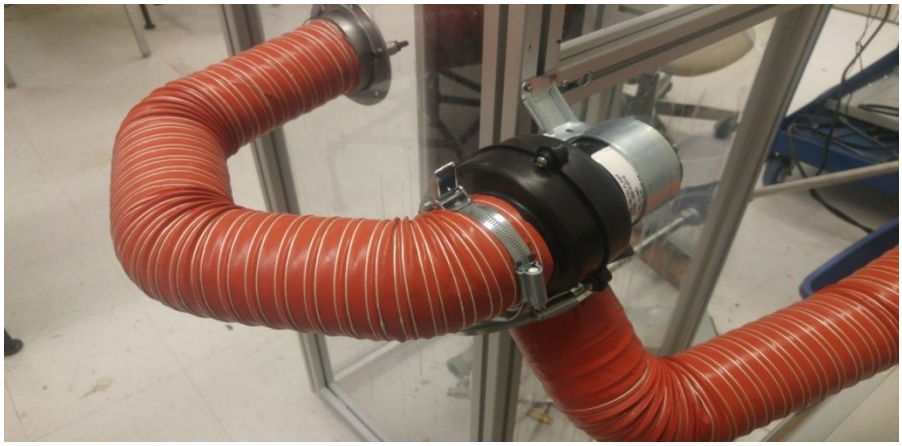

Figure 2-13 - Actual image of the vacuum pump and duct hose

(a) (b)

Figure 2-14 -(a) Frame 3D model (b) Frame 3D model with the setup

2.7 Gases for premixed flame and methane for pyrolysis

In this experiment, two premixed laminar flames were used for the pyrolysis of methane. In the first case, commercial grade compressed propane (99.5% pure) was used as the fuel for the premixed flame. In the second case, bottled methane (99.97% pure) was used as fuel for the premixed flame, and this bottle was always used to provide the methane flow for pyrolysis. The mass flow controller for fuel has the range of 0 to 5 l_n/min (Bronkhorst EL-FLOW Prestige Mass Flow Controller) and the one for methane has the range of 0 to 15.25 l_n/min (Bronkhorst EL-FLOW Prestige Mass Flow Controller). Filtered building air was passed through a flow controller calibrated for air for flow ranges of 2 to 100 l_n/min (Bronkhorst EL-FLOW Prestige Mass Flow Controller). Inline filters were used for both propane and methane bottle before the MFCs to protect them. The mass flow rates reported in this study were all in normal conditions which were temperature of 0 °C and pressure of 101325 Pa.

2.8 Igniting the flame

The airflow rate was set to 35 l_n/min for propane flame and 34.8 l_n/min for methane flame; for the fuel mass flow controller flow rate was set to 1.430 l_n/min with the propane flame and 1.62 l_n/min with methane flame (the calculation is shown in Appendix B). Then, the burner was ignited inside the fume hood by a hand held butane lighter; after having a stable premixed flame the burner was fitted above the quartz chamber with the two alignment pins to guide the burner into place. The burner was tightened in place with two 3 mm bolts. The flame could be seen through the quartz, or through the slits made on top four blocks when the insulation was used. An oxygen sensor (Innovate motorsport LM-1) was used to fine tune to a slightly rich flow rate of fuel for the premixed flame. The oxygen sensor shows air-fuel equivalence ratio (λ), when inside the products of a flame; which can be defined as;

$$Air - fuel\ equivalence\ ratio\ = \lambda = \frac{(\frac{n_{air}}{n_{fuel}})_{actual}}{(\frac{n_{air}}{n_{fuel}})_{stochiometric}} \qquad 2\text{-}1$$

$$Fuel - air\ equivalence\ ratio\ =\ \varphi = \frac{1}{\lambda} \qquad 2\text{-}2$$

By holding the oxygen sensor at the outlet of the exhaust tube air-fuel equivalence ratio can be read, then the propane flow rate can be manipulated until the stoichiometric flow rate is found (λ=φ=1). Since the flame needs to be slightly rich, with the propane flame experiment air flow was set to 35 l_n/min and propane to 1.43 l_n/min and with the methane flame experiment air was set to 34.8 l_n/min and methane was set to 1.62 l_n/min, in both cases air-fuel equivalence ration (λ) would be 0.95 (or φ = 1.05) and the total flow rate of air and fuel would be the same. After finding the right flow rate for propane and methane set-up needs to reach its steady state. This can be done by observing the temperature at the exit of the reactor and letting this temperature reach a maximum stable number and then start sampling the exhaust. A fast response K type thermocouple was attached to the exhaust tube right after it leaves the quartz chamber; the steady state temperature of this point is 150°C, so after getting to this temperature sampling can be done. Figure 2-15 shows two typical flames produced by this setup. The image on the left is at the beginning of the experiment when there was not a significant collection of carbon particles stuck to the quartz wall, and the image on the right is after carbon particles are collected on the quartz wall.

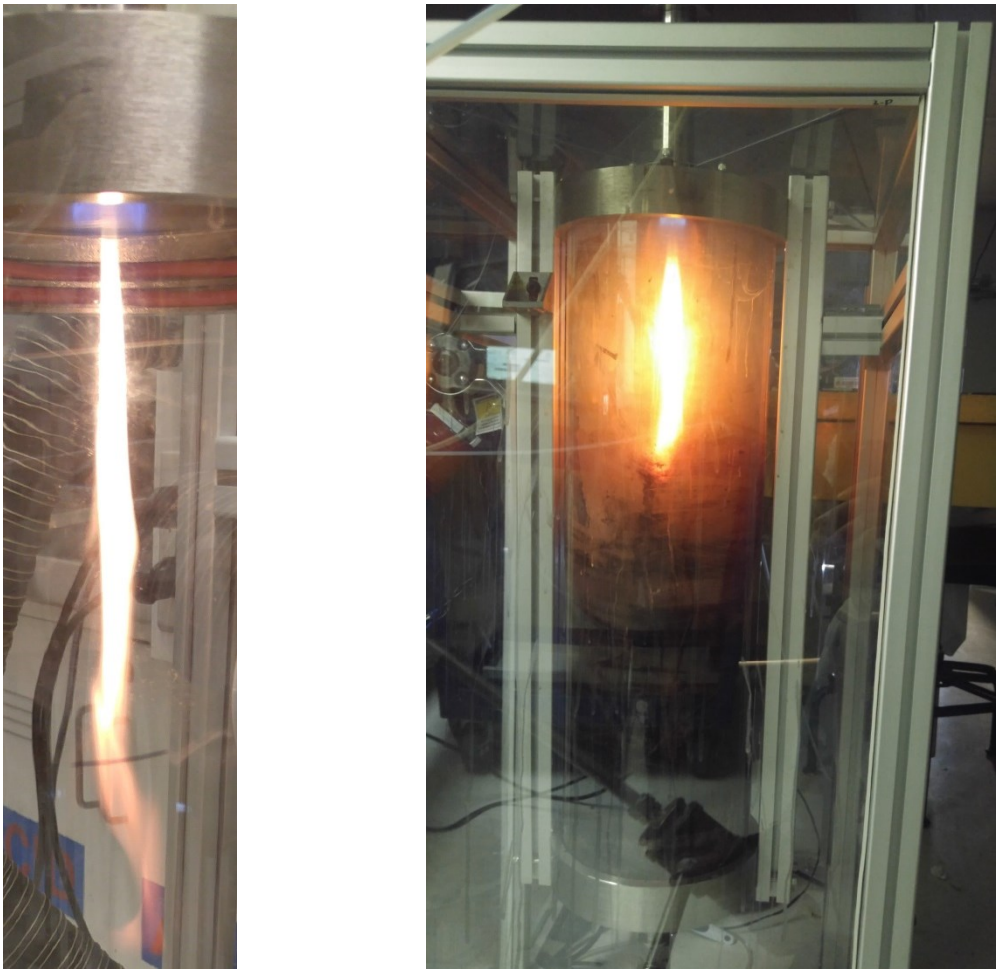

Figure 2-15- The propane flame and methane pyrolysis with the pyrolysis methane flow rate of 0.5 l_n/min

2.9 Gas Phase Measurements of Products

A gas chromatograph (GC) analyzer (Agilent 7890B), shown in Figure 2-16, was used to measure the concentration of many of the gas-phase components in the exhaust. The GC has 3 channels, the first channel works with Argon as the carrier gas using a thermal conductivity detector (TCD) for measuring hydrogen and helium. The second channel uses hydrogen as the carrier gas with TCD detection to measure oxygen, nitrogen, CO, and CO_2. The third channel is a flame ionization detector (FID) with hydrogen as the carrier gas, which is used to measure all hydrocarbons. Table 2-1 shows a list of all the columns that are used in the GC. Columns are used to separate the components in the sample in time and send them to the detectors to be examined. The

component can be separated based on solubility, volatility, polarity, specific chemical interaction or other properties.

Table 2-1- Details of the columns used in GC

Column number	Length (m)	Diameter (mm)	Model number
1	60	0.25	CP8780
2	0.5	2	G3591-81023
3	1.83	2	G3591-81037
4	2.44	2	G3591-80022
5	0.91	2	G3591-81135
6	1.83	2	G3591-81035

FID channel uses hydrogen as the carrier gas, nitrogen as the make-up gas and air. In this channel sample with carrier gas are passed through a hydrogen-air flame, burning of an organic component creates ions; these ions will be collected and produce a current that can be used to find the concentration of hydrocarbons. Detector temperature is set at 250 °C, hydrogen flow rate is 40 mL/min, air is 400 mL/min and nitrogen is 25 mL/min.

TCD channel has a filament and thermal conductivity of two flows are compared to find the concentration of a component, first a flow of pure carrier gas passes over the filament and then a flow will be switched to a flow of carrier gas plus sample; the power that holds the filament temperature constant in these two cases will be used to measure the concentration of each component in the sample. An auxiliary TCD channel uses argon as the carrier gas because the channel is used to measure hydrogen concentration in the sample. Detector temperature is set at 200 °C for both TCD channels and the pure carrier gas flow rate is 45 mL/min.

Figure 2-16 - Agilent 7890B GC [44]

ChemStation software was used to define a calibration table and process the results from GC. Eight calibration bottles from Praxair Inc. were used to calibrate the GC for the gases in the exhaust. Table 2-2 shows the ranges of the gases in all of these standards. The uncertainty on all the concentrations reported in the table is ±2% of the reported number according to manufacturer report.

Table 2-2- Concentration in % for all component in the standards

Standard #	H_2	CO	CO_2	O_2	CH_4	C_2H_6	C_3H_8	N_2
1	0.4018	19.95	-	-	0.1002	0.09975	0.09937	79.449
2	-	0.01	-	0.1005	-	-	-	99.889
3	4.005	-	-	-	0.9947	1.013	1.008	92.979
4	19.93	-	-	-	4.971	4.994	5.07	65.035
5	-	0.0998	5.01	1.01	-	-	-	93.88
6	-	3.005	19.95	19.99	-	-	-	57.055
7	-	0.6016	10.01	3.992	-	-	-	85.396
8	0.04	9.983	-	-	0.0105	0.0107	0.0102	89.946

GCs identify the various gases in the mixture by the retention time. Calibration curves can be defined based on peaks available for a particular gas. For example, Figure 2-17 for CO_2 shows there are 3 peaks available from standards 5, 6 and 7. By adding these peaks into the calibration table a linear curve was defined. Each peak in the calibration table would represent a response factor based on its concentration in the standard and the area found by the GC. These standards were chosen with suitable ranges to cover the results of the experiment. Furthermore, by having this calibration table all the results would be valid and close (experimental uncertainty estimated later) to the actual amount.

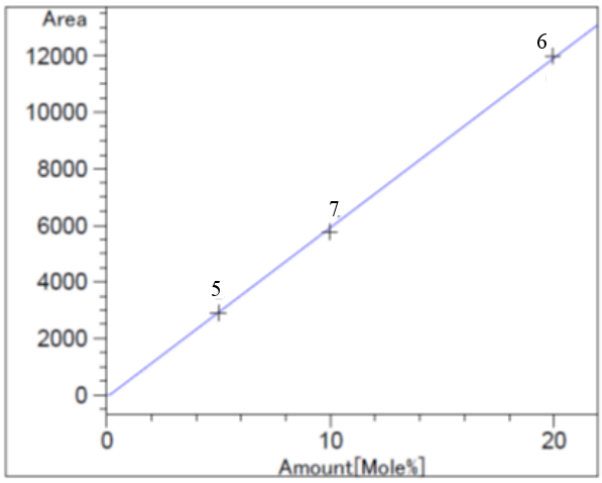

CO_2

Retention time = 1.794 s

TCD channel,

Calibration curve : y = mx +b

m = 600.40693

b = -81.82183

x = amount (mole %)

y = area (found by TCD channel)

(a) (b)

Figure 2-17 - Details of CO2 Calibration (a) curve (b) formula

2.10 Temperature Measurements

Temperature distribution was measured by a K-type thermocouple in two separate experiments. In the first experiment, the temperature distribution for various points inside the quartz chamber was measured before loading the insulation blocks in the chamber. A 1.27 cm NPT hole on the top steel fitting was used to reach inside the quartz tube. The thermocouple is covered by a metal sheath with the outside diameter of 0.16 cm and has an exposed junction. The thermocouple was passed through a support tube with an OD of 0.635 cm and ID of 0.21 cm, and then it was bent with the tube into an L-shape to allow it reach the centerline of the quartz tube. The thermocouple support tube was marked with 5 cm increments to measure *z* (axial) component of thermocouple junction's position. The support tube was also fitted with an indicator and a protractor, shown in Figure 2-18; to measure the angle of thermocouple junction's position. With the help of the setup shown in Figure 2-19, the temperature for a specified *r* (radial) and *z* position inside the chamber could be measured.

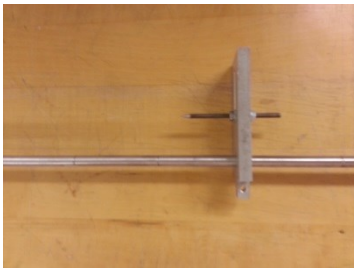

(a)

(b)

Figure 2-18 - Temperature measurement tools (a) depth indicator (b) protractor

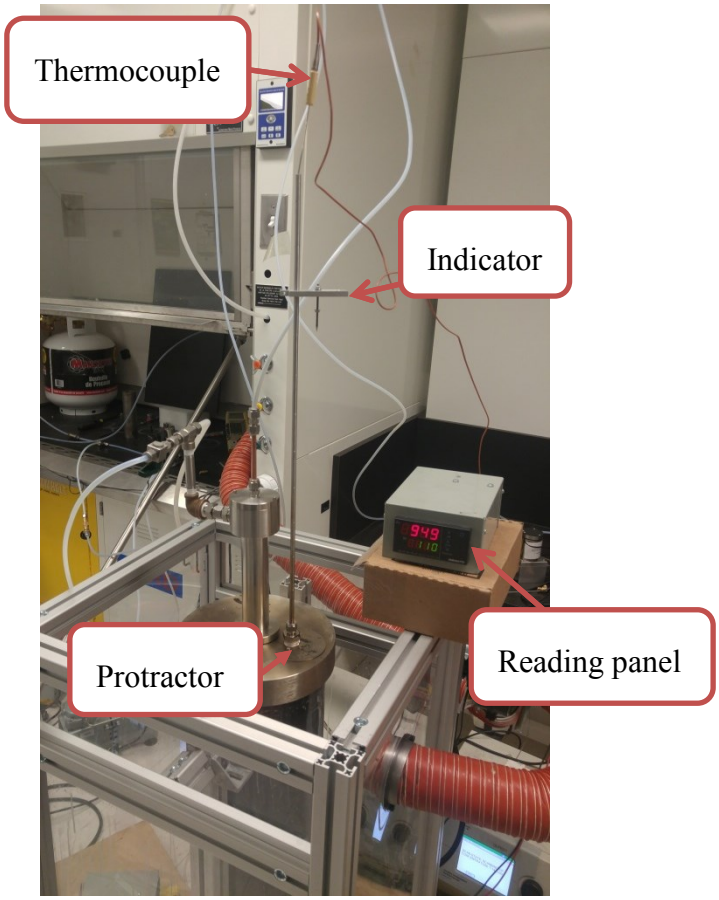

Figure 2-19- Temperature measurement experiment

In a second experiment, the temperature distribution was measured when the quartz chamber was filled with insulation blocks. In this case, the thermocouple was passed through the middle tube that was used for pyrolysis methane. As result, the temperature was only measured for the flame (both propane and methane) with no pyrolysis reaction.

The temperature distribution for the centerline was measured at different heights. Figure 2-20 (a) shows the temperature measurement along the centerline and Figure 2-20 (b) shows the tip of the thermocouple inside the quartz chamber during the measurements.

(a) (b)

Figure 2-20 -(a) centerline temperature measurements experiment (b) thermocouple inside the flame

2.11 CO Detectors

Due to high concentrations of CO produced in the pyrolysis of methane by a premixed flame, CO detectors (ToxiRAE 3 model by Honeywell), Figure 2-21 were used with every experiment. These detectors are capable of measuring CO presence in the environment with the resolution of 1 ppm with a range of 0 to 1999 ppm. Response time is less than 12 seconds. The alarm is set on 25 ppm that means if the concentration of CO in the lab environment reaches 25 ppm the detector will start beeping. These detectors were on and carried by every person who works in the lab while the experiment was running.

Figure 2-21 - CO detector

CHAPTER 3. METHANE PYROLYSIS IN A PREMIXED FLAME

3.1 Introduction

In the first set of experiments methane pyrolysis in the products of a premixed propane/air flame was investigated. In these experiments, the flame was turned on with flow rates given in Chapter 2 to have a slightly fuel-rich propane flame (φ = 1.05). Different flow rates of methane were introduced into the flame and the GC measured the concentrations of the gas-phase components in the products. A second set of experiments was conducted with a premixed methane/air flame. Identical experiments were conducted over 5 days and the scatter in data was taken as a measure of uncertainty for each result. Methane conversion into hydrogen was calculated based on the results from the GC; also a carbon balance was done considering the results of components with C from GC (thereby trying to estimate of the amount of carbon to form black carbon particles). Temperature measurements are also reported.

3.2 Experiments conducted

For each of the rich premixed flames different flow rates of methane were introduced. The flow rates consider for pyrolysis methane in these experiments were 0, 0.5, 1, 1.5, 2 and 5 l_n/min. In the first experiment, only the post-flame gases were sampled (methane = 0 l_n/min), then methane flow rate was increased to the various amounts, and each case was sampled with GC. These different experiments were repeated for 5 days to find uncertainty in the measurements. For the methane flow rate of 1 l_n/min, the test was done 5 times each day while for all other flow rates just one sample was taken per day.

3.3 Temperature measurements

As it is explained in Chapter 2, temperature for different points inside the quartz chamber was measured for two cases. The first one was 3D measurements with no insulation and for a propane flame with pyrolysis methane flow rate of 0 and 0.5 l_n/min. The results of these experiments are shown in Figure 3-1.

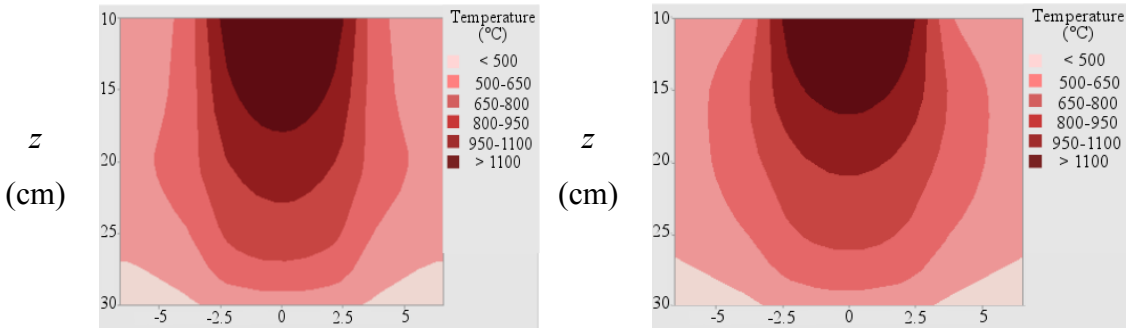

r - Radius measured from center line of the quartz tube (cm)

(a)

r - Radius measured from center line of the quartz tube (cm)

(b)

Figure 3-1- Temperature distribution inside the quartz tube around the propane flame (*z*=0 and *r*=0 shows the tip of the burner) for (a) no pyrolysis methane flow, and (b) with pyrolysis methane flow rate of 0.5 l_n/min

It can be seen from temperature diagrams in Figure 3-1 that in each case only a small region around the flame has temperatures over 1000 (°C). For a couple of centimeters radially or axially away from the flame, the temperature would not be expected to be high enough for the pyrolysis of methane. Also after introducing methane in Figure 3-1 (b) the region with the highest temperature gets smaller. Insulation was added to inside the quartz tube to lessen heat loss to the environment.

In the second experiment, after adding insulation blocks, temperature was measured for just the centerline of the propane and methane flame with no pyrolysis methane flow rate. The same steady state as gas sampling was considered before reading temperature,

i.e. the temperature at the exhaust tube right after it leaves the quartz chamber had reached 150 °C and then temperature measurements inside the quartz chamber were done for the center line. In this experiment z represent the distance from the burner surface on the centerline; so $z = 0$ means thermocouple sits at the burner surface and then it was moved downward for various heights and temperature was recorded. Results can be seen in Figure 3-2. When there is no pyrolysis methane flow rate by adding insulation blocks temperature gradient gets smaller and higher temperatures are recorded for similar points compared to the experiments with no insulation blocks.

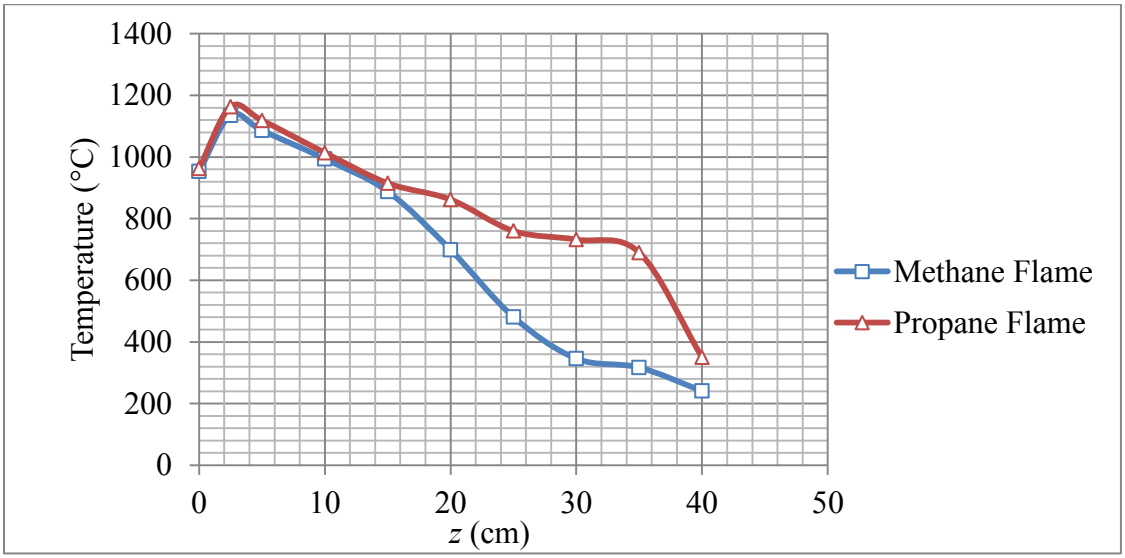

Figure 3-2- Temperature distribution for the center line with methane and propane flame - with insulation blocks

3.4 Gas Chromatography results

Table 3-1 shows the calibration table for the GC with the specific retention times that represent a certain compound. Based on the actual mole percentage of each compound in each calibration standard (Table 2-1) and the area found by the GC, a response factor is obtained, and the mole percentage of each compound can be estimated based on this response factor and area found by GC in the actual experiment. Two standards were checked prior to each sampling to make sure that there was no drift in the calibration table. The results from one of these drift-checks for standards number 3 and 7 are shown

in Table 3-2. As it can be seen, the results captured from GC for standard 3 and 7 are close to the actual amounts, except oxygen, which is not reported for the experiment as it is not used in the H and C balances.

Table 3-1- Calibration table for GC

Compound	Retention Time (s)	Standard #	Amount [mole%]	Area	Response Factor
H_2	0.784	8	4.00000e-2	20.68922	1.93337e-3
		1	4.01800e-1	205.80989	1.95229e-3
		4	19.93000	1.02188e4	1.95033e-3
CO_2	1.840	5	5.01000	2906.58447	1.72367e-3
		7	10.01000	5777.69351	1.72785e-3
		6	19.95000	1.19685e4	1.66688e-3
O_2	2.884	2	1.01000	461.13037	2.19027e-3
		7	3.99200	1614.30603	2.47289e-3
N_2	3.148	6	57.05500	2.67775e4	2.13071e-3
		4	65.03500	3.08341e4	2.10919e-3
		1	79.44900	3.65881e4	2.17145e-3
		7	85.39600	3.93243e4	2.17158e-3
		8	89.94600	4.14921e4	2.16778e-3
		3	92.97900	4.28880e4	2.16795e-3

		5	93.88000	4.34027e4	2.16300e-3
CO	4.873	7	6.01600e-1	294.69719	2.04142e-3
		6	3.00500	1443.06067	2.08238e-3
		8	9.98300	4731.73730	2.10980e-3
		1	19.95000	9397.84375	2.12283e-3
CH_4	2.491	8	1.05000e-2	8.00218	1.31214e-3
		1	1.00200e-1	78.16411	1.28192e-3
		3	9.94700e-1	783.58661	1.26942e-3
		4	4.97100	3942.46769	1.26089e-3
C_2H_6	2.549	8	1.01300e-2	15.71374	6.44659e-4
		1	9.97500e-2	153.02618	6.51849e-4
		3	1.01300	1551.70453	6.52830e-4
		4	4.99400	7726.84701	6.46318e-4
C_3H_8	2.654	8	1.02200e-2	23.66238	4.31909e-4
		1	9.93700e-2	230.29179	4.31496e-4
		3	1.00800	2318.11035	4.34837e-4
		4	5.07000	1.16683e4	4.34511e-4

Table 3-2 - Results from GC for standards number 3 and 7 prior the sampling								
	H_2	CO	CO_2	O_2	CH_4	C_2H_6	C_3H_8	N_2
Standard 3 Measured %	4.0519	-	-	-	0.9955	1.0084	1.0090	92.935
Standard 3 Actual%	4.005	-	-	-	0.9947	1.013	1.008	92.979
% diff.	1.1%	-	-	-	0.08%	0.45%	0.1%	0.04%
Standard 7 Measured %	-	0.603	9.762	4.538859	-	-	-	85.096
Standard 7 Actual %	-	0.602	10.01	3.992	-	-	-	85.396
% diff	-	0.27 %	2.48 %	15%	-	-	-	0.35%

The sampling was done for 5 days in the row for each flame (propane and methane) to find the error bars on the results from GC. On each day, the flame was turned on and the burner was placed on the quartz chamber. The temperature of a certain point at the outlet (as shown in Figure 2-1) was measured for each test to ensure the system was stable before sampling. The first test was done for the flame itself with no methane introduced into the system. For sampling, the diaphragm pump was turned on for 2 minutes to make sure all valves inside the GC were filled with sample and then the pump was turned off for 1 minute so the pressure drops into atmospheric pressure inside the valves within the GC. After that, the test was started by hitting the start button on the GC. To analyze all components available in the exhaust, a total time of 7 minutes was needed

for each test. Within this range, all gases in the exhaust were found and the absolute mole percentage of each component was found based on the calibration table. The reported results from the GC are called external standard percentage (ESTD %), which represents the mole fraction of each compound as a percentage of all compounds. Since all the compounds from combustion and pyrolysis are assumed to be known and are identified by the GC, this number can be considered as the absolute mole percentage of each compound. The total mole percent of all compounds doesn't always add up to 100%; in this case, results can be normalized, but for finding the methane conversion into hydrogen efficiency absolute mole % are reported. After sampling the flame-only case, methane was introduced into the system with the flow rate of 0.5 l_n/min. After 5 minutes of stabilization the GC was used to measure exhaust composition. Then methane flow rate was then increased to 1 l_n/min. For this flow rate, the experiment was repeated 5 times on each day, which means there are 25 experiments in total for methane flow rate of 1 l_n/min; flow rates of 1.5, 2 and 5 l_n/min were sampled once each day and for 5 days.

By repeating the experiments for 5 days, the average result was reported for each scenario; furthermore, uncertainty in the mean of the measurements was calculated. The main components in the exhaust are H_2, CO, CO_2, CH_4, C_2H_6, C_3H_8, and N_2. Part of these results is needed to find methane destruction efficiency and methane conversion into hydrogen efficiency. Carbon balance was done using the results from GC by measuring the mass of the carbon in the hydrocarbons, CO and CO_2 and deducting this mass from the mass of the carbon in pyrolysis methane at the inlet, however the results showed very low conversion of methane into black carbon, and the uncertainty in the measurements can lead to unrealizable negative conversion. Oxygen concentrations measured by GC were not reported in this study due to issues with repeatability.

For each pyrolysis methane flow rate, results for a specific compound were measured for 5 days. To find the average concentration for each component the following equation was used:

$$x_{ave} = \frac{\sum_{i=1}^{N} x_i}{N} \tag{3-1}$$

where x_i is the concentration of component x at day i and N is total number of experiments, which is either 5 or 25 depending on the inlet methane flow rate.

Uncertainty in the mean of measurement can be found with the following equations:

$$P_x = t_{\frac{\alpha}{2},\upsilon} \frac{S_x}{\sqrt{N}} \tag{3-2}$$

where S_x is standard deviation of the results, P_x is the precision uncertainty which is the uncertainty in the mean of the measurements, values for t-distribution for desired confidence interval of 95% is dependent on υ and α. $\upsilon = N - 1$ and it is called number of degrees of freedom. α is dependent on the confidence interval, for confidence interval of 95%, α is 0.05. For 5 experiments $t_{0.025,4}$ would be 2.775 and for 25 experiments $t_{0.025,24}$ would be 2.064.

$$U_x = \sqrt{{P_x}^2 + {B_x}^2} \tag{3-3}$$

U_x is the total uncertainty in the mean. B_x is the bias uncertainty of GC which represents the accuracy of GC. Bias uncertainty can be found based on the calibration table of the GC, according to the calibration table shown in Table 3-1 and Figures 3-3 to 3-8. The largest offset on each compound can be used to find the accuracy of the GC for that compound. In this case, for each compound the area measured by GC is given in the table, the calibration curve formula also can be used to find the mole percentage for that compound. The difference between the calibrated amount and the actual amount shows the accuracy of device and can be used for bias uncertainty.

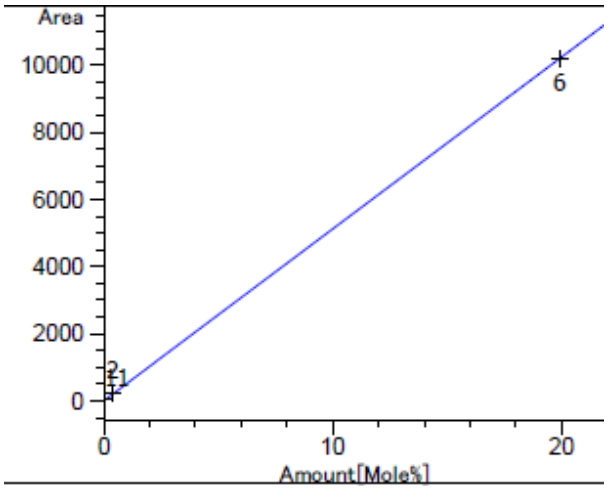

Hydrogen

Retention time = 0.784 s

TCD channel,

Calibration curve : y = mx +b

m = 512.71557

b = -0.0050297

x = amount (mole %)

y = area

Bias Uncertainty 0.001 mole %

Figure 3-3 - Calibration curve and formula - hydrogen

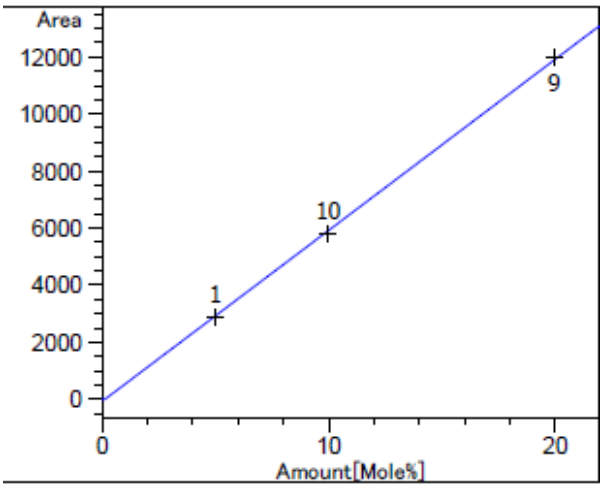

CO_2

Retention time = 1.794 s

TCD channel,

Calibration curve : y = mx +b

m = 600.40693

b = -81.82183

x = amount (mole %)

y = area (found by TCD channel)

Bias Uncertainty -0.03 mole%

Figure 3-4 - Calibration curve and formula - CO_2

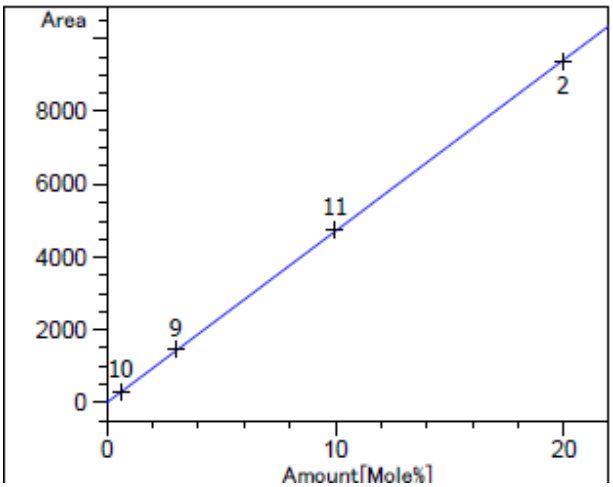

CO

Retention time = 5.133 s

TCD channel,

Calibration curve : y = mx +b

m = 471.81810

b = 0 (forced to origin)

x = amount (mole %)

y = area (found by TCD channel)

Bias Uncertainty -0.03 mole%

Figure 3-5 - Calibration curve and formula - CO

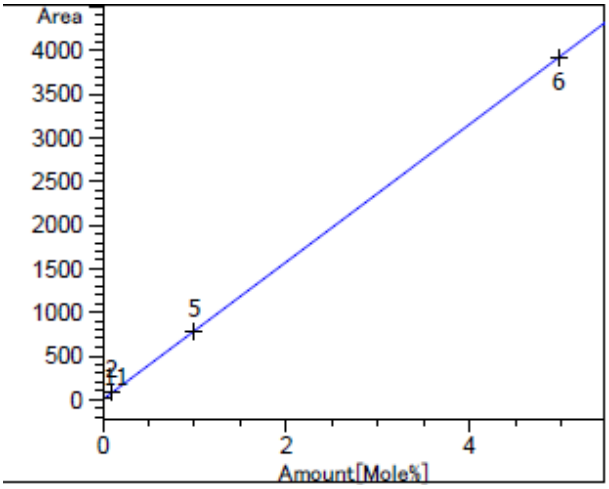

Methane

Retention time = 2.492 s

TCD channel,

Calibration curve : y = mx +b

m = 789.99637

b = -0.805708

x = amount (mole %)

y = area (found by TCD channel)

Bias Uncertainty 0.01 mole%

Figure 3-6 - Calibration curve and formula - Methane

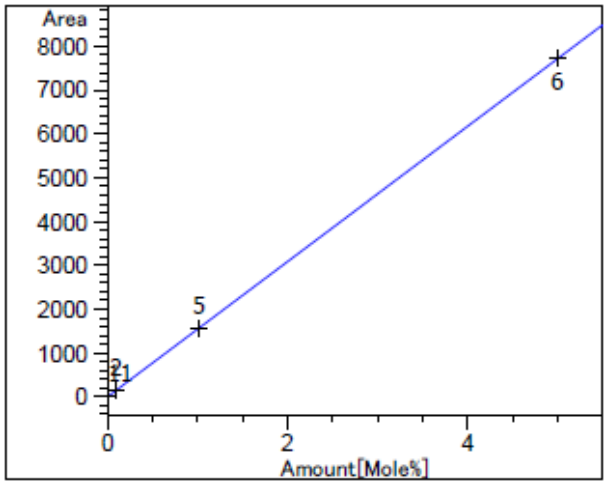

Ethane

Retention time = 2.492 s

TCD channel,

Calibration curve : y = mx +b

m = 1545.02700

b = -3.09766

x = amount (mole %)

y = area (found by TCD channel)

Bias Uncertainty 0.01 mole%

Figure 3-7- Calibration curve and formula - Ethane

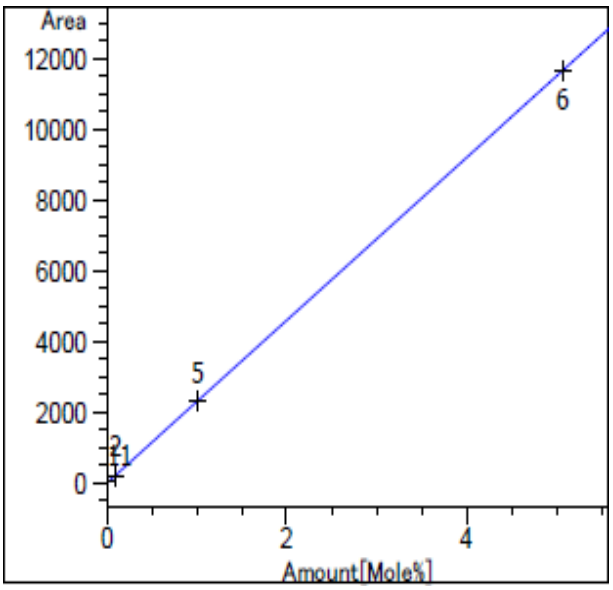

Propane

Retention time = 2.655 s

TCD channel,

Calibration curve : y = mx +b

m = 2302.68805

b = -0.219459

x = amount (mole %)

y = area (found by TCD channel)

Bias Uncertainty 0.001 mole%

Figure 3-8 - Calibration curve and formula - Propane

3.4.1 GC results for propane flame

The average and uncertainty in the mean of the 5-days measurements with propane flame can be found in Figure 3-9 and Figure 3-10. Raw data of these 5-days measurements are shown in Appendix E. The average and uncertainty in the mean numbers are shown in Appendix F.

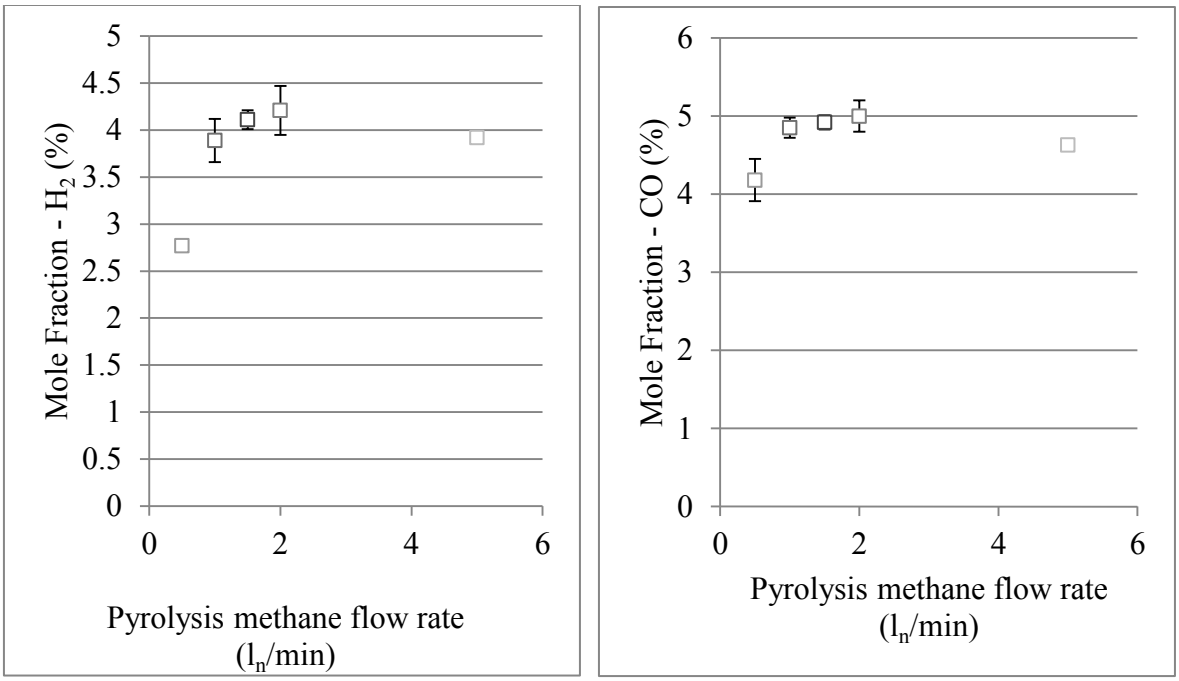

H_2 CO

Figure 3-9 - Average mole % based on pyrolysis methane flow rate for the propane flame - Some error bars are smaller than the marker size

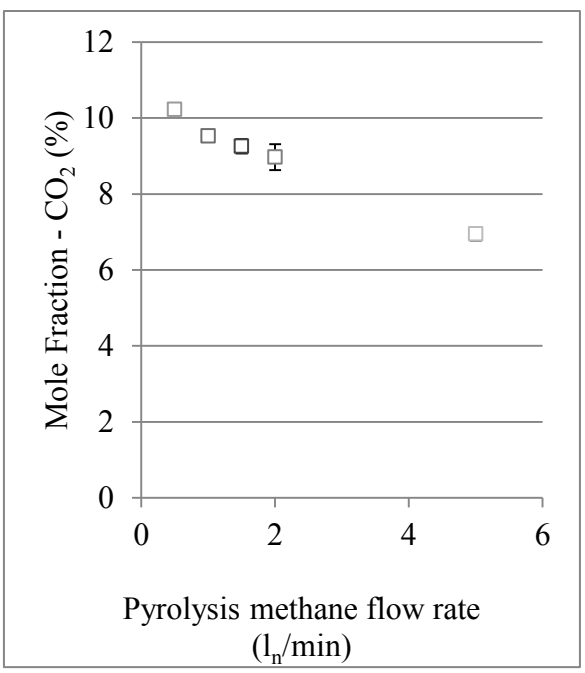

CO_2

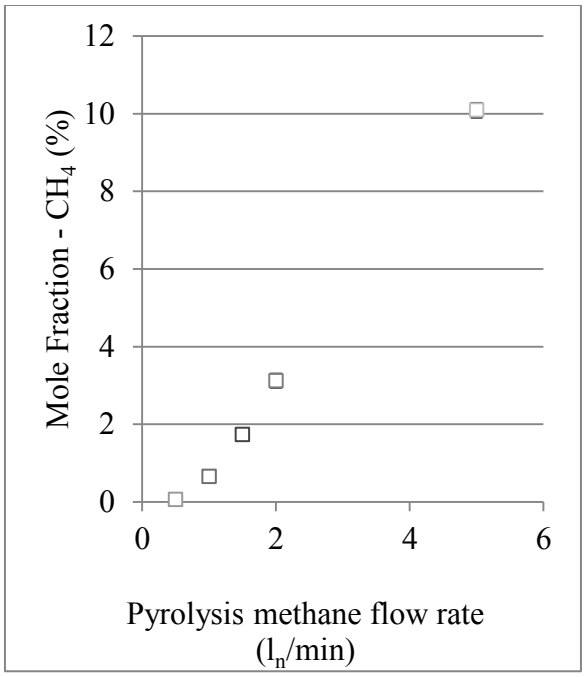

CH_4

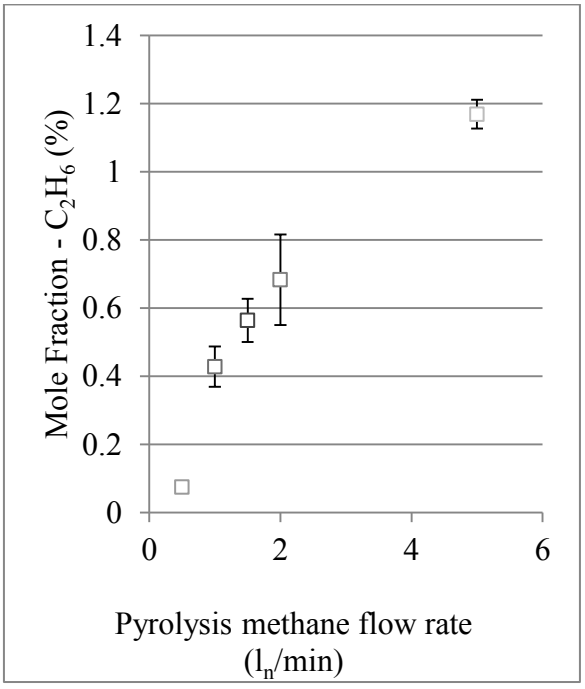

C_2H_6

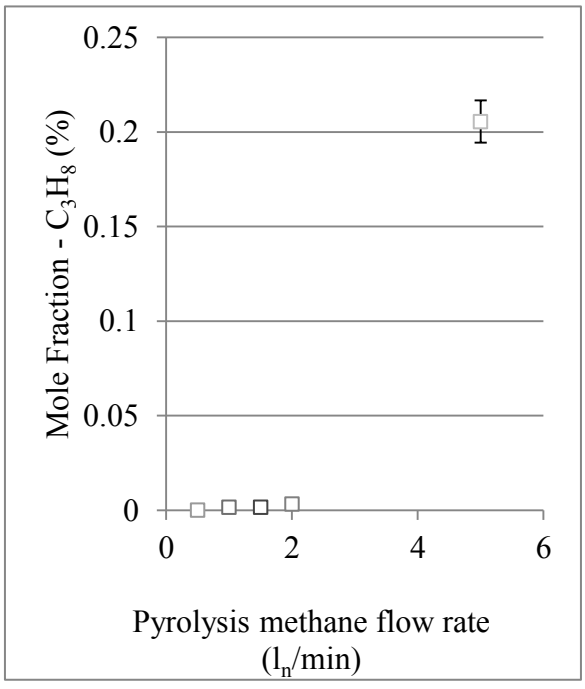

C_3H_8

Figure 3-10 - Average mole % based on pyrolysis methane flow rate for the propane flame - Some error bars are smaller than the marker size

3.4.2 GC results for methane flame

The same sets of experiments were done using a premixed methane flame. In this experiment, propane is replaced by methane and a premixed methane-air flow was burned. The total flow rate of this experiment was equal to the propane flame experiment. Air flow rate was equal to 34.8 l_n/min and methane as fuel has the flow rate of 1.62 l_n/min. Fuel-air equivalence ratio (φ) was 1.05 which is same as the propane flame experiment. The experiments were repeated for different pyrolysis methane flow rates from 0 to 5 and for 5 days. The average and uncertainty in the mean of the 5-day measurements with methane flame can be found in Figure 3-11 and Figure 3-12. Raw data of these 5-days measurements are shown in Appendix E. The average and uncertainty in the mean numbers are shown in Appendix F.

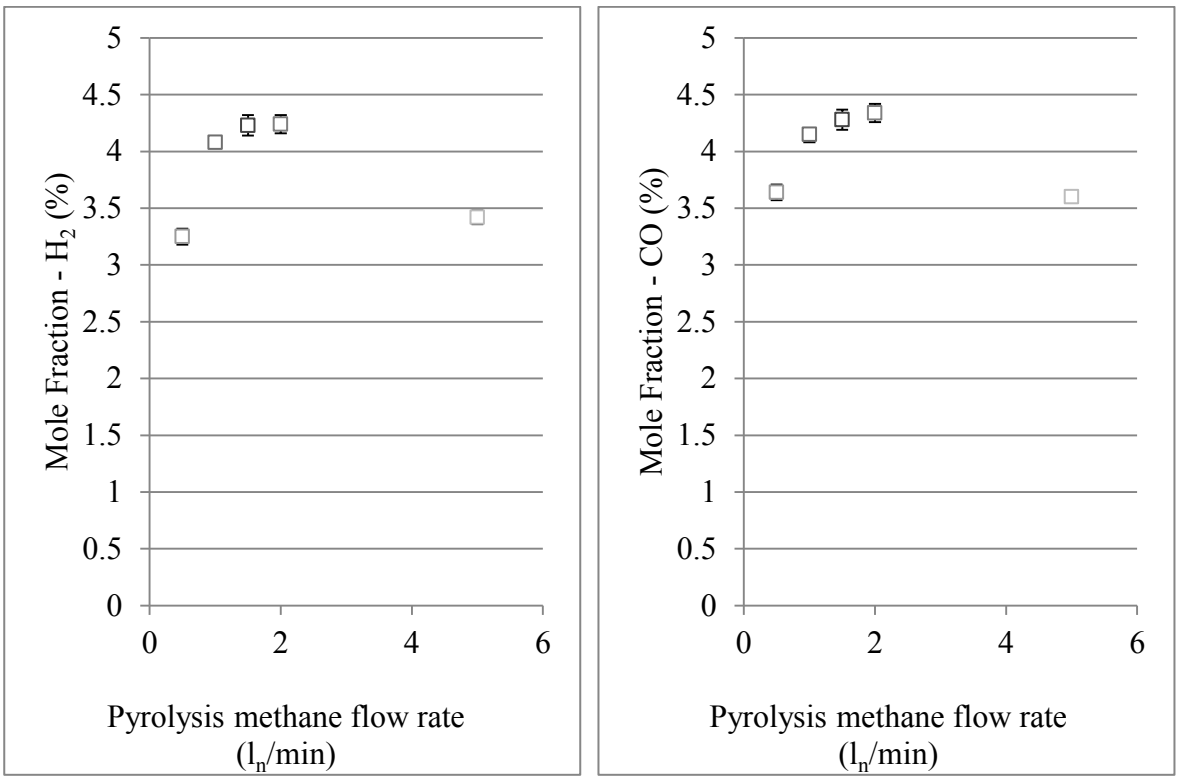

H_2 CO

Figure 3-11 - Average mole % based on pyrolysis methane flow rate for the methane flame - Some error bars are smaller than the marker size

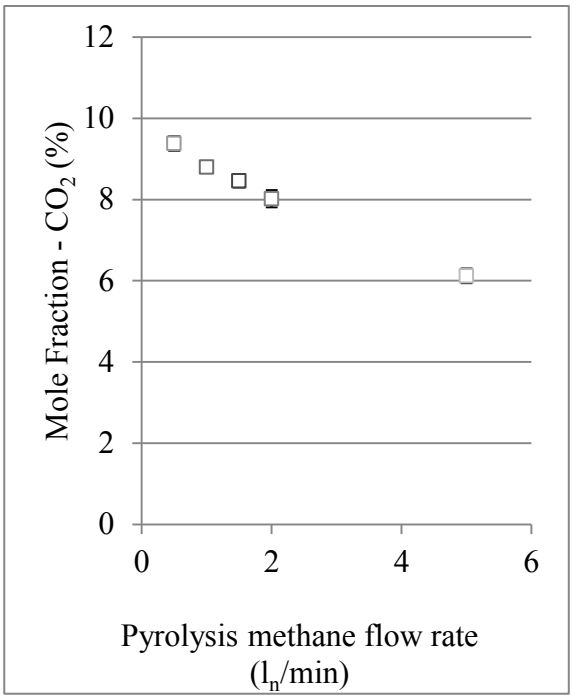

CO_2

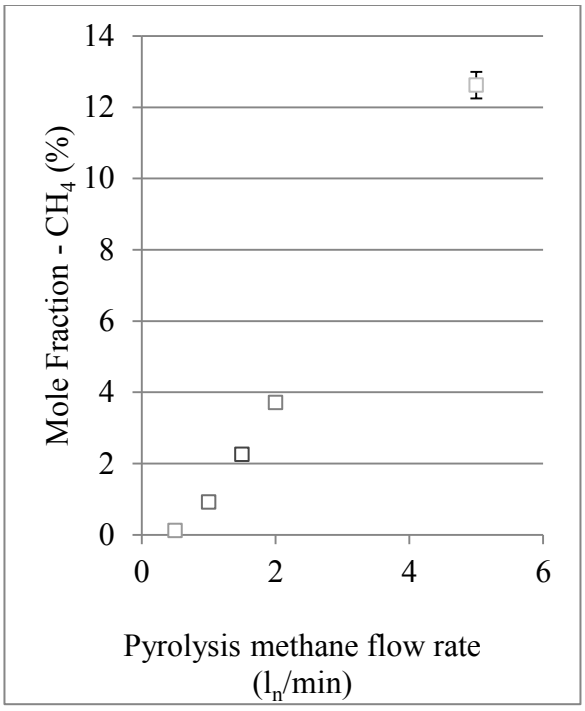

CH_4

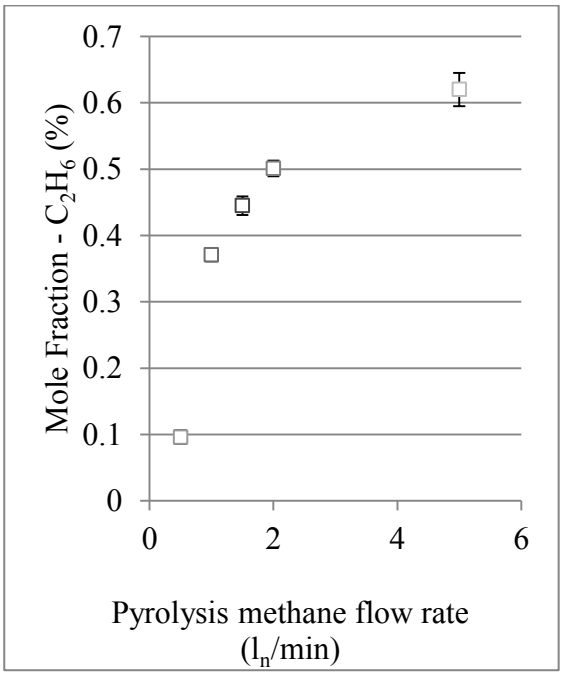

C_2H_6

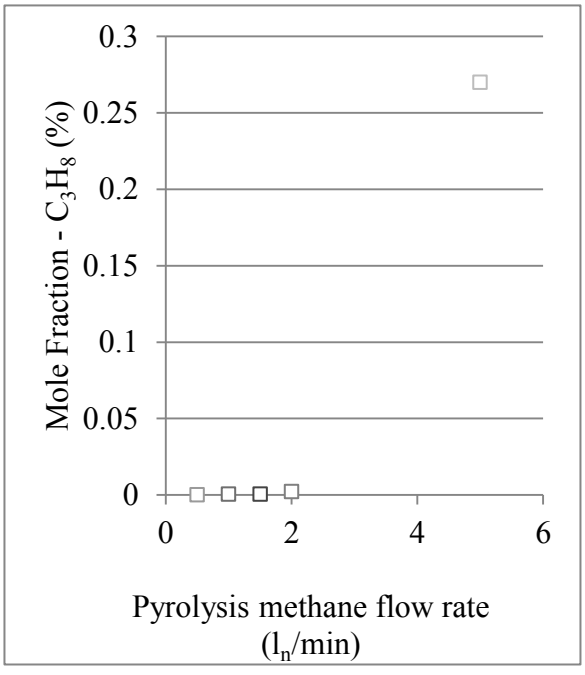

C_3H_8

Figure 3-12 - Average mole % based on pyrolysis methane flow rate for the methane flame - Some error bars are smaller than the marker size

3.4.3 Methane destruction efficiency

Methane destruction efficiency can be calculated for both flames, which is the mass ratio of the converted methane to the inlet methane:

$$\eta_{\text{methane destruction}} = \frac{\dot{m}_{\text{converted methane}}}{\dot{m}_{\text{ pyrolysis methane at the inlet}}} \tag{3-4}$$

To calculate $\dot{m}_{\text{converted methane}}$ in equation (4-17) the following equations can be used:

$$\dot{m}_{\text{ pyrolysis methane at the inlet}} = \dot{m}_{\text{converted methane}} + \dot{m}_{\text{unconverted methane}} \tag{3-5}$$

For each flame and pyrolysis methane flow rate the mole fraction percentage of methane obtained from GC can be used to calculate $\dot{m}_{\text{unconverted methane}}$. $\dot{m}_{\text{ pyrolysis methane at the inlet}}$ can be obtained by the mass flow rate set point for pyrolysis methane. The methane destruction efficiency can be measured using equation (3-4). It has to be mentioned that in the methane flame experiment there will be a mass flow rate of unburned methane in the outlet but this can be neglected comparing to mass flow rate of pyrolysis methane due to the small fuel-air equivalence ratio (φ=1.05). The results for methane conversion efficiency for both flames are shown in Figure 3-13.

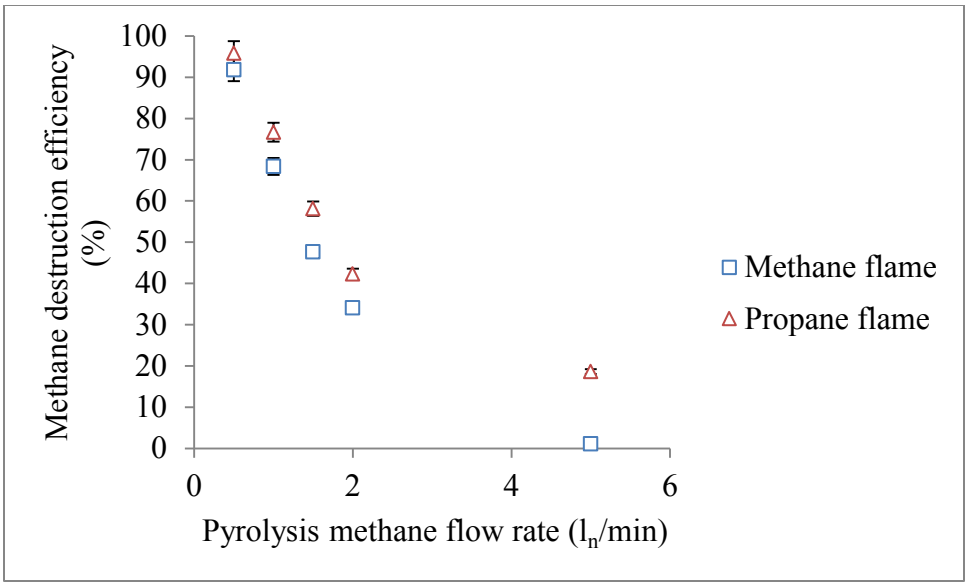

Figure 3-13 – Methane destruction efficiency for different pyrolysis methane flow rate for both flames with error bars (some error bars are smaller than the marker size)

The results show that methane conversion (into hydrogen, carbon and other compounds) efficiency is higher with lower pyrolysis methane flow rate. Furthermore, the propane flame has higher conversion efficiency as it has higher temperature distribution comparing to the methane flame.

3.4.4 Methane conversion into hydrogen efficiency for the propane flame

Results from the GC can be used to find the methane conversion efficiency into hydrogen, which is the main objective of the project. Hydrogen mole percentage at the exhaust calculated from the GC results and the inlet flow rate of methane can be used to find the efficiency of methane conversion into hydrogen by:

$$\eta_{H_2} = \frac{\dot{m}_{H_{2_{out}}}}{\dot{m}_{H_{2_{in}}}} \tag{3-6}$$

Where η_{H_2} is the methane conversion efficiency into hydrogen, $\dot{m}_{H_{2_{out}}}$ is the mass flow rate of the produce hydrogen at the outlet measured by GC and $\dot{m}_{H_{2_{in}}}$ is the mass of

the hydrogen in the pyrolysis methane that was introduced to the reaction chamber. As it was mentioned before, the results from GC are not normalized and they represent the actual mole percentage of each compound according to the total mole at the outlet. The measurement of nitrogen, since it is essentially inert in these conditions, can be used to find the total moles at the outlet. Products of the experiment were tested with a 5 gas analyzer and results for NO_x concentration show 50 to 180 ppm of NO_x for different methane flow rates (Appendix G). Due to the small concentration of NO_x, it can be neglected and N_2 would be considered as the only product containing nitrogen atoms. Based on inlet molar flow rate of nitrogen and the results of the GC for nitrogen, the total number of moles can be found. The overall conversion reaction is shown schematically in Figure 3-14.

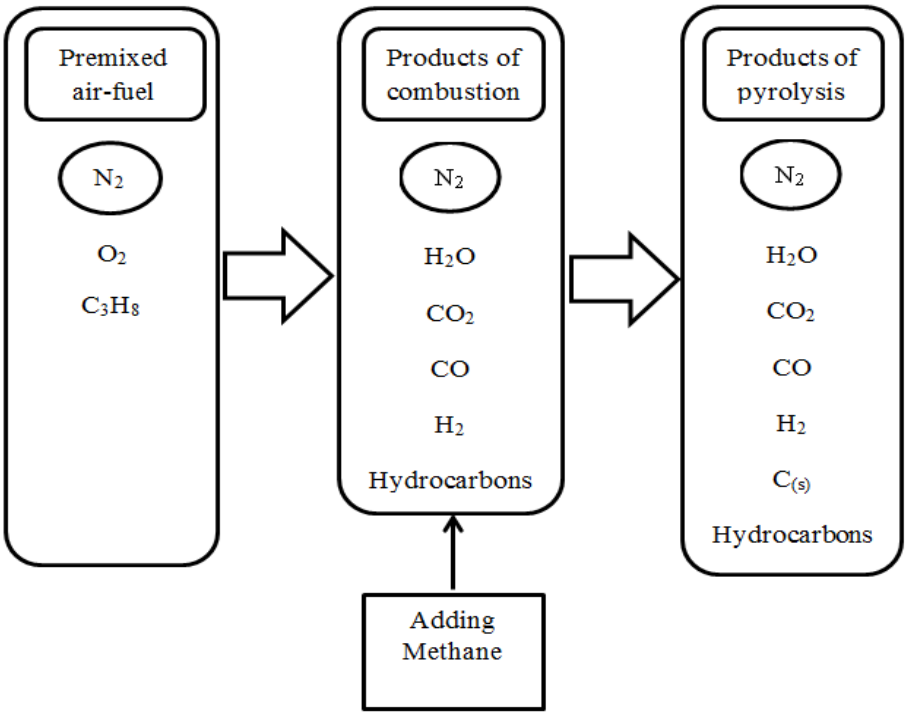

(a) (b) (c)

Figure 3-14 – The overall process that shows N_2 would remain unchanged during the whole process as it doesn't invole in any reaction – (a) air and fuel (propane) are mixed to be burnt (b) methane will be added to the hot products of air-propane combustion (c) final products of methane pyrolysis in products of air-propane combustion

Equation (3-7) shows combustion of air and propane which happens in Figure 3-14 (a); Equation (3-8) shows the reaction of methane pyrolysis after adding methane into the hot products of combustion in Figure 3-14 (b). n_1 to n_{19} are the mole fractions of each component. First air and propane are mixed and burned, and then methane is added to the hot products of propane flame and will be decomposed mainly into carbon and hydrogen.

$$n_1C_3H_8 + n_2(O_2 + 3.76N_2) \rightarrow n_3CO_2 + n_4H_2O + n_5N_2 + n_6H_2 + n_7CO \qquad (3\text{-}7)$$

$$n_8CO_2 + n_9H_2O + n_{10}N_2 + n_{11}H_2 + n_{12}CO + n_{13}CH_4 \qquad (3\text{-}8)$$

$$\rightarrow n_{14}CO_2 + n_{15}H_2O + n_{16}N_2 + n_{17}H_2 + n_{18}CO + n_{19}C_{(s)} + \text{hydrocarbons}$$

Nitrogen is a non-reacting compound and can be used for actual mole calculation. Mass of nitrogen is conserved, therefore in reactions (3-7) and (3-8) moles of nitrogen would be the same ($3.76n_2 = n_{10} = n_{16}$). In another word:

$$(\dot{n}_{N_2})_{inlet} = (\dot{n}_{N_2})_{outlet} \quad (3\text{-}9)$$

Moles of nitrogen that enters the reaction chamber would be same as the moles of nitrogen at the outlet. Mole fraction of nitrogen measured by GC at the outlet can be defined as follow:

$$(\dot{n}_{N_2})_{outlet} = y * \dot{N}_{\text{total,outlet}} \quad (3\text{-}10)$$

Where *y* is the mole fraction percentage of nitrogen found by GC and $\dot{N}_{total,outlet}$ is the unknown variable that is needed to be found. According to equation (3-9) moles of nitrogen at the outlet is equal to the inlet moles of nitrogen, so equation (3-10) can be written as:

$$(\dot{n}_{N_2})_{inlet} = y * \dot{N}_{\text{total,outlet}} \quad (3\text{-}11)$$

According to the equation (3-11), by calculating $(\dot{n}_{N_2})_{inlet}$ from the flow rate set point of air, $\dot{N}_{\text{total,outlet}}$ can be found. For the propane flame $\dot{n}_{N_2\ \text{inlet}}$ can be found using the following equations:

$$\dot{n}_{\text{air inlet}} = \frac{\dot{m}_{\text{air}}}{M_{\text{air}}} \quad (3\text{-}12)$$

$$\dot{m}_{\text{air}} = \rho_{air}\dot{V}_{\text{air}} \tag{3-13}$$

Moles of inlet air can be found by equation (3-12), where $\dot{m}_{air}$ the mass flow is rate of air and can be obtained from equation (3-13). M_{air} is the molar mass of air. ρ is the density of air at normal conditions mentioned in chapter 2, and $\dot{V}_{\text{air}}$ is volumetric flow rate of air. So $\dot{n}_{\text{air inlet}}$ will be 0.025 mol/s and considering that dry air contains 78.09% nitrogen, $(\dot{n}_{\text{N}_2})_{\text{inlet}}$ would be 0.019 mol/s.

$\dot{N}_{\text{total,outlet}}$ in equation (3-11) can be found by having $\dot{n}_{\text{N}_2\text{ inlet}}$. By having the total moles at the outlet and mole fraction of hydrogen measured by GC, the mass of produced hydrogen can be calculated and the efficiency of methane conversion into hydrogen can be calculated with Equation (3-6). The hydrogen yield by the propane flame itself was deducted from the hydrogen produced by pyrolysis methane to make sure only the efficiency of methane conversion into hydrogen was considered.

3.4.5 Methane conversion efficiency for methane flame

Based on the results from pyrolysis of methane in the premixed methane-air flame, efficiency of methane conversion into hydrogen can be calculated with the same procedure as explained in section 3.4.4 for the propane-air flame. The methane conversion into hydrogen efficiency for both flames is shown in Figure 3-15.

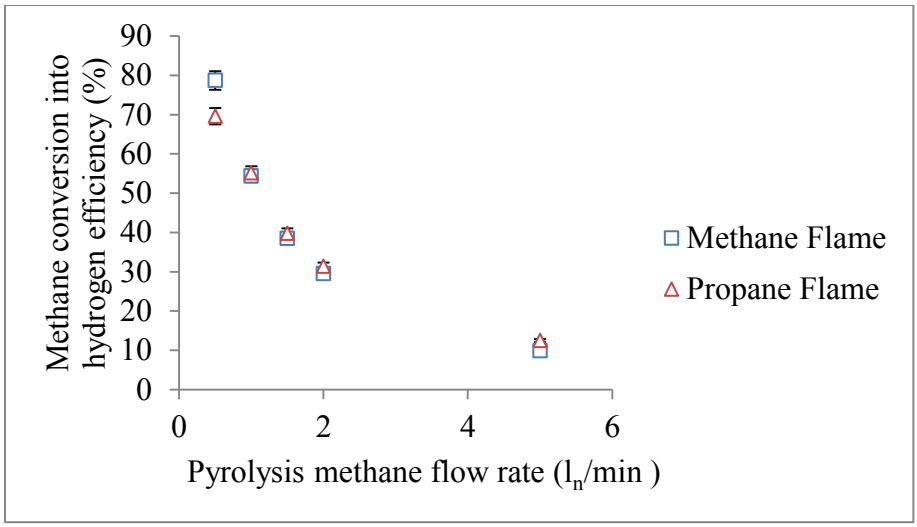

Figure 3-15 - Methane conversion into hydrogen efficiency – Methane and propane flame with error bars (some error bars are smaller than the marker size)

The results from methane conversion into hydrogen for the propane shows that an efficiency of 69% can be obtained with pyrolysis methane flow rate of 0.5 l_n/min. By increasing the pyrolysis methane flow rate, methane conversion into hydrogen efficiency decreases. There are two major reasons causing this efficiency to drop which are a shorter residence time and the cooling effect of introduced methane with higher flow rates. For the flow rate of 5 l_n/min most of the methane would leave the reaction chamber unconverted. The result from methane pyrolysis in the methane flame shows similar results to the propane flame. The highest conversion is reached at methane pyrolysis flow rate of 0.5 l_n/min which is 78%. By increasing the pyrolysis methane flow rate the efficiency would decrease. According to Figure 3-13 methane destruction efficiency is higher with the propane flame because of the higher temperature distribution, but Figure 3-15 shows that for both flames the hydrogen conversion is almost the same for any pyrolysis methane flow rate, that means that pyrolysis methane in the propane flame experiment is also converted to other components than hydrogen.

Based on the mass of produced hydrogen the thermal energy of the produced hydrogen can be measured, the thermal energy of the fuel and pyrolysis methane also can

be measured based on their mass flow rates. Figure 3-16, shows the thermal energy of the produced hydrogen based on the total input thermal energy.

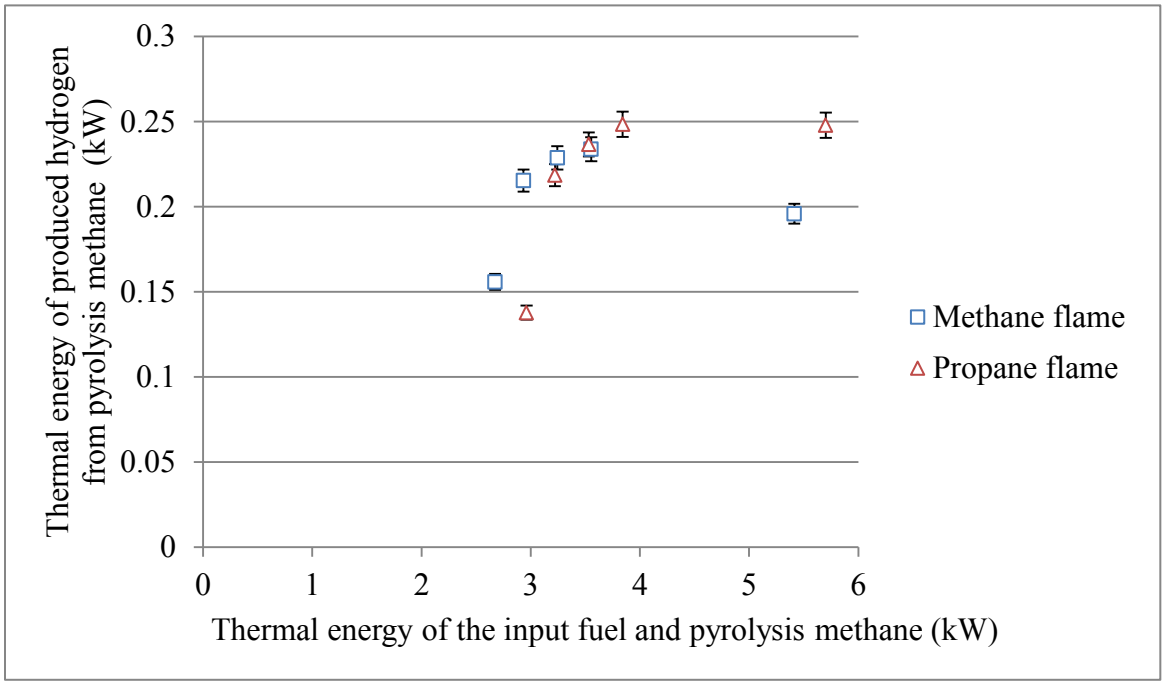

Figure 3-16- Thermal energy (kW) of the produced hydrogen based on the total input thermal energy (kW) with error bars (some error bars are smaller than the marker size)

3.5 Conclusion

The results from the methane conversion into hydrogen shows that with the current system the highest conversion efficiency of 69% and 78% can be obtained by propane and methane flame respectively. The gas chromatography results show that most of the produced carbon atoms in the pyrolysis reaction are forming mainly CO molecules. Temperature distribution inside the reaction chamber shows that insulation blocks are needed in order to provide the needed temperature for the pyrolysis reaction, but there is a dramatic temperature drop in the reaction chambers for the points away from the flame. Temperature and residence time were found to be two dominant parameters in the methane conversion efficiency into hydrogen.

CHAPTER 4. CONCLUSIONS AND FUTURE WORK

4.1 Conclusion

Pyrolysis of methane in the products of a premixed laminar flame was investigated in this project. The main goal of this study was to have an experimental analysis of methane pyrolysis by a laminar premixed flame. Based on a literature review, it appears that is the first time this approach was used for direct thermal cracking, as most of the experimental of methane cracking were done in a shock tube, gas-phase tube reactors, or bubbling through molten metals. This project was motivated by using a premixed flame as the high temperature source to provide the energy for methane cracking.

Two flames were used in the experiment one with propane as the fuel and the other one with methane as the fuel. Temperature distribution inside the reaction chamber was measured with and without insulation blocks inside the quartz reaction chamber. Due the uncertainties in designing the experiment, a COMSOL model was used to get a better understanding of the temperature distribution and time scales inside the reaction chamber before and after adding insulation blocks (Appendix D). The model showed that adding these blocks were needed in the system to provide the temperatures needed for the pyrolysis reaction.

Maximum temperature of 1170 °C and 1135 °C was measured experimentally for propane and methane flame respectively inside the reaction chamber after adding insulation blocks. Temperature measurements show that by adding insulation blocks the overall temperature inside the quartz chamber increases which provides the needed conditions for pyrolysis reaction. Temperature distribution found from experiments had a large difference from the adiabatic temperature of a propane or methane flame (~2400 K) and also the model that was simulated with COMSOL (Appendix D), such a difference was unclear in the setup and future work is needed to investigate this.

Gas analysis for both flames was done at the exhaust of the reaction chamber by a gas chromatography (GC). Pyrolysis of methane in a rich premixed propane-air (air flow rate of 35 l_n/min and propane flow rate of 1.43 l_n/min) and a methane-air flame (air flow rate of 34.8 l_n/min and propane flow rate of 1.62 l_n/min) were studied for different pyrolysis methane flow rates (0.5, 1, 1.5, 2 and 5 l_n/min). In both cases the fuel-air equivalence ratio and the total flow rate of air and fuel was kept constant. Efficiency of methane conversion into hydrogen was measured using the results from GC analyzer; the results show maximums of 69% and 78% of methane conversion into hydrogen for the pyrolysis methane flow rate of 0.5 l_n/min with propane and methane flames, respectively. By increasing the pyrolysis methane flow rate the methane conversion into hydrogen efficiency decreases, and is believed to be highly dependent on the residence time for this setup. Increasing pyrolysis methane flow rate increases CO concentration at the exhaust while CO_2 concentration decreases; which strongly suggested that the produced carbon atoms from methane cracking tend to form CO molecules and that the oxygen for this reaction came from the flame's CO_2.

4.2 Future work

The results from this study show good conversion rate of methane into hydrogen using a premixed flame. However, there are areas that future works need to focus on to develop the pyrolysis of methane using a premixed flame. The following points are recommended.

- Developing a numerical model to investigate the mechanism of methane cracking with the given temperature distribution of this set-up and presence of the combustion products.
- Decreasing temperature gradient inside the reaction chamber by using a new material for the reaction chamber and a better insulation.
- Separating the pyrolysis methane flow from the combustion products in order to prevent carbon atoms to produce CO and reach better methane to carbon black conversion rate.

- Increasing the residence time on the pyrolysis reaction by using a different method for methane injection, such as placing a larger diameter pyrolysis tube with high heat conductivity directly in contact with the flame in order to produce more black carbon formation.
- Characterizing the produced carbon black by size in order to find the suitable market for the black carbon produced in this process.
- Consider constructing a non-quartz reaction chamber to allow for better insulation and sealing, at the expense of poorer flow visualization.

References

[1] H. F. Abbas and W. M. A. W. Daud, "Hydrogen production by methane decomposition : A review," *Int. J. Hydrogen Energy*, vol. 35, pp. 1160–1190, 2010.

[2] T. Karl, J. Melillo, and T. Peterson, "Global cLimate change impacts in the United States,", A state of knowledge report from the U.S. global change research program, Cambrige university press, 2009.

[3] A. Abánades, E. Ruiz, and E. . . Ferruelo, "Experimental analysis of direct thermal methane cracking," *Int. J. Hydrogen Energy*, vol. 36, pp. 12877–12886, 2011.

[4] M. Steinberg, "Fossil fuel decarbonization technology for mitigating global warming," *Int. J. Hydrogen Energy*, vol. 24, pp. 771–777, 1999.

[5] L. Kostiuk, J. Olfert, and M. Secanell, "Thermal decomposition of natural gas in a gas-phase oxygen deficient environment," Technical information for the purpose of proposal review, Edmonton, 2015.

[6] N. Z. Muradov, "CO2 -Free production of hydrogen by catalytic pyrolysis of hydrocarbon fuel," *Energy and Fuels*, vol. 12, pp. 41–48, 1998.

[7] N. Z. Muradov, "How to produce hydrogen from fossil fuels without CO_2 emission," *Int. J. Hydrogen Energy*, vol. 18, pp. 211–215, 1993.

[8] G. Marbán and T. Valdés-solís, "Towards the hydrogen economy?," *Int. J. Hydrogen Energy*, vol. 32, pp. 1625–1637, 2007.

[9] "ElectroChem, Inc. About fuel cells. available from, www. fuelcell.com/aboutcels.html; 2002.," 2002. .

[10] P. Moriarty and D. Honnery, "Hydrogen's role in an uncertain energy future," *Int.*

J. Hydrogen Energy, vol. 34, pp. 31–39, 2009.

[11] M. Momirlan and T. N. Veziroglu, "Current status of hydrogen energy," *Renew. Sustain. Energy Rev.*, vol. 6, pp. 141–179, 2002.

[12] S. Rodat, S. Abanades, J. Coulié, and G. Flamant, "Kinetic modelling of methane decomposition in a tubular solar reactor," *Chem. Eng. J.*, vol. 146, pp. 120–127, 2009.

[13] A. Tsutsumi, "Thermodynamics of water splitting," *Energy carriers Convers. Syst.*, vol. 1, pp. 136–146.

[14] B. Gaudernack and S. Lynum, "Hydrogen from natural gas without release of CO2 to the atmosphere," *Int. J. Hydrogen Energy*, vol. 23, pp. 1087–1093, 1996.

[15] M. Steinberg, "The Hy-C process (thermal decomposition of natural gas) potentially the lowest cost source of hydrogen with the least CO_2 emission," *Energy Convers. Manag.*, vol. 36, pp. 791–796, 1995.

[16] P. L. Spath and M. K. Mann, "Life cycle assessment of hydrogen production via natural gas steam reforming,", Technical report, National Renewable Energy Laboratory, Golden, CO, USA, 2001.

[17] D. Y. C. Leung, G. Caramanna, and M. M. Maroto-valer, "An overview of current status of carbon dioxide capture and storage technologies," *Renew. Sustain. Energy Rev.*, vol. 39, pp. 426–443, 2014.

[18] J. M. Lane and P. L. Spath, "Technoeconomic analysis of the thermocatalytic decomposition of natural gas," Technical report, National Renewable Energy Laboratory, Golden, CO, USA, 2001.

[19] E. Shpilrain, V. Shterenberg, and V. Zaichenko, "Comparative analysis of different natural gas pyrolysis methods," *Int. J. Hydrogen Energy*, vol. 24, pp. 613–624, 1999.

[20] World Health Organization, “Carbon Black, Titanium Dioxide, and Talc,” IARC Monographs on the Evaluation of Carcinogenic Risks to Humans, vol. 93, pp. 43–190, 1984.

[21] R. Adams, “Focus on Pigments,”, An international newsletter, pp. 2-3, 2007.

[22] M. Gautier, V. Rohani, L. Fulcheri, and J. P. Trelles, “Influence of temperature and pressure on carbon black size distribution during allothermal cracking of methane,” *Aerosol Sci. Technol.*, vol. 50, pp. 26–40, 2015.

[23] D. Paxman, S. Trottier, M. R. Flynn, L. Kostiuk, and M. Secanell, “Experimental and numerical analysis of a methane thermal decomposition reactor,” *Int. J. Hydrogen Energy*, vol. 42, pp. 25166–25184, 2017.

[24] S. Rodat, S. Abanades, J. Sans, and G. Flamant, “Hydrogen production from solar thermal dissociation of natural gas: development of a 10 kW solar chemical reactor prototype,” *Sol. Energy*, vol. 83, pp. 1599–1610, 2009.

[25] M. Steinberg, “Production of hydrogen and methanol from natural gas with reduced CO2 emossion,” *Int. J. Hydrogen Energy*, vol. 23, pp. 419–425, 1998.

[26] V. Kevorkian, C. E. Heath, and M. Boudart, “The decomposition of methane in shock waves,” *J. Phys. Chem. J. Phys. Chem.*, vol. 64, pp. 964–968, 1960.

[27] G. Patrianakos, M. Kostoglou, and A. Konstandopoulos, “One-dimensional model of solar thermal reactors for the co-production of hydrogen and carbon black from methane decomposition,” *Int. J. Hydrogen Energy*, vol. 36, pp. 189–202, 2010.

[28] “Skinner, G. B., Proc. Div. Fuel Chem., American Chemical Society Meeting, St. Louis, Missouri, March 21-30, 1961.” .

[29] F. Billaud, C. Gueret, and J. Weill, “Thermal decomposition of pure methane at 1263 K. Experiments and mechanistic modelling,” *Thermochim. Acta*, vol. 211, pp. 303–322, 1992.

[30] M. Dresselhaus, “Basic research needs for the hydrogen economy,”, Report presented by Argonne national laboratory, USA, 2003.

[31] M. Steinberg and H. C. Cheng, “Modern and prospective technologies for hydrogen production from fossil fuels,” *Int. J. Hydrogen Energy*, vol. 14, pp. 797–820, 1989.

[32] N. Ozalp, K. Ibrik, and M. Al-meer, “Kinetics and heat transfer analysis of carbon catalyzed solar cracking process,” *Energy*, vol. 55, pp. 74–81, 2013.

[33] E. Bilgen and J. Galindo, “High temperature solar reactors for hydrogen production,” *Int. J. Hydrogen Energy*, vol. 6, pp. 139–152, 1981.

[34] A. Steinfeld, “Solar thermochemical production of hydrogen - a review,” *Sol. Energy*, vol. 78, pp. 603–615, 2005.

[35] A. Kobayashi and M. Steinberg, “The thermal decomposition of methane in a tubular reactor,” Thechnical report, Brookhaven national laboratory, Upton, NY (United States), 1991.

[36] M. Younessi-Sinaki, E. a. Matida, and F. Hamdullahpur, “Kinetic model of homogeneous thermal decomposition of methane and ethane,” *Int. J. Hydrogen Energy*, vol. 34, pp. 3710–3716, 2009.

[37] J. Appel, H. Bockhorn, and M. Frenklach, “Kinetic modeling of soot formation with detailed chemistry and physics: laminar premixed flames of C_2 hydrocarbons,” *Combust. Flame*, vol. 121, pp. 122–136, 2000.

[38] B. J. McBride, S. Gordon, and M. A. Reno, “Coefficients for calculating thermodynamic and transport properties of individual species,”, NASA technical memorandum 4513, Cleveland, OH, United States, 1993.

[39] “http://www.chromacademy.com/lms/sco10/03-Why-choose-Gas-Chromatography-a.html?fChannel=1&fCourse=2&fSco=10&fPath=sco10/03-Why-choose-Gas-Chromatography-a.html.” .

[40] R. Hatchard, “The development and analysis of an ultra-low emissions furnace,” University of Alberta, M.Sc. Thesis, 1996.

[41] C. H. Berman, R. J. Gill, and H. F. Calcote, “Enhanced flame stability and soot radiation using electric fields,”, Technical report, AeroChem Research Labs, Princeton, NJ (USA), 1989.

[42] M. R. Johnson, “Development of a low emissions, lean premixed, natural gas burner,” University of Alberta, M.Sc. Thesis, 1995.

[43] “http://www.matweb.com/index.aspx.” .

[44] “www.agilent.com/en-us/products/gas-chromatography/gc-systems/7890b-gc-system.” .

[45] S. G. Zavarukhin and G. G. Kuvshinov, “The kinetic model of formation of nanofibrous carbon from CH_4-H_2 mixture over a high-loaded nickel catalyst with consideration for the catalyst deactivation,” *Appl. Catal. A Gen.*, vol. 272, pp. 219–227, 2004.

[46] G. P. Smith, D. M. Golden, M. Frenklach, N. W. Moriarty, B. Eiteneer, M. Goldenberg, C. T. Bowman, R. K. Hanson, S. Song, J. William C. Gardiner, V. V. Lissianski, and Z. Qin, “http://www.me.berkeley.edu/gri_mech/.” .

[47] A. Holmen, O. Olsvik, and O. A. Rokstad, “Pyrolysis of natural gas: chemistry and process concepts,” *Fuel Process. Technol.*, vol. 42, pp. 249–267, 1995.

[48] “navier.engr.colostate.edu.” Colorado State University.” .

[49] “www.comsol.com/model/thermal-decomposition-2164.” .

Appendix A. Engineering drawings

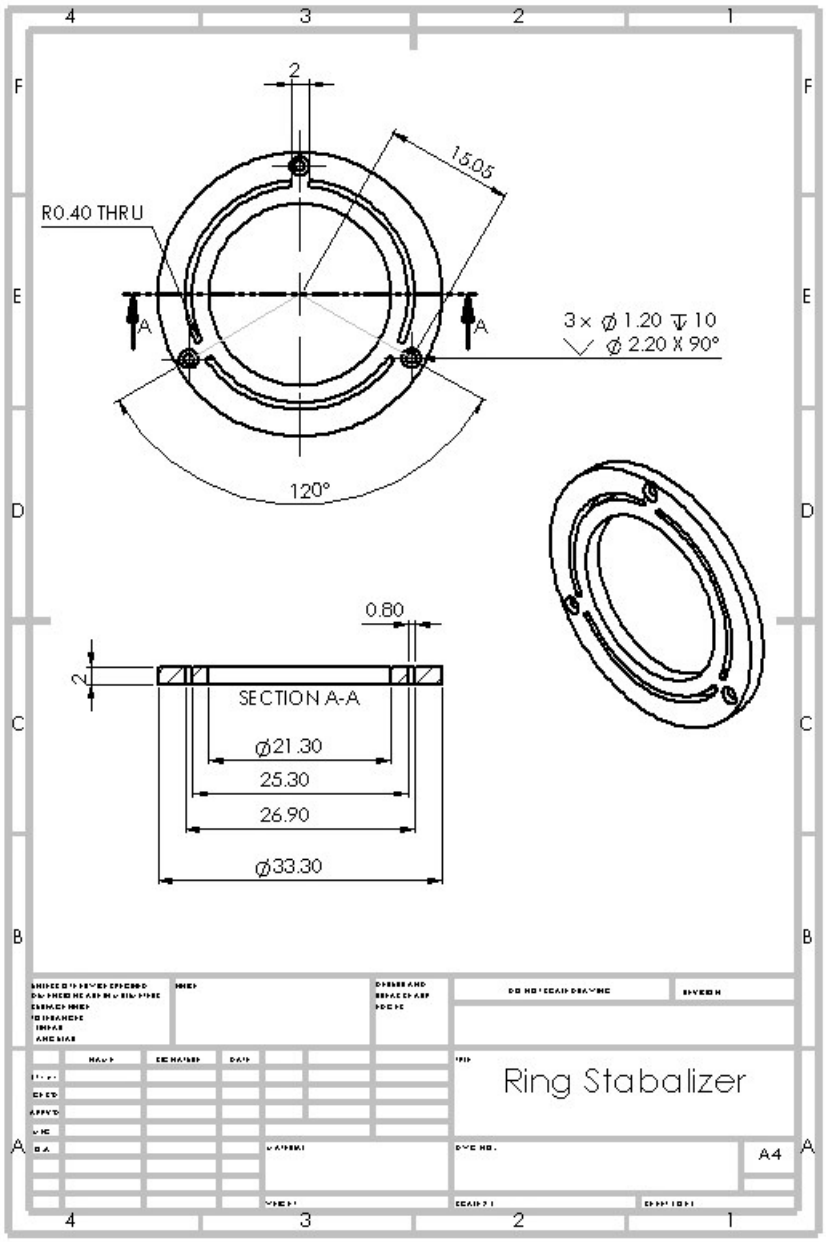

Figure A-1 - ring stabilizer (all dimensions in mm)

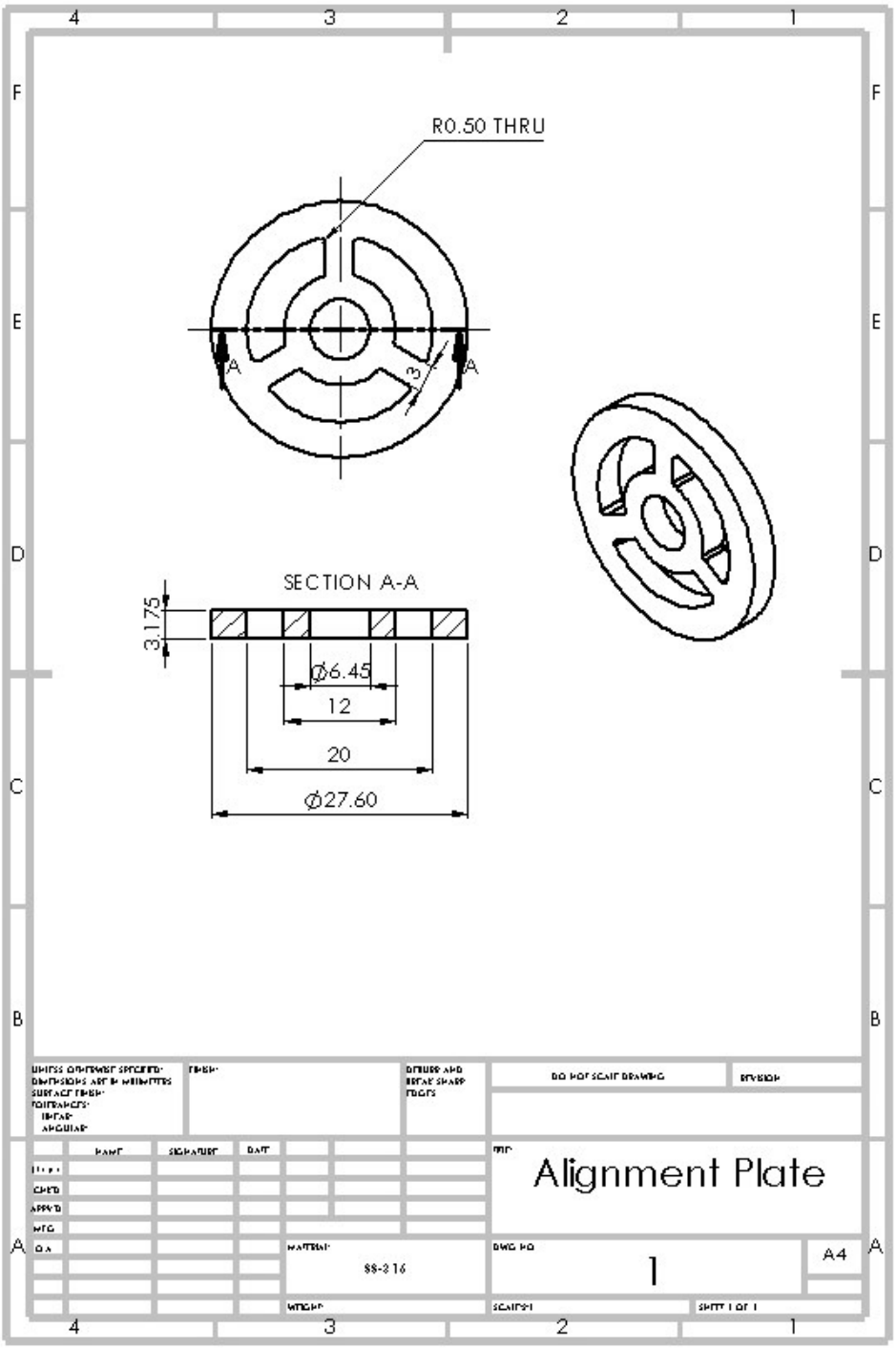

Figure A-2 – Alignment plate (all dimensions in mm)

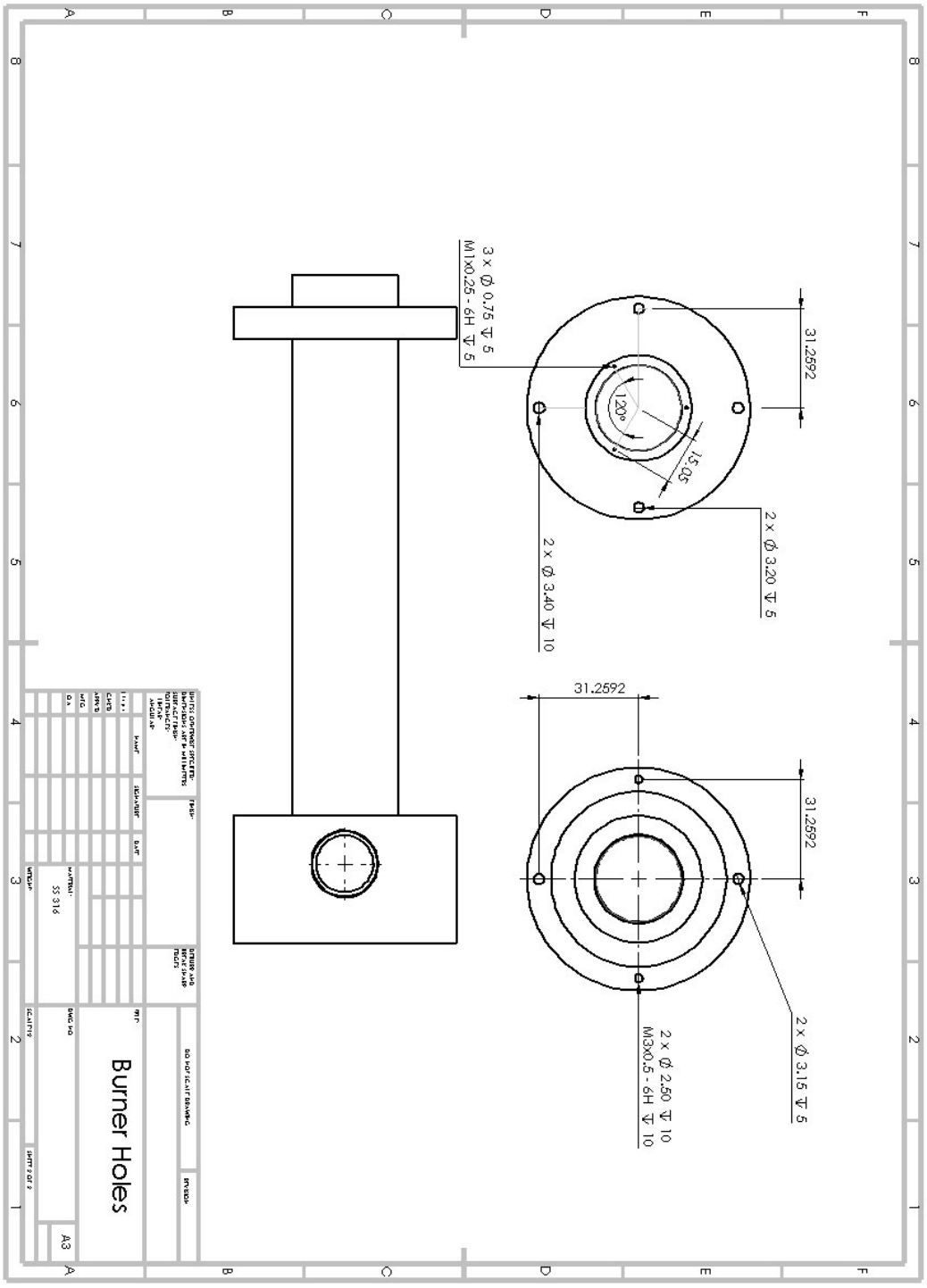

Figure A-3 - Burner holes - All dimensions in mm

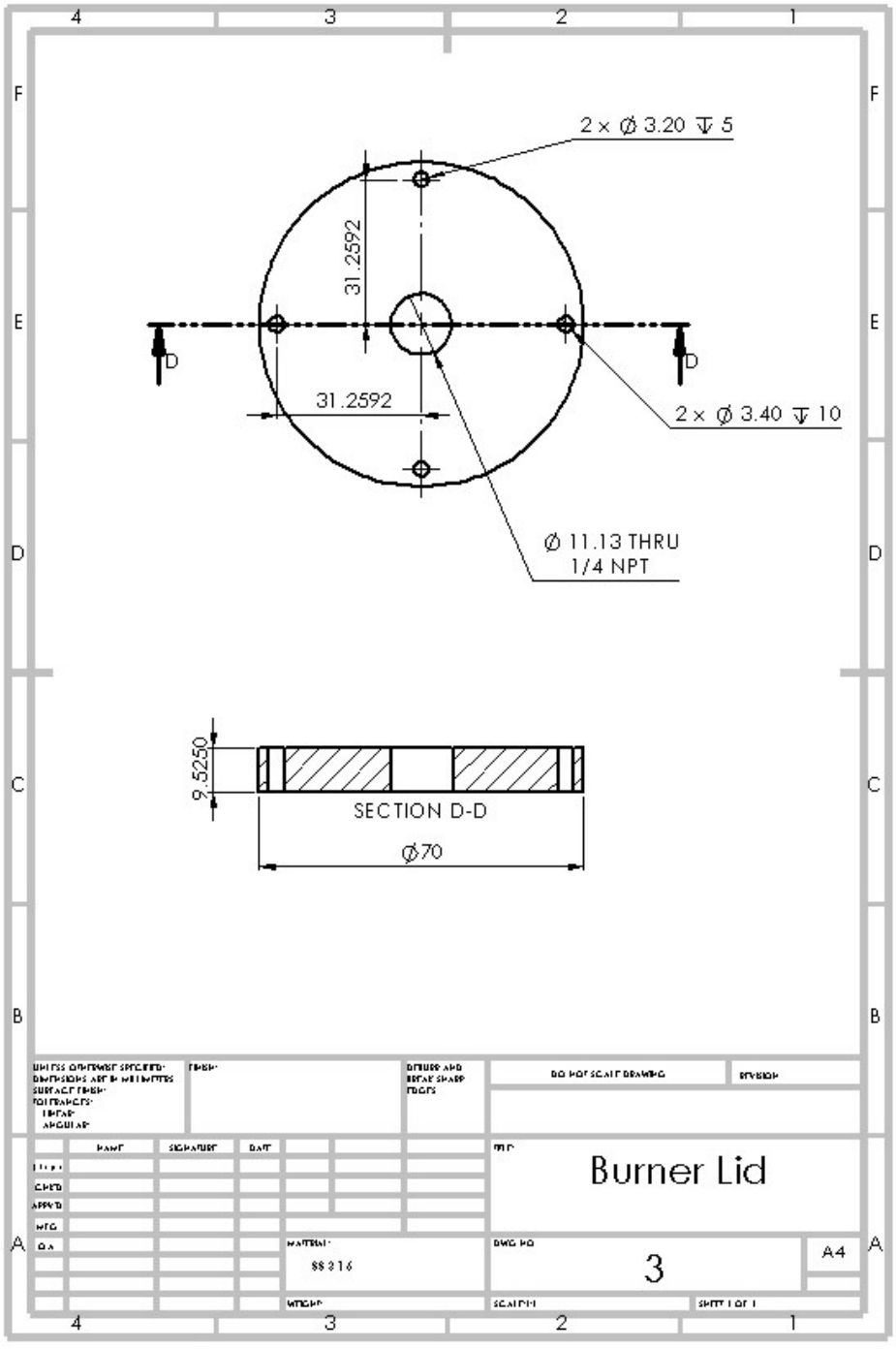

Figure A-4 - Burner lid drawings - all dimension in mm

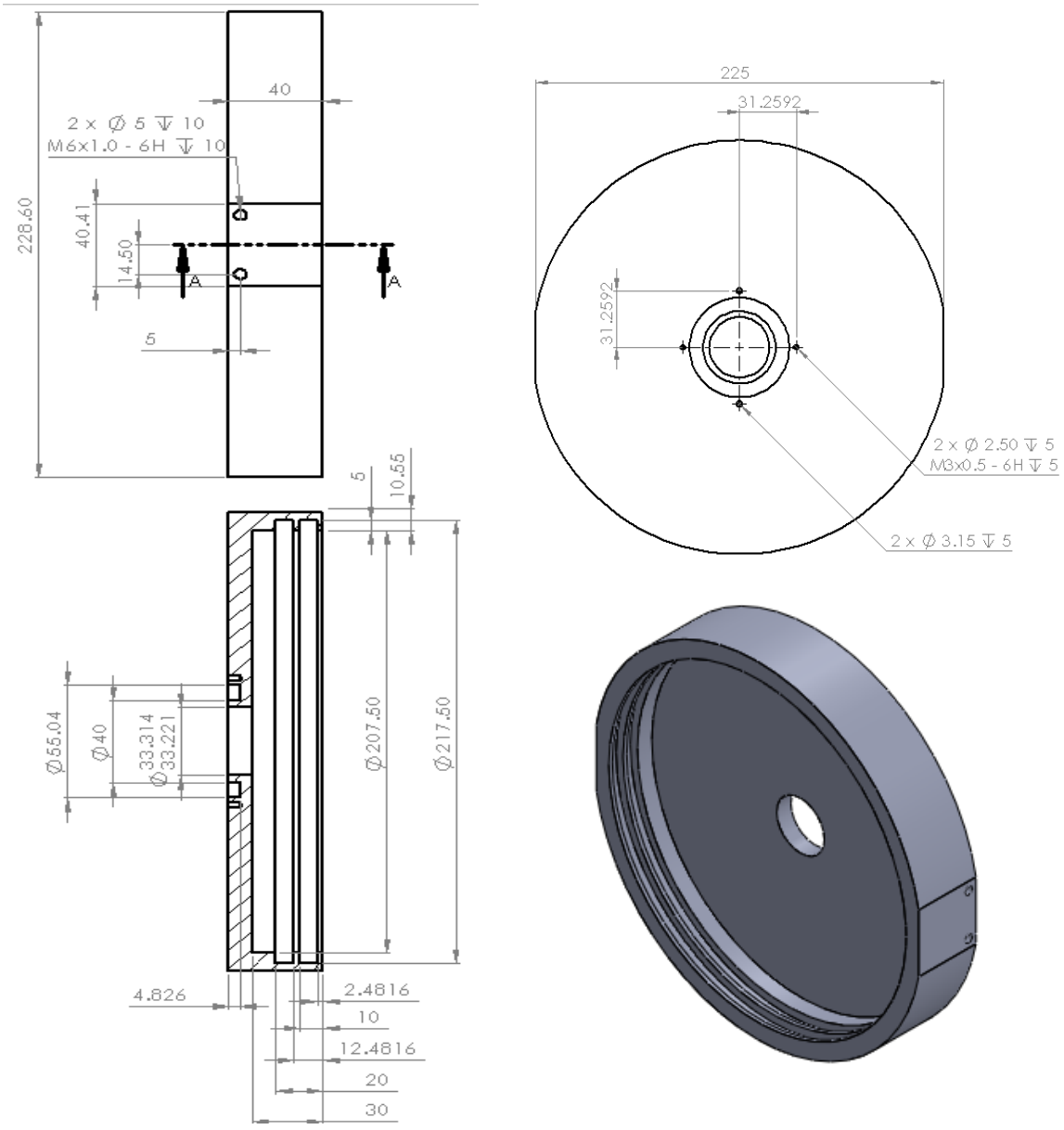

Figure A-5 - Top fitting drawings - all dimensions in mm

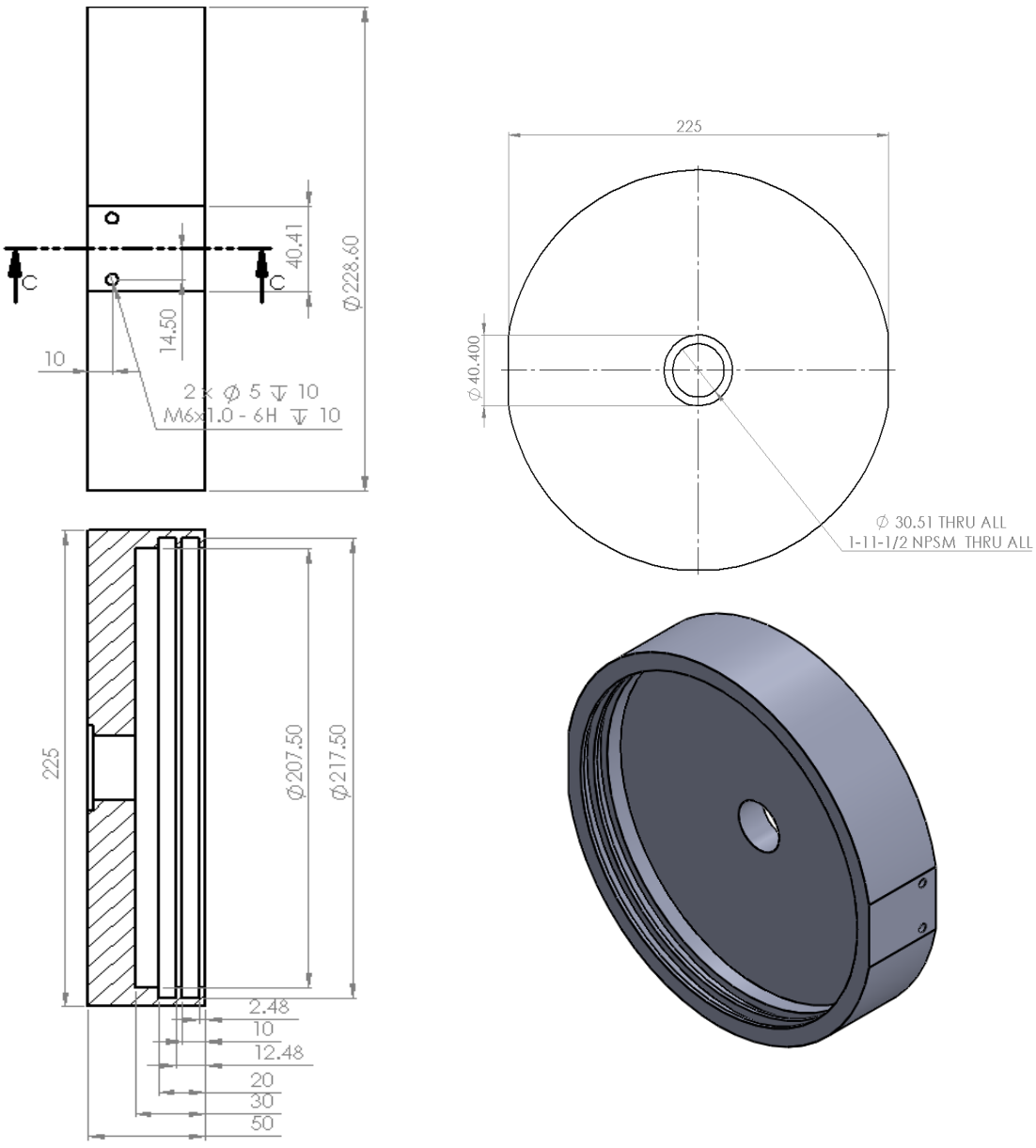

Figure A-6 - Bottom fitting drawings - all dimensions in mm

Appendix B. Flow rate calculations

B-1. Propane as fuel

The flow rates are needed to be calculated for fuel, air and pyrolysis methane so the whole set-up would be 8 kW. The stoichiometric reaction of combustion is as follow:

$$C_3H_8 + 5(O_2 + 3.76N_2) \rightarrow 3CO_2 + 4H_2O + 18.8N_2 \quad \text{(B-1)}$$

Energy equation can be written for this reaction, considering that the process starts at ambient temperature and goes to a temperature *T*, which is temperature of the premixed propane-air flame. By solving the energy equation, *T* can be found:

$$h_{f,C_3H_8} = h_{f,CO_2} + h_{f,H_2O} + \int_{300}^{T} (3Cp_{CO_2} + 4Cp_{H_2O} + 18.8Cp_{N_2})\, dT \quad \text{(B-2)}$$

Where

h_{f,C_3H_8} = Enthalpy of formation of C_3H_8

h_{f,CO_2} = Enthalpy of formation of CO_2

h_{f,H_2O} = Enthalpy formation of H_2O

C_p = specific heat in constant pressure

$$-104.7 = 3(-393.5) + 4(-248.82) + \int_{300}^{T} (3Cp_{CO_2} + 4Cp_{H_2O} + 18.8Cp_{N_2})\, dT$$

Third order equations available for *Cp* in thermodynamic tables:

$$Cp = a + bT + cT^2 + dT^3 \quad \text{(B-3)}$$

Where

a = {N_2 = 28.9 , H_2O = 32.24 , CO_2 = 22.26}

b = {N_2= -0.1571 * 10^{-2}, H_2O = 0.1923 * 10^{-2} , CO_2 = 5.981 * 10^{-2} }

c = {N_2= 0.8081 * 10^{-5} , H_2O = 1.055* 10^{-5} , CO_2 = -3.501 * 10^{-5}}

d = {N_2= -2.873* 10^{-9} , H_2O = -3.595 * 10^{-9} , CO_2 = 7.469 * 10^{-9} }

Solving the energy equation for T = 2444.33 K = 2171.18 °C

After introducing methane into the hot products of combustion, methane will be decomposed as the following equation:

$$x\ CH_4 \rightarrow xC + 2xH_2 \qquad \Delta H_f = 74.87 \text{ kJ/mole} \tag{B-4}$$

Where x is number of moles of methane that is needed to drop the system temperature to 1400 K. Considering that methane flow rate would drop the combustion products temperature down to 1400 K at the outlet another energy equation can be written to find the moles of methane needed to drop the total temperature to 1400 K at the exhaust; In this equation temperature of C and H_2 as the products of methane decomposition are considered to rise from 300 K to 1400 K and temperature of combustion products (CO2, H2O and N2) would drop from 2444.33 K to 1400K:

$$1000x\ (-74.87) = 12x(0.708\ (1400-300)) + 4x\ (14.307\ (1400-300)) + \int_{2444.33}^{1400} (3Cp_{CO_2} + 4Cp_{H_2O} + 18.8Cp_{N_2})\ dT \tag{B-5}$$

By solving equation (B-5) moles of methane would be x = 7.29 mole

Considering same specific energy for methane and propane = 50 MJ/kg

If burning 1 mole of propane and decomposing 7.29 moles of methane the whole energy of the system would be: $\frac{1*44+7.29*16}{1000} * 50\ MJ/Kg = 8.032\ MJ$. For the set-up to be 8 kW the scaling factor would be 8032/8 = 1004.

So the mole needed would be:

Mole of propane = 1/1004 => mass flow rate (propane) = 0.0438 gr/s

Mole of methane = 7.29/1004 => mass flow rate (methane) = 0.1161 gr/s

Volume flow rate:

$\dot{V}_{air}$ = 33.467 lpm

$\dot{V}_{propane}$ = 1.307 lpm

$\dot{V}_{methane}$ = 10.62 lpm

The flow rates for air and propane were changed and the fuel-air equivalence ratio of the products were checked with an oxygen sensor at the exhaust to make sure the flame was slightly rich, for this purpose fuel-air equivalence ratio was considered to be 1.05, as result the flow rates for air and propane were set on 35 slpm and 1.43 slpm respectively.

B-2. Methane as fuel

For the experiments with the methane flame and finding the right flow rates for methane as fuel and air, two parameters were kept constant with the propane flame so the result would be comparable. The total flow rate of air and fuel and fuel-air equivalence ratio of methane flame is same as the propane flame. This was done by using an oxygen sensor at the exhaust while running the methane flame in the system and changing the flow rates so same total flow rate and fuel-air equivalence ratio (φ =1.05) is reached. The methane flow rate as the fuel was set on 1.62 slpm and air flow rate was set on 34.8 slpm.

Appendix C. Insulation loading tool

Each 5.08 thick block weighs about 5 kg, removing these blocks inside the quartz by hand was impossible. A tool was designed, see Figure C-1, to load and unload blocks. It consists of a 30 cm long handle that is attached into a medium soft rubber cylinder with durometer of 40A and diameter of 3.8 cm and 4.4 cm long. The rubber is in between the handle and a M10 bolt that goes through the rubber to the handle; as result by placing the rubber inside the insulation block's hole and bending the handle and then turning the handle the bolt starts to move upward and will squeeze the rubber in the middle, since the rubber expand radially it makes it possible to pick up the block and place inside the quartz after placing the block inside the handle can be turned back to release the rubber and take the tool out.

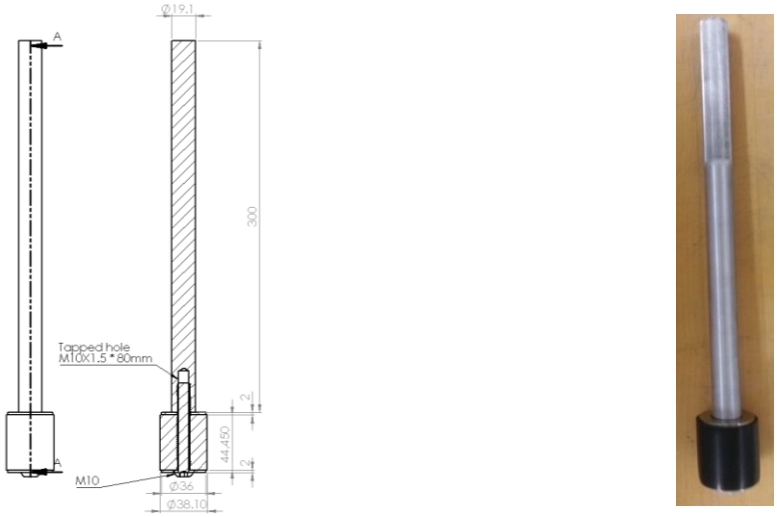

Figure C-1 - Pick up tool for insulation blocks

Appendix D. Reactor Simulation

D-1. Introduction

A model of the proposed reacting flow was investigated with COMSOL simulation. In the model, methane enters the reaction chamber through a 0.635 cm tube and co-flows with hot gases. Two cases were considered for this simulation. First was with no insulation blocks where the reaction chamber had the same diameter as the quartz chamber. Since the reaction chamber is axi-symmetric, equations can be solved for a 2D model and just half plane. The geometry defined in the first model consists of three rectangles; one had a width of 0.3 cm (methane tube radius), and height of 68 cm (quartz chamber height). The second and third rectangle had widths of 1 cm (burner radius) and 10 cm (quartz chamber radius) respectively and height of 68 cm, as shown in Figure D-1. For the second case, the reaction chamber is reduced to a rectangle with a width of 2 cm and height of 68 cm and two rectangles with the width of 0.3 cm (methane tube) and 1 cm (burner) and height of 68 cm, as shown in Figure D-2. The second case was to investigate the effect of insulation blocks on the temperature distribution results.

By the beginning of the process, heat and mass start to diffuse into each other and the time-space history was followed. The inlet flow rate for both methane and hot products and all boundary conditions were known. The model was a multi-physics problem that makes this problem a suitable case for COMSOL. For the aforementioned project, these physics were considered: conservation of mass, conservation of momentum (Navier-Stokes equations), chemical reaction of pyrolysis, energy equation, and species mass diffusion. COMSOL Multi-physics can be used to systematically set up and solve increasingly sophisticated models using predefined physics interfaces.

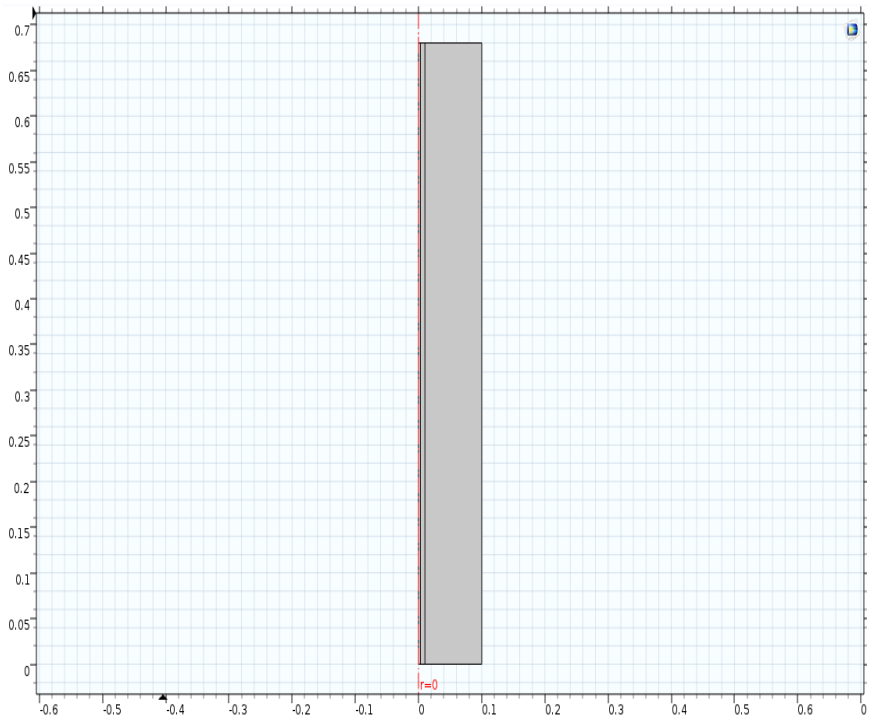

Figure D-1 - Geometry of COMSOL model - without insulation

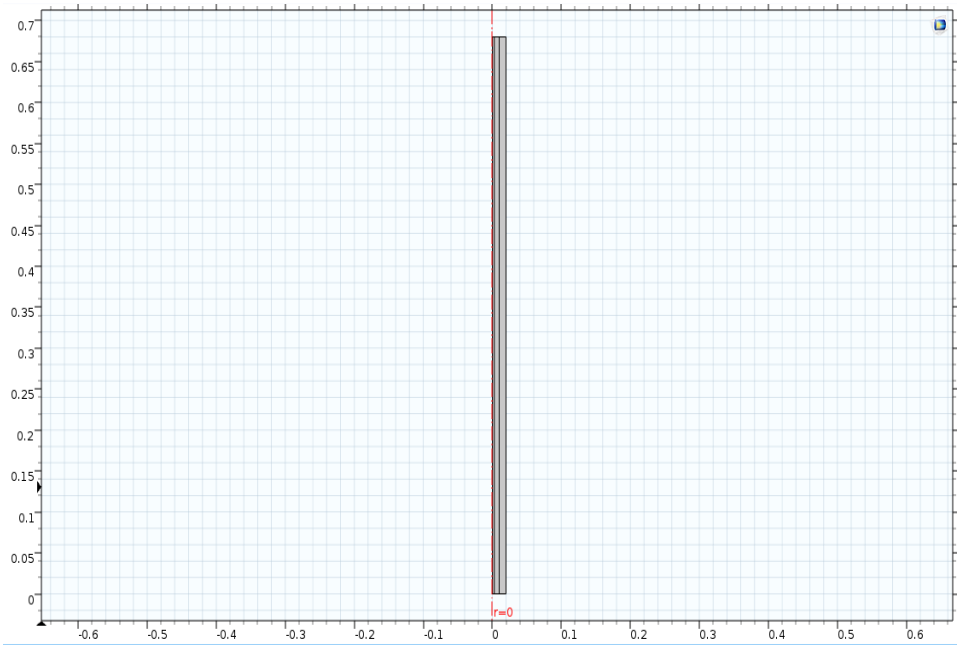

Figure D-2- Geometry of COMSOL model - with insulation

D-2. Review

In the work done by Zavarukhin *et al* [45], methane decomposes over a high-nickel catalyst (Ni/Al_2O_3) according to the overall chemical reaction:

$$CH_4 \rightarrow C_{(s)} + 2H_{2_{(g)}} \tag{D-1}$$

under atmospheric pressure, with temperate ranging from 490 to 590 °C and volume fraction of hydrogen between 0 and 40%, the following reaction rate expression was reported:

$$r = K \frac{p_{CH_4} - \frac{p_{H_2}^2}{K_P}}{\left(1 + K_H \sqrt{p_{H_2}}\right)^2} \tag{D-2}$$

where p_{CH_4} and p_{H_2} are partial pressures of methane and hydrogen. Zavarukhin *et al* [65] have defined equations for K_H, K_P, and K. The limitation of this work was that they have considered pyrolysis in the presence of a catalyst, and due to the fact that the temperature is relatively low. In the current project temperatures were over 1100°C and there is no catalyst. The higher temperature and the fact there is no catalyst will mean that the reaction rate will be very different, so the rate parameters used in equation (D-2) will not be useful for current project; however, the procedure they followed can be very useful. An analysis has been done to simulate the combustion of methane using the GRI-3.0 mechanism, incorporating a detailed reaction mechanism of 53 species taking part in 325 reactions. The files describing the reaction kinetics and thermodynamics of the GRI-3.0 mechanism are can be found in [46]. CHEMKIN data input files were used for kinetic and thermodynamic data for the current project.

D-3. Simulation

The experimental set-up was simulated by COMSOL to investigate temperature distribution. It is helpful to simulate this process by COMSOL software to have a clear

perspective of pyrolysis before running the experiment. The pyrolysis happens when methane comes into contact with hot products from combustion.

Modeling the system starts with zero dimension in COMSOL software just to investigate the reaction engineering. There are very limited sources available for kinetic analysis of methane pyrolysis. The kinetics of the decomposition of methane can be described using the resulting mechanism as follows. In the first step, methane atoms bonds will be broken and smaller molecules and radicals are formed. Then aromatic species will start to form, mainly from the recombination of propargyl (C_3H_3) radicals as well as the reaction of n-C_4H_3 (HCCCHCH) or n-C_4H_5 ($CH_2CHCHCH$) with acetylene. Then polycyclic aromatic hydrocarbons (PAHs) will be formed through H abstraction–C_2H_2 addition mechanism. By coalescence of two PAH molecules solid carbon particles are produced [36].For the simulation, the reaction mechanism in COMSOL the work done by Holmen *et al* [47] can be used. They had investigated the pyrolysis reactions up to hydrogen and acetylene formation. In their source, they have gone through kinetics of methane conversion to acetylene and hydrogen and they had calculated all the Arrhenius parameters for reactions. Their model includes 28 reactions with 17 species which are shown in Table D-1. In the model the modified Arrhenius equation is considered.

$$k = k_0 \cdot T^n e^{\frac{-E_a}{RT}} \tag{D-3}$$

k_0 = Pre-exponential factor, 1/s

E_a = Activation energy, kJ/mole

R = Universal gas constant of 8.314 J/mole·K

T = Reaction temperature, K

n = constant

The rate of reaction (mole/$m^3 \cdot s$) can be defined as:

Table D-1 – Arrhenius parameters for methane pyrolysis mechanism up to hydrogen formation based on the work done by Holmen *et al* [47]

Number	Reaction	k_0 [1/s]	n	E_a[J/mol]
1	CH4⇔CH3+H	3.51E+15	0	434720
2	CH4+H⇔CH3+H2	2.25E+04	3	36650
3	CH3+CH3⇔C2H6	1.01E+15	-0.64	0
4	C2H6+H⇔ C2H5+H2	5.54E+2	3.5	21627
5	CH3+CH3⇔C2H4+H2	1E+16	0	133760
6	C2H4+H⇔C2H3+H2	1.32E+6	2.53	51238
7	CH3+C2H3⇔C3H6	1E+13	0	0
8	C3H6+⇔C3H5+H2	5E+12	0	6270
9	C3H5⇔C2H2+CH3	1.16E+10	0	180576
10	C2H4⇔C2H2+H2	7.94E+12	0.44	371016
11	C2H6+CH3⇔C2H5+CH4	0.55	4	34677
12	C2H5⇔C2H4+H2	1E+16	0	133760
13	C2H4+CH3⇔C2H3+CH4	6.62	3.7	39760
14	C2H3⇔C2H2+H	1.93E+28	-4.783	213694
15	C3H6⇔C3H5+H	1E+15	0	367840
16	C2H3+C2H3⇔C2H4+CH4	1.81E+11	0	72314
17	C4H6+H⇔C4H5+H2	1E+14	0	62700

18	C4H5⇔C4H4+H	1E+14	0	173052
19	C2H+H⇔C2H2	1.81E+14	0	0
20	C2H3+C2H2⇔C4H5	1.1E+12	0	16720
21	C3H3+C3H3⇔C2H5+H	1.8E+12	0	43472
22	C4H5+C2H2⇔C6H6+H	6.02E+12	0	37620
23	C2H4⇔C2H3+H	1E+16	0	451440
24	C2H5+C2H2⇔C2H6+C2H	2.71E+11	0	97812
25	C2H5+H⇔C2H6	3.07E+13	0	0
26	C2H4⇔C2H2+H2	7.94E+12	0.44	371016
27	C2H3+H⇔C2H2+H2	9.64E+13	0	0
28	C3H6+CH3⇔C3H5+CH4	1.58E+12	0	0

Their model can be used to calculate the heat term from pyrolysis reaction and add this term to the energy equation to get a better result on the temperature distribution; it also can be used to track the concentration of specific species will be used in transport of diluted species. In this model, the combustion products were modeled as compounds that are essentially inert (e.g., N_2), or fully oxidized compounds (*e.g.*, CO_2 and H_2O) that were considered stable. Experimental results will later show this to be an error of assumption.

Space dependent model can be generated and other physics related to the simulation can be defined: transport of diluted species, chemistry, heat transfer in fluids, laminar flow. Methane is to come into contact with hot gasses formed from stoichiometric combustion of propane with air:

$$C_3H_8 + 5(O_2 + 3.76N_2) \rightarrow 3CO_2 + 4H_2O + 18.8N_2 \qquad \text{(D-4)}$$

After this reaction happens a mixture of $3CO_2$ + $4H_2O$ + $18.8N_2$ at 2400 K (calculations of this temperature is shown in Appendix B) is available but for simplicity, only N_2 was considered to enter the system at 2400K as about 73 mole% of the mixture consists of N_2. At the injection point, the hot N_2 comes into contact with CH_4 at 300K.

D-4. Chemistry

The chemistry module of COMSOL keeps track of species concentration over time for transports of species equation. In the model for simplicity and making the whole model solvable only the concentration of methane and hydrogen were considered to avoid a huge number of equations. In this model the time-dependent concentration of methane and hydrogen is taken from the model by Holmen *et al* [47] for pyrolysis reaction their model defines mechanism of methane pyrolysis up to hydrogen formation. The reactions and Arrhenius parameters were added to the software, CHEMKIN data input files were used for kinetic and thermodynamic data. The reversible reactions rate can be found with by the following equation

$$r_j = k_j^f \prod_{i=1} c_i^{-\nu_{ij}} - k_j^r \prod_{i=1} c_i^{\nu_{ij}} \tag{D-5}$$

where k (1/s) is defined in equation (1-6) and c_i is the concentration of species i. r_j can be calculated for the reaction j and chemical species i with the respective reaction orders ν_{ij} using the Arrhenius parameters from Holme *et al* [47] model.

D-5. Momentum Transport

The time-dependent continuity equation for compressible flows is as follows:

$$\frac{\partial \rho}{\partial t} + \nabla \cdot (\rho \mathbf{u}) = 0 \tag{D-6}$$

The Navier-Stokes equations are second-order nonlinear partial differential equations, which govern momentum transport and are solved by default in the single-phase flow interfaces,:

$$\rho\frac{\partial \boldsymbol{u}}{\partial t} + \rho\boldsymbol{u} \cdot \nabla\mathbf{u} = -\nabla p + \nabla \cdot \left(\mu(\nabla\mathbf{u} + (\nabla\mathbf{u})^{T}) - \frac{2}{3}\mu(\nabla \cdot \mathbf{u})I\right) + \boldsymbol{F} \qquad \text{(D-7)}$$

μ: Dynamic viscosity ($N{\cdot}s/m^2$)

u: Velocity (m/ s)

ρ: Density of the fluid (kg/m^3)

p: Static pressure (Pa),

and F is the body force term (N/m^3)

D-5-1. Boundary and initial conditions for fluid mechanics:

- Incompressible flow.
- Temperature is found by coupled heat transfer equation.
- All the coefficients in all equations are used from GRI data-base [46].
- No slip on the quartz wall.
- Methane enters the chamber through the smallest rectangle at normal speed of 0.26314 m/s,
- N_2 enters through the rectangle with the width of 0.01 at normal speed of 1.026 m/s.
- All products leave the chamber at the outlet with no pressure difference

Figure D-3 and Figure D-4 show the boundary and initial conditions for momentum equation without and with insulation respectively.

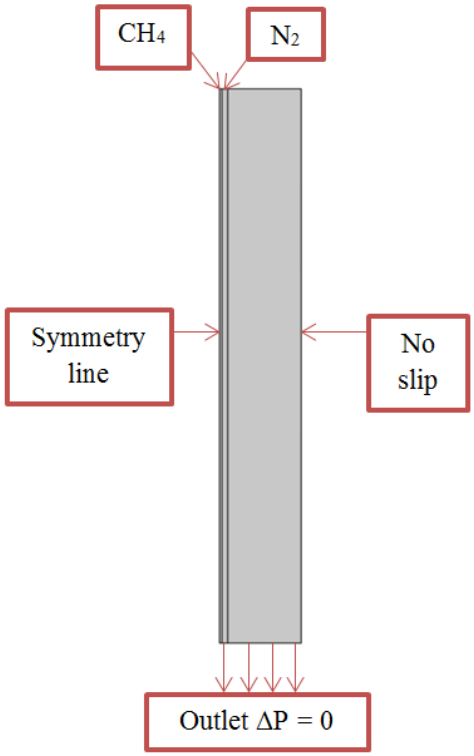

Figure D-3 - Boundary conditions - without insulation

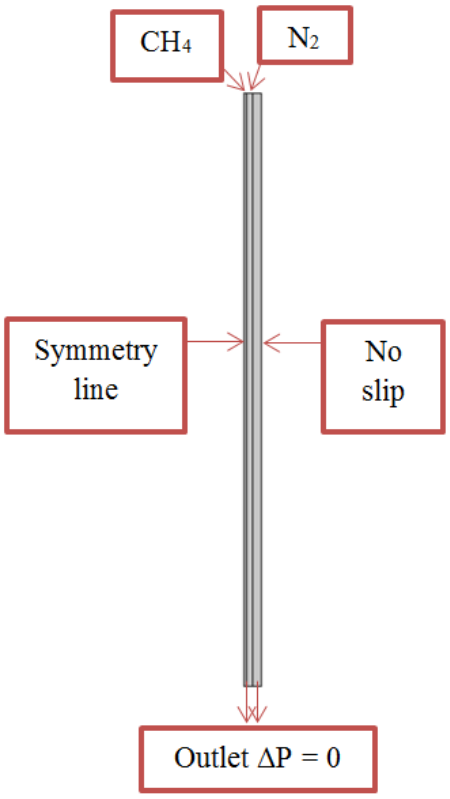

Figure D-4 - Boundary conditions - with insulation

D-6. Energy Transport

The energy balance equation applied to the reactor domain considers heat transfer through convection and conduction:

$$\nabla \cdot (-k\nabla \mathrm{T}) + \rho C_p \frac{\partial T}{\partial t} + \rho C_p(\boldsymbol{u} \cdot \nabla)T = Q \qquad \text{(D-8)}$$

C_p: Specific heat capacity (J/kg·K)

k: Thermal conductivity (W/m·K)

Q: Sink or source term (W/m^3)

D-6-1. Boundary and initial conditions for energy

- Time-dependent model is solved,
- The initial temperature of the chamber is 300 K.

- Heat source inside the chamber due the chemical reactions is added.
- Methane enters at 300 K.
- N_2 at 2400 K.
- At the side wall and outlet there is convective heat flux with room air (assumes that the conduction resistance through the quartz is zero),

Figure D-5 shows boundary and initial conditions for energy equation.

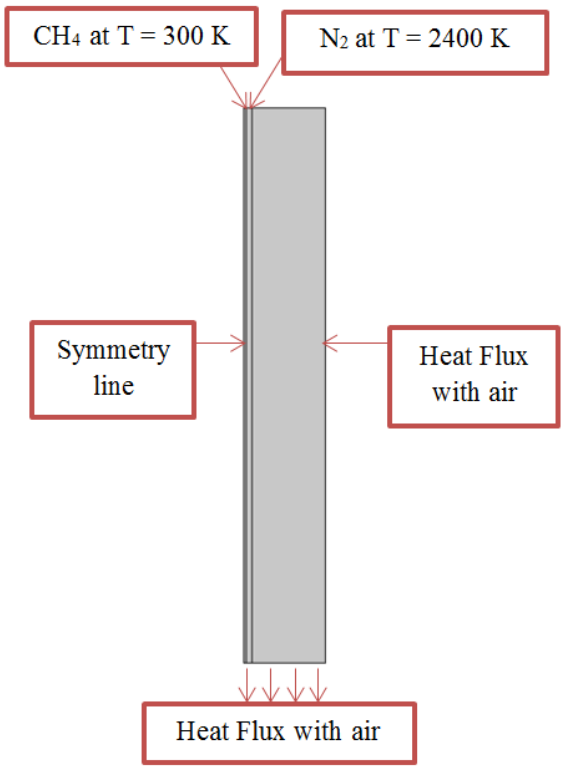

Figure D-5 -Boundary conditions - without insulation

By adding insulation, the assumption would be that ideally there is no heat transfer on the side wall and it is thermally insulated, as shown in Figure D-6.

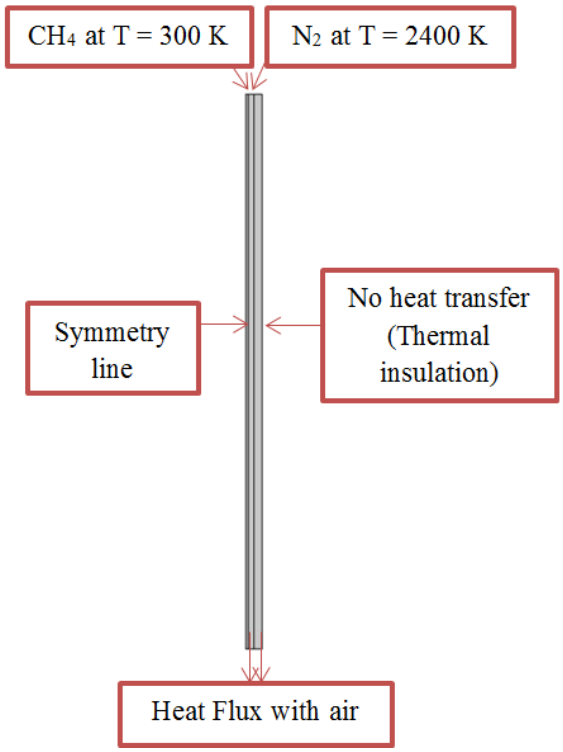

Figure D-6 - Boundary conditions – with insulation

D-7. Species Mass Transport

The mass transfer in the reactor domain could be given by the general advection-diffusion equation:

$$\frac{\partial C}{\partial t} = \nabla \cdot (D_i \nabla c_i) - \nabla \cdot (\mathbf{u} c_i) + R_i \qquad \text{(D-9)}$$

D_i: diffusion coefficient (m^2/s)

R_i: Reaction term ($mole/m^3 \cdot s$)

D-7-1. Boundary and initial conditions for species mass transport

- Only three species were considered in the equation in order to make the equation solvable. Diffusion coefficients were defined for CH_4, N_2, and H_2 as the main product of methane pyrolysis.

- No species mass flux on the side wall.
- The initial concentration of all compounds is zero except nitrogen.
- Reaction rates are taken from chemistry physic in the model.
- Methane and nitrogen enter the chamber with concentration of 0.011 moles/m^3 and 0.2 moles/m^3 respectively.
- The outflow is at the bottom.

After writing the necessary transport equations, it is vital to find the properties in transport equations such as thermal conductivity, heat capacity, viscosity, density, and diffusivity. These parameters can be found using reference [48]. This reference can be used to find transport properties, chemical equilibrium and homogeneous kinetics.

D-8. Coupling Transport Equations

Taking equations (D-7), (D-8) and (D-9) into account it can be seen the whole process in the system depends on both temperature distribution and fluid flow. In the equation (D-8), the velocity vector would be derived after solving the momentum equation. In addition, reaction term (*Ri*) in equation (D-9) is derived after solving the energy equation (D-8), due to the fact that it varies in terms of temperature. The simplest procedure is a stepwise method:

- The momentum transport equation can be solved separated from energy and mass transport equations
- The energy transport can be solved using results from the last step.
- Now, having results from energy and momentum transport, the mass transport equation can be solved.

This structure suggests that it is possible to solve the problem sequentially. Another method is to first solve the momentum transport and energy transport problem, then add the mass transport and investigate the difference. The last step leads to a fully coupled problem [49]. The momentum transport depends on the energy transport [49]. The energy transport depends on both momentum and mass transport (added heat of reaction) [49]. The mass transport depends on both the momentum transport and the energy transport. All equations describing transport phenomena should be solved simultaneously [49].

D-9. Results

The model was solved for the actual geometries for the two cases for 50 seconds. It can be seen in the temperature results that the system gets into a steady temperature profile after first 20 s when there is no insulation; Figure D-7 shows temperature distribution inside the quartz chamber with no insulation for t = 0, 20 and 50 s. By adding insulation blocks to the system the model gets into constant temperature profile after 5 seconds; Figure D-8 shows temperature distribution inside the quartz chamber for this case for t = 0, 2 and 5 s. As it is clear by adding the insulation blocks the temperatures needed for pyrolysis of methane can be provided in the reaction chamber.

This model suggests that for providing temperatures over 1400 K, adding insulation into the system is needed to initiate and sustain the pyrolysis reaction. As it can be seen in the model with no insulation only a small area around the flame has temperatures over 1000 K, by adding insulation into the model a large volume would have high enough temperatures for methane pyrolysis.

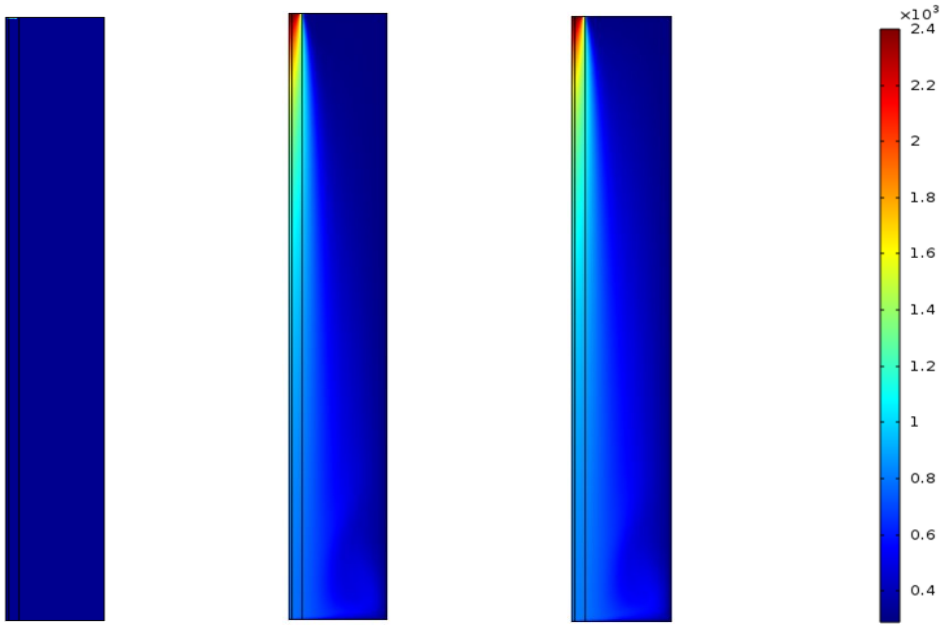

$t = 0$ s $t = 20$ s $t = 50$ s Temperature (K)

Figure D-7- 2D Temperature distribution for the COMSOL model without insulation

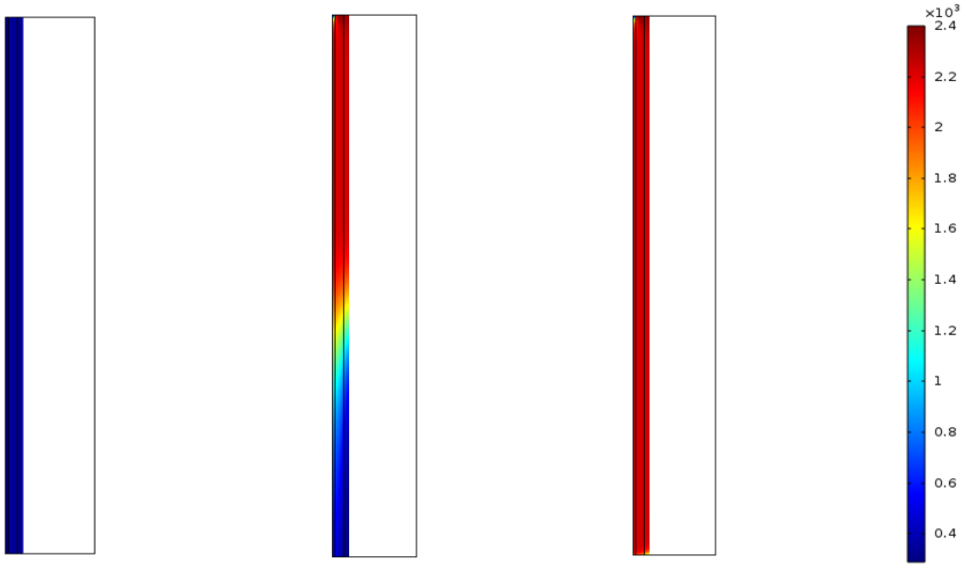

t = 0 s $t = 2$ s $t = 5$ s Temperature (K)

Figure D-8- 2D Temperature distribution for the COMSOL model with insulation

Appendix E. GC results

E-1. Propane Flame

Table E-1 to **Error! Reference source not found.** show the mole percentage of all known gases measured by GC at the exhaust for experiments that have been done in 5 days to investigate pyrolysis of methane inside a propane flame.

Table E-1 - Mole % of products for different methane flow rates from GC - First day

Total	H_2	CO	N_2	CO_2	C_3H_8	C_2H_6	CH_4	Pyrolysis CH_4 (l_n/min)
94.4443	0.80431	0.54862	79.5003	12.3929	0.0014	0.00473	0.02171	0
94.5426	2.76453	3.65861	77.1467	10.1117	0	0.0723	0.05598	0.5
97.4045	3.80365	4.77847	75.521	9.43397	0.00388	0.37946	0.54857	1
95.27	3.81384	4.77705	75.3171	9.44991	0.00384	0.38253	0.53709	1
95.8021	3.86351	4.81381	75.8344	9.35025	0.00537	0.39912	0.54662	1
95.0847	3.84379	4.25065	75.7	9.37198	0.00066	0.39108	0.53803	1
97.3714	3.88807	4.82171	75.85	9.33304	0.00065	0.39919	0.54663	1
95.8929	4.09377	4.7948	74.7563	9.18309	0.00087	0.51738	1.5727	1.5
98.1434	4.12604	4.77073	73.8644	8.96944	0.00149	0.60597	3.03877	2
97.5006	3.99287	4.63121	67.2874	6.79796	0.19272	1.23294	10.3888	5

Table E-2- Mole % of products for different methane flow rates from GC - Second day

Total	H_2	CO	N_2	O_2	CO_2	C_3H_8	C_2H_6	CH_4	Pyrolysis CH_4 (l_n/min)
96.0466	0.812503	1.26595	79.58555	1.94317	12.43533	0	0.004101	0	0
95.37992	2.70595	4.20637	77.10869	1.02534	10.22786	0	0.05898	0.046733	0.5
101.0064	3.84277	4.82596	78.38424	3.61245	9.41067	0.003862	0.383188	0.543254	1
98.47216	4.17698	4.8612	77.36504	1.0353	9.51074	0.000839	0.563318	0.958747	1
98.77685	3.77998	4.8025	76.64709	2.8841	9.44816	0.000928	0.456289	0.757806	1
103.9505	3.80986	4.8321	80.15071	4.43858	9.4649	0.000844	0.467757	0.785768	1
100.5282	3.82609	4.8338	78.70341	2.47536	9.4398	0.000899	0.470818	0.778065	1
102.4373	4.26502	4.97807	77.7361	3.68496	9.05489	0.002373	0.67942	2.03642	1.5
97.49865	4.43807	5.20541	74.09854	1.2336	8.6123	0.005646	0.790627	3.11446	2
97.63792	3.91724	4.59177	67.58457	3.23938	6.8309	0.21395	1.1692	10.09091	5

Table E-3 - Mole % of products for different methane flow rates from GC - Third day

Total	H_2	CO	N_2	O_2	CO_2	C_3H_8	C_2H_6	CH_4	Pyrolysis CH_4 (l_n/min)
95.45152	0.795682	1.123456	79.39236	1.10411	13.00712	0.000778	0.005453	0.02256	0
95.41951	2.7712	4.27345	77.0596	1.021	10.1568	0	0.078352	0.05911	0.5
97.91875	3.85	4.7804	76.2046	2.62891	9.42333	0.00063	0.41288	0.618	1
96.68052	3.9033	4.8196	76.5058	0.99756	9.41046	0.000696	0.4211	0.622	1
96.71334	3.78401	4.86465	76.49915	1.0123	9.43679	0.000877	0.43813	0.67743	1
103.4154	4.68374	5.09725	79.49969	2.78285	9.67345	0.000968	0.658945	1.0185	1
97.65787	4.07198	4.92059	76.97589	1.01608	9.3717	0.000858	0.51498	0.78579	1
98.60009	4.0568	5.03156	75.2252	2.92736	9.10146	0.001974	0.58838	1.66736	1.5
98.24551	4.42073	5.27803	74.37063	1.23126	8.58515	0.00633	0.89397	3.45941	2
97.82619	3.88561	4.59037	67.64597	3.24456	6.87179	0.22057	1.19232	10.175	5

Table E-4 - Mole % of products for different methane flow rates from GC - fourth day

Pyrolysis CH_4 (l_n/min)	CH_4	C_2H_6	C_3H_8	CO_2	O_2	N_2	CO	H_2	Total
0	0.02316	0.005354	0.000747	12.47145	1.083	80.45705	1.31196	0.830847	96.18357
0.5	0.0614	0.08022	0	10.1918	1.03248	77.86338	4.35333	2.79678	96.37939
1	0.60693	0.40027	0.000631	9.50976	1.00557	76.81548	4.866	3.8181	97.02274
1	0.5879	0.392922	0.000749	9.54168	1.00639	76.62511	4.86889	3.82196	96.8456
1	0.5777	0.3905	0.000766	9.55787	1.00763	76.6704	4.89029	3.83476	96.92992
1	0.569431	3.9066	0.000754	9.54474	1.00858	76.82676	4.9111	3.8575	100.6255
1	0.565	0.3911	0.000716	9.54626	2.35381	77.03053	4.92061	3.86498	98.67301
1.5	1.66548	0.517199	0.001043	9.36039	2.53767	77.22416	4.8666	4.07449	100.247
2	2.93155	0.55931	0.001552	9.26349	0.98044	74.968	4.85919	4.0167	97.58023
5	9.80426	1.133237	0.20827	6.9752	3.21445	68.22066	4.66143	3.91704	98.13455

Table E-5- Mole % of products for different methane flow rates from GC - fifth day

Total	H_2	CO	N_2	O_2	CO_2	C_3H_8	C_2H_6	CH_4	Pyrolysis CH_4 (l_n/min)
98.42255	0.847364	1.31563	82.22057	1.23766	12.7562	0.00135	0.00738	0.0364	0
99.89619	2.82887	4.40726	79.5836	2.4507	10.47139	0	0.087381	0.066989	0.5
99.99843	3.81103	4.89453	77.98973	2.44391	9.83062	0.004581	0.396424	0.627606	1
100.3201	3.83634	4.92507	78.07731	2.67076	9.77819	0.000931	0.402193	0.629277	1
100.2092	3.86022	4.9354	77.89956	2.6993	9.7975	0.000726	0.39869	0.617841	1
100.3273	3.8567	4.95432	77.83727	2.85525	9.82875	0.000783	0.39344	0.600746	1
98.74677	3.87801	4.97325	77.96428	1.1542	9.78276	0.000718	0.396106	0.597442	1
98.86813	4.08499	4.95636	76.87211	1.1373	9.58172	0.00104	0.517634	1.71698	1.5
99.36125	4.02675	4.89361	76.27122	1.12215	9.44536	0.001634	0.56569	3.03484	2
105.7265	3.8919	4.68241	72.31389	6.26789	7.27102	0.1922	1.11577	9.99139	5

E-2. Methane Flame

Error! Reference source not found. to **Error! Reference source not found.** show e mole percentage of all known gases at the exhaust for experiments that have been done in 5 days to investigate pyrolysis of methane inside a methane flame.

Table E-6 - Mole % of products for different methane flow rates from GC - First day

Total	H_2	CO	N_2	O_2	CO_2	C_3H_8	C_2H_6	CH_4	Pyrolysis CH_4 (l_n/min)
100.079	0.905529	0.939444	85.7354	1.25993	11.19629	0.000188	0.002767	0.039465	0
100.2423	3.32541	3.71244	82.46928	1.21121	9.31941	0.000213	0.092368	0.111979	0.5
100.189	4.11083	4.15802	80.61918	1.18416	8.83063	0.000678	0.369543	0.915918	1
100.4331	4.16788	4.20896	80.84782	1.18681	8.7358	0.000739	0.37733	0.907769	1
100.631	4.19367	4.22686	81.01073	1.18819	8.73707	0.000709	0.381641	0.892144	1
100.8104	4.20179	4.24279	81.15983	1.19107	8.76095	0.000738	0.381624	0.871561	1
100.892	4.22801	4.26895	81.20215	1.19104	8.76148	0.000713	0.382999	0.856618	1
100.8123	4.33589	4.37589	79.836	1.17035	8.41271	0.001875	0.45247	2.22715	1.5
100.5896	4.21025	4.38148	78.36016	1.30415	7.96231	0.002785	0.496052	3.87241	2
100.8105	3.37202	3.59518	70.62413	3.88144	6.08297	0.002921	0.606457	12.64535	5

Table E-7- Mole % of products for different methane flow rates from GC - Second day

Total	H_2	CO	N_2	O_2	CO_2	C_3H_8	C_2H_6	CH_4	Pyrolysis CH_4 (l_n/min)
99.57439	0.928543	0.927929	85.21585	1.25185	11.15342	0.000903	0.005022	0.090873	0
99.85634	3.28621	3.64437	82.19702	1.20633	9.29196	0.000413	0.09791	0.132123	0.5
99.76817	4.03597	4.11182	80.36335	1.17941	8.7732	0.000834	0.360682	0.942909	1
100.0174	4.10452	4.13836	80.55665	1.18117	8.71256	0.000825	0.376295	0.947004	1
100.0078	4.10511	4.15865	80.54312	1.18112	8.73622	0.000861	0.37163	0.911115	1
100.1067	4.14242	4.19688	80.60348	1.18125	8.70617	0.000852	0.379392	0.89628	1
99.99596	4.15345	4.1993	80.49484	1.18007	8.71905	0.000854	0.375309	0.873083	1
99.83774	4.23874	4.28429	79.10716	1.15941	8.4342	0.001933	0.44007	2.17194	1.5
99.57017	4.2951	4.38037	77.64881	1.13892	7.9276	0.002835	0.507937	3.6686	2
99.55949	3.42066	3.60435	70.07308	3.41447	6.04215	0.001264	0.618302	12.38521	5

Table E-8 - Mole % of products for different methane flow rates from GC - Third day

Total	H_2	CO	N_2	O_2	CO_2	C_3H_8	C_2H_6	CH_4	Pyrolysis CH_4 (l_n/min)
99.2512	0.889346	0.905462	85.01218	1.24935	11.18805	0	0.002179	0.004629	0
99.1903	3.19647	3.56553	81.72341	1.19782	9.28637	0.000188	0.097107	0.123408	0.5
99.35986	3.92637	4.01294	80.17314	1.17561	8.73235	0.000856	0.349477	0.989118	1
99.4034	3.96068	4.04996	80.17183	1.1766	8.70892	0.000826	0.35776	0.976829	1
99.2375	3.99861	4.06587	79.98263	1.17208	8.69594	0.000915	0.361726	0.959729	1
99.41094	4.05238	4.10131	80.08315	1.17376	8.68159	0.000886	0.366579	0.951288	1
99.41291	4.08102	4.12616	80.05526	1.17297	8.66823	0.000856	0.368927	0.939484	1
99.26158	4.14072	4.21013	78.68976	1.15244	8.33267	0.001891	0.436224	2.29775	1.5
98.9608	4.24547	4.32143	77.1785	1.13162	7.88926	0.002739	0.504057	3.68772	2
99.30019	3.40746	3.56369	69.76053	3.40053	5.97973	0.003158	0.625241	12.55985	5

Table E-9 - Mole % of products for different methane flow rates from GC - fourth day

Pyrolysis CH_4 (l_n/min)	CH_4	C_2H_6	C_3H_8	CO_2	O_2	N_2	CO	H_2	Total
0	0.027632	0.003954	0	11.32045	1.25588	85.15036	0.927551	0.897341	99.58317
0.5	0.117942	0.096711	0	9.36233	1.20726	82.01862	3.655	3.25434	99.7122
1	0.936523	0.370489	0.000446	8.80148	1.18084	80.25605	4.11692	4.04693	99.70968
1	0.920691	0.375388	0.000555	8.74938	1.17895	80.16598	4.15089	4.10068	99.64251
1	0.898186	0.377687	0.000532	8.75333	1.17848	80.0963	4.17628	4.12009	99.60088
1	0.876474	0.377937	0.000567	8.78686	1.17788	80.05478	4.19964	4.13916	99.6133
1	0.875214	0.383541	0.00054	8.78624	1.18034	80.22041	4.21201	4.15354	99.81183
1.5	2.22654	0.44578	0.001644	8.47676	1.16188	78.98973	4.28548	4.23811	99.82592
2	3.65751	0.502117	0.002563	8.03391	1.13874	77.43217	4.38694	4.28982	99.44377
5	12.40425	0.590812	0.00287	6.13256	3.28922	69.90248	3.59038	3.41423	99.3268

Table E-10- Mole % of products for different methane flow rates from GC - fifth day

Pyrolysis CH_4 (l_n/min)	CH_4	C_2H_6	C_3H_8	CO_2	O_2	N_2	CO	H_2	Total
0	0.044695	0	0	11.48387	1.25974	85.34657	0.940976	0.887185	99.96304
0.5	0.123063	0.094488	0	9.62508	1.21467	82.44299	3.60608	3.19614	100.3025
1	0.98827	0.360101	0.000442	9.0342	1.18789	80.72972	4.05461	3.94341	100.2986
1	0.979443	0.367875	0.000472	8.98834	1.18575	80.65272	4.08559	3.97736	100.2376
1	0.956968	0.368893	0.000529	8.986118	1.18692	80.66681	4.11688	4.0179	100.301
1	0.942527	0.370819	0.000522	8.98234	1.1871	80.66734	4.12834	4.05204	100.331
1	0.928028	0.373354	0.00058	8.98854	1.18563	80.57426	4.15477	4.08356	100.2887
1.5	2.379	0.450975	0.001453	8.66529	1.1668	79.35397	4.22353	4.18266	100.4237
2	3.69153	0.497395	0.002286	8.31244	1.14908	78.05196	4.23917	4.1442	100.0881
5	13.11556	0.660132	0.003179	6.35402	3.04493	70.6045	3.65344	3.51391	100.9497

Appendix F. Uncertainty in the mean for GC results

Based on the results shown in Appendix F, average mole percentage and uncertainty in the mean can be measured for all components as explained in chapter 3. The results of these calculation for both propane and methane flame are show in Table F-1 and Table F-2.

Table F-1 - Average mole % and uncertainty in the mean – propane flame

Pyrolysis methane flow rate	H_2 mole %	Pyrolysis methane flow rate	CO mole %	Pyrolysis methane flow rate	CO_2 mole %
0	0.82 ± 0.03	0	1.11 ± 0.29	0	12.61 ± 0.23
0.5	2.77 ± 0.06	0.5	4.18 ± 0.27	0.5	10.23 ± 0.12
1	3.89 ± 0.23	1	4.85 ± 0.13	1	9.53 ± 0.14
1.5	4.11 ± 0.10	1.5	4.92 ± 0.09	1.5	9.26 ± 0.19
2	4.21 ± 0.26	2	5.00 ± 0.20	2	8.97 ± 0.34
5	3.92 ± 0.05	5	4.63 ± 0.05	5	6.95 ± 0.17
	CH_4 mole %		C_2H_6 mole %		C_3H_8 mole %
0	0.02 ± 0.02	0	0.005 ± 0.001	0	0.0009 ± 0.0005
0.5	0.06 ± 0.01	0.5	0.075 ± 0.014	0.5	0
1	0.65 ± 0.11	1	0.428 ± 0.059	1	0.0015 ± 0.0010
1.5	1.73 ± 0.16	1.5	0.564 ± 0.063	1.5	0.0015 ± 0.0012
2	3.12 ± 0.18	2	0.683 ± 0.133	2	0.0033 ± 0.0024
5	10.09 ± 0.19	5	1.169 ± 0.042	5	0.2055 ± 0.0112

Table F-2 - Average mole % and uncertainty in the mean – methane flame

Pyrolysis methane flow rate	H_2 mole %	Pyrolysis methane flow rate	CO mole %	Pyrolysis methane flow rate	CO_2 mole %
0	0.90 ± 0.02	0	0.93 ± 0.03	0	11.27 ± 0.17
0.5	3.25 ± 0.07	0.5	3.64 ± 0.07	0.5	9.38 ± 0.18
1	4.08 ± 0.03	1	4.15 ± 0.04	1	8.80 ± 0.05
1.5	4.23 ± 0.09	1.5	4.28 ± 0.09	1.5	8.46± 0.16
2	4.24 ± 0.08	2	4.34 ± 0.08	2	8.02 ± 0.21
5	3.42 ± 0.06	5	3.60 ± 0.05	5	6.12 ± 0.18
	CH_4 mole %		C_2H_6 mole %		C_3H_8 mole %
0	0.05 ± 0.04	0	0.003 ± 0.010	0	0.0002 ± 0.0001
0.5	0.12 ± 0.01	0.5	0.096 ± 0.010	0.5	0.0002±0.0001
1	0.92 ± 0.02	1	0.371 ± 0.010	1	0.0006 ± 0.0001
1.5	2.26 ± 0.10	1.5	0.445 ± 0.014	1.5	0.0017 ± 0.0001
2	3.71 ± 0.11	2	0.501 ± 0.012	2	0.0026 ± 0.0001
5	12.62 ± 0.37	5	0.620 ± 0.025	5	0.27 ± 0.0001

Appendix G. 5 Gas analyzer results

Results from a 5 gas analyzer are shown in Table G-1 which proves low concentration of NO_x at the exhaust for the pyrolysis of methane in a propane flame.

Table G-1 – Results from 5 gas analyzer for the propane flame (for various fuel-air equivalence ratios and methane pyrolysis flow rates)

Volumetric flow rates (l_n/min)	O_2 (%)	CO (%)	CO_2 (%)	HC ppm	NO_x ppm
Air = 35 Propane = 1.370 Methane = 0	0.1	0.12	13.5	0	181
Air = 35 Propane = 1.570 Methane = 0	0.1	4.03	11.4	0	71
Air = 35 Propane = 1.770 Methane = 0	0.1	7.7	9.9	1	52
Air = 35 Propane = 1.170 Methane = 0	3.3	0.01	11.6	0	79
Air = 35 Propane = 1.370 Methane = 0 .5	0.1	3.5	11.9	20	110
Air = 35 Propane = 1.370 Methane = 1	0.1	4.35	11	230	112
Air = 35 Propane = 1.370 Methane = 1.5	0.1	4.38	10.7	585	94
Air = 35 Propane = 1.370 Methane = 5	2.2	4.25	9.5	3120	57

Appendix H. GC columns details

Figure H-1, shows the schematic of the columns, valves and detectors in the gas chromatograph analyzer used in the study. All valves are in off position and the part numbers of the columns are given below the figure.

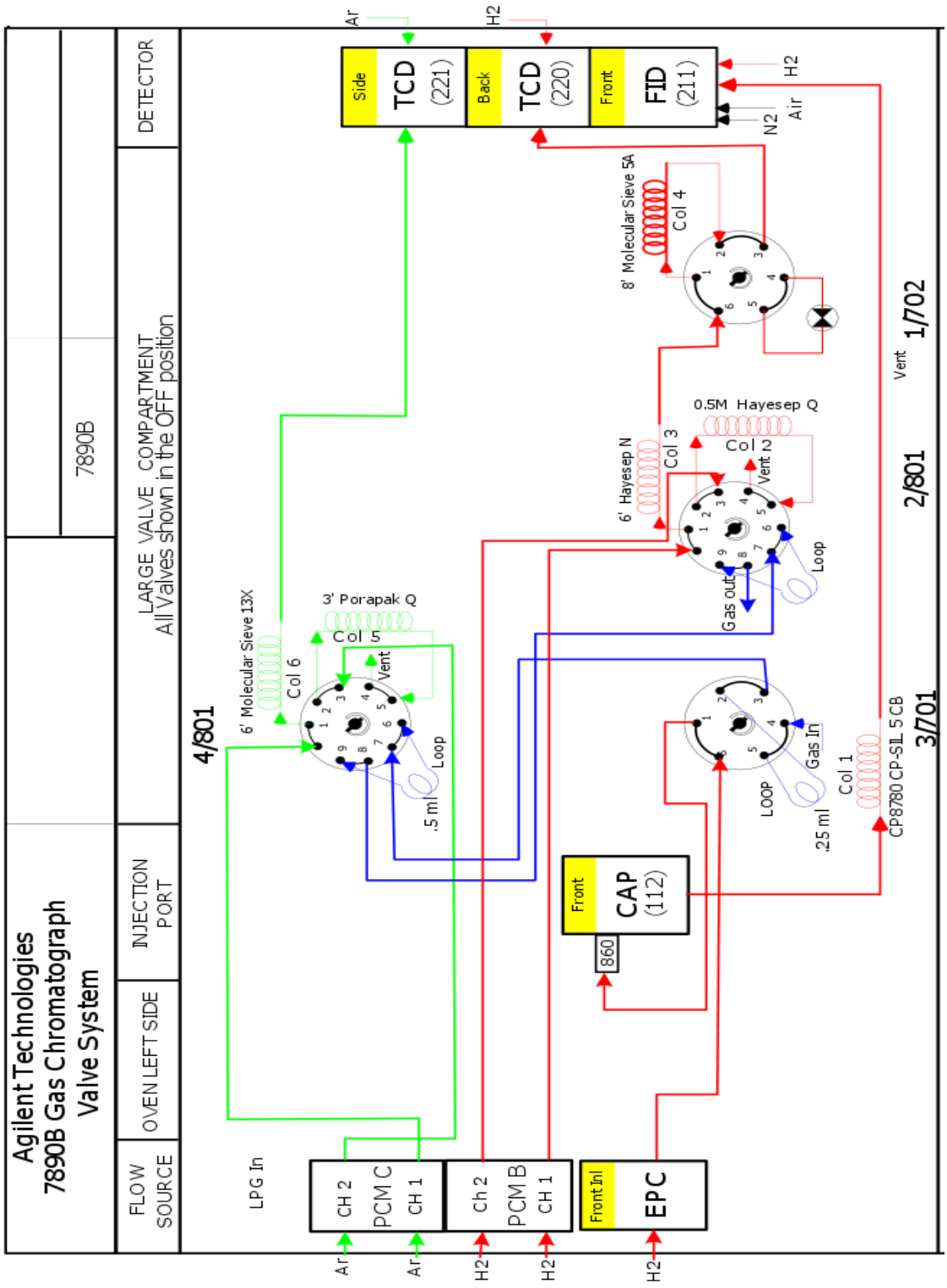

Figure H-1 – Schematic of columns, valves and detectors in GC (Agilent 7890B)

H-1. GC Summary

Run Time	7 min
Post Run Time	0 min
Oven	
Equilibration Time	0.5 min
Max Temperature	165 °C
Maximum Temperature Override	Disabled
Slow Fan	Disabled
Temperature	
Set point	On
(Initial)	80 °C
Hold Time	7 min
Post Run	50 °C
Front SS Inlet H2	
Mode	Split
Heater	On 150 °C
Pressure	On 21.411 psi
Total Flow	On 53.479 mL/min
Septum Purge Flow	On 1 mL/min
Gas Saver	Off
Split Ratio	25 :1
Split Flow	50.461 mL/min

H-2. Columns

Column Outlet Pressure	0 psi
Column #1 (CP8780)	
Temperature Range	-60 °C—325 °C (325 °C)
Dimensions	60 m x 250 µm x 1 µm
Column lock	Unlocked
In	Front SS Inlet H2
Out	Front Detector FID
(Initial)	80 °C
Pressure	21.411 psi
Flow	2.0184 mL/min
Average Velocity	45.056 cm/sec
Holdup Time	2.2195 min
Pressure	
Set point	On
(Initial)	21.411 psi
Post Run	10 psi

Column #2 (G3591-81023)

Temperature Range	-60 °C—325 °C (325 °C)
Packed	
Column lock	Unlocked
In	Aux PCM B H2
Out	Other
Pressure	
Set point	On
(Initial)	5 psi
Hold Time	0.01 min
Post Run	5 psi
Program	
#1 Rate	30 psi/min
#1 Value	0.5 psi
#1 Hold Time	0.55 min
#2 Rate	30 psi/min
#2 Value	5 psi
#2 Hold Time	0 min

Column #3 (G3591-81037)

Temperature Range	-60 °C—325 °C (325 °C)
Packed	
Column lock	Unlocked
In	PCM B H2
Out	Back Detector TCD
Pressure	
Set point	On
(Initial)	35 psi
Post Run	30 psi

Column #5 (G3591-81135)

Temperature Range	-60 °C—325 °C (325 °C)
Packed	
Column lock	Unlocked
In	Aux PCM C ArMe
Out	Other
Pressure	
Set point	On
(Initial)	10 psi
Hold Time	0.01 min
Post Run	10 psi
Program	

#1 Rate	30 psi/min
#1 Value	0.5 psi
#1 Hold Time	0.3 min
#2 Rate	30 psi/min
#2 Value	10 psi
#2 Hold Time	0 min

Column #6 (G3591-81035)

Temperature Range	-60 °C—325 °C (325 °C)
Packed	
Column lock	Unlocked
In	PCM C ArMe
Out	Aux Detector TCD
Pressure	
Set point	On
(Initial)	25 psi
Post Run	10 psi

Front Detector FID

Makeup	N2
Heater	On 250 °C
H2 Flow	On 40 mL/min
Air Flow	On 400 mL/min
Makeup Flow	On 25 mL/min
Carrier Gas Flow Correction	Does not affect Makeup or Fuel Flow
Flame	On

Back Detector TCD

Makeup	H2
Heater	On 200 °C
Reference Flow	On 45 mL/min
Makeup Flow	Off
Filament	On
Negative Polarity	Off

Aux Detector TCD

Makeup	N2
Heater	On 200 °C
Reference Flow	On 45 mL/min
Makeup Flow	Off
Filament	On
Negative Polarity	On

Valve 1

Switching Valve Off

Valve 2

Switching Valve Off

Valve 3

Switching Valve Off

Valve 4

Switching Valve Off

PCM B

PCM B

PCM B H2 Supplies Column 3

Aux PCM B H2

Aux PCM B H2 Supplies Column 2

PCM C

PCM C ArMe

PCM C ArMe Supplies Column 6

Aux PCM C ArMe

Aux PCM C ArMe Supplies Column 5

Run Time Events

Run Time Events

#1 Time	0.01 min
#1 Event	Valve
#1 Position	Valve 3
#1 Set point	On
#2 Time	0.01 min
#2 Event	Valve
#2 Position	Valve 4
#2 Set point	On
#3 Time	0.01 min
#3 Event	Valve
#3 Position	Valve 2
#3 Set point	On
#4 Time	0.5 min
#4 Event	Valve
#4 Position	Valve 3
#4 Set point	Off
#5 Time	0.6 min
#5 Event	Valve

#5 Position	Valve 4
#5 Set point	Off
#6 Time	0.7 min
#6 Event	Valve
#6 Position	Valve 2
#6 Set point	Off
#7 Time	1.4 min
#7 Event	Valve
#7 Position	Valve 1
#7 Set point	On
#8 Time	2.6 min
#8 Event	Valve
#8 Position	Valve 1
#8 Set point	Off